Finite strip elastic buckling solutions for thin-walled metal columns with perforation patterns

Frank Harrison Smith

Thesis submitted to the faculty of the Virginia Polytechnic Institute and State University
in partial fulfillment of the requirements for the degree of

Master of Science
In
Civil Engineering

Cristopher D. Moen, Committee Chairman
Matthew R. Eatherton
William J. Wright

August 1, 2013
Blacksburg, Virginia 24061

Keywords: elastic buckling, perforation, hole, finite strip analysis, local buckling, global buckling, distortional buckling, pallet rack

Frank Harrison Smith

Finite strip elastic buckling solutions for thin-walled metal columns with perforation patterns

ABSTRACT

Presented are approximate finite strip methods for use in predicting elastic buckling strength of cold-formed steel columns. These methods were developed by examining elemental behavior of cross-sections in eigen-buckling analyses and validated using a large database of finite element rack-type columns with perforation patterns. The influence of perforations is accounted by reduced thicknesses related to the plate buckling coefficient and transverse web rotational stiffness in the prediction of local and distortional buckling respectively. Global buckling prediction including the influence of perforations uses critical elastic loads of an unperforated section multiplied by the ratio of weighted to gross cross-sectional moment of inertia for flexural buckling and the ratios of weighted to gross cross-sectional warping torsion constant and weighted to gross St. Venant torsional constant for flexural-torsional buckling. Concern for end-user was given and methods are presented in a way for incorporation into governing design standards.

ACKNOWLEDGEMENTS

To my advisor, Dr. Cris Moen, for his encouragement to achieve something better, to always ask the question “Why?”, for his guidance and funding I am indebted.

To my parents, Gilbert and Catherine, whose expectations and trust have pushed me to be a better person – I am grateful. To my brother, Parker, for his support I am grateful as well.

To my fiancée, Nora, who has lifted my spirits and whose words “be productive” have prodded my efforts more than once – I am blessed.

And to my committee members, Dr. William Wright and Dr. Matthew Eatherton, I am thankful for their reviewing of this research.

TABLE OF CONTENTS

LIST OF FIGURES

LIST OF TABLES

CHAPTER 1. INTRODUCTION

1.1. Background

Since the characteristics of thin-walled steel post-buckling strength were quantified in the early half of the 1900s, structural cold-formed steel has seen an expansion in use. A shortlist of the benefits of the material includes that it is lightweight, transportable, potentially stackable, infinitely recyclable, noncombustible, and easily workable. Because of its high strength to weight ratio, fields as diverse as building construction, storage rack and appliance manufacturing, and aerospace engineering have relied on cold-formed steel to provide strength for main force resisting systems.

These applications have forced design of cold-formed steel to specific conditions. Member cross-sections have been developed that prevent certain types of buckling through lip or elemental stiffeners. Free elements in cross-sections have allowed for fastening and construction of entire cold-formed steel systems. More importantly to this research is how the implementation of holes in cross-sections affects buckling behavior. To save weight and allow access for inspections in aerospace structures, holes are punched along member lengths. To allow for conduit to be passed through wall and ceiling systems in buildings, stud and joists are manufactured with holes spaced at regular intervals. To let warehouses determine best rack arrangements, storage rack systems include perforation patterns along lengths of columns that allow adjustability of shelving. Without consideration for holes, strength of cold-formed steel in many applications may be overestimated.

Strength prediction of cold-formed steel has relied on effective widths to estimate post buckling capacity of individual elements within a cross-section. These effective widths are used to more easily model how stresses are carried within a plate element – at the center and unsupported edges of a plate, less stress can be carried than at stiffened edges. An effective area composed of the effective element widths is then used to calculate local buckling capacity (a buckling mode where instability of individual elements contributes to the overall instability of the member). This process may be iterative, becomes burdensome as cross-sections become more complex, and ignores the static equilibrium and stiffening effects of the interaction between cross-sectional elements. Separate strength equations are provided for global buckling modes where the entire member buckles as a whole and distortional buckling where flanges in open shapes flexuarlly buckle outward but are restrained by the web.

To stem use of difficult equations, a method that uses software has been developed in recent years to predict capacity of thin-walled metallic members. The Direct Strength Method (DSM) (AISI, 2007; Schafer, 2008) is an extension of column curve based design of hot-rolled steel that relates slenderness to buckling capacity for the three buckling modes – local, global, and distortional buckling. Slenderness values are constructed in such a way that uses critical elastic buckling loads and the squash load of the column, e.g., $\lambda_c=(P_y/P_{cre})^{0.5}$. Critical elastic buckling loads can be easily calculated by inputting cross-section geometries and material properties into software that runs finite strip or general beam theory analyses.

The incorporation of holes in cold-formed steel members complicates the design process. This has been addressed in the DSM for members used in residential,

commercial, and light industrial construction through modifications in determining critical elastic buckling loads, incorporating inelastic buckling into DSM curves, and limiting capacity to that of the net section, $P_{y,net}$, rather than the squash load, P_y (Moen and Schafer, 2009a; Moen and Schafer, 2011). The modifications to the process of determining critical elastic buckling loads to account for the influence of large, discretely spaced holes has been done through implementation of reduced cross-sectional thicknesses for distortional buckling, using weighted average cross-sectional properties in classical buckling equations for global buckling, and examining the worst case condition of local buckling at the location of holes or in the gross-section between holes. Literature on this topic will be incorporated into the next publishing of the American Iron and Steel Institute's (AISI) North American Specification for the Design of Cold-Formed Steel Structural Members (2012).

Perforation patterns characteristic of rack sections are the focus of this research; these perforations differ from discrete holes in that they are typically smaller in size and are arranged in tightly spaced arrays along an a cross-sectional element's length. The influence of periodic perforations on local buckling strength of pallet rack sections has been captured in the past through experimental determination of an effective cross-sectional area (CEN, 2009; RMI, 2012). The engineer is left to use rational analysis to account for other buckling modes. This research is a part of efforts to expand the DSM to include periodic perforations (Casafont et al., 2012).

1.2. Motivation

Developing prediction methods for pallet rack columns with periodic perforations is beneficial for two reasons. The first is that physical testing for strength prediction

required by governing standards in the US of the Rack Manufacturer's Institute (RMI) (2012) and in Europe of the European Committee for Standardization (CEN) (2009) can be reduced or eliminated, representing potentially a large cost savings for the rack industry. The second is that reliability in quantifying strength of distortional and global buckling can be improved if a prediction method explicitly states how to quantify the influence of perforations.

The decision to explore elastic buckling prediction of columns with periodic perforations stems from efforts to expand the Direct Strength Method to give designers a larger toolbox for strength prediction. Because of the DSM's ease of use, it is becoming the preferred method of cold-formed steel design, solidifying examination of the method to include periodic perforations. The key point in making the DSM account for perforations is to quantify the effect of perforations on elastic strength of local, distortional, and global buckling; DSM curves have already been calibrated considering unperforated rack uprights along with many other standard shapes – see pre-qualified shapes in AISI's North American standard (2007).

Additionally, research was motivated to consider the end use of the methods. Behavior based predictions are presented that are easy to implement for novice users and robust enough to give product engineers a large design space. While the research strictly examines web perforations in finite element models, local buckling is derived in a general sense that may be applied to any stiffened element in a cross-section with perforation patterns and global and distortional buckling prediction methods are potentially applicable to shapes with flange holes as well. That the methods are general in nature may spell their use in other fields besides rack manufacturing, such as design of

perforated stiffeners in aerospace applications and perforated architectural cladding in building applications.

CHAPTER 2. LITERATURE REVIEW

Discrete holes and the smaller holes of perforation patterns have found applications in cold-formed steel compression members for many years. Investigations on their effects on buckling behavior have typically started from examinations on discrete holes in uniaxially loaded simply supported plates subject local buckling. Observations from these studies have helped define ways to treat the effects of holes in full cross-sectional members. Separate studies have helped define procedures to treat distortional and global buckling modes of cross-sections with perforation patterns and discrete holes. To begin a review of literature, an obvious starting point is research involving plates with holes.

2.1. Uniaxially loaded simply supported plates with holes

An early investigation into a hole's effect on plate buckling was funded by the Navy Department of the US Bureau of Aeronautics to better understand the stabilizing effects of the common practice of stiffening edges of holes in fuselage and wing construction of airplanes (Levy et al., 1947). Theoretical elastic buckling of the plate was examined and charts were developed for constants to be used when solving for the critical elastic buckling load. The solution was performed with an energy approximation using a trigonometric series for the plate deflection function, *w*. The numerical method was not compared to experimental results. The study found that even at unstiffened hole diameters as great as half the width of the plate, the critical buckling load was reduced by less than 15 percent in comparison to an unperforated plate.

Research by Schlack (1964) investigated elastic buckling in square plates with circular holes using a Ritz energy approach. The displacement function, *w*, was phrased as a polynomial series and found that reduction in critical load in comparison to cases without holes to be no greater than 15 percent for holes with a diameter no greater than 30 percent of the plate width. The theoretical model was found to be very accurate through physical experimentation. Critical elastic buckling loads in experiments were defined to occur at the inflection point of load-deflection curves.

Kawai and Ohtsubo (1968) investigate a more general application of a Rayleigh-Ritz energy solution using an initial stress distribution from a finite element study and using a power series displacement function, *w*. Similar results to Schlack (1964) were found for smaller holes. Stress distributions found from finite element modeling of plates with large holes led to a compelling simplified model: plate buckling will occur in the unstiffened strips adjacent to the hole. This is beneficial to designers as it forgoes the more rigorous mathematics required when using an energy solution.

"Compressive buckling of perforated plate elements" by Pennington Vann (1971) studies the following in compression: elastic buckling of square plates with single circular holes with and without hole stiffeners using finite element analysis and testing, elastic buckling of rectangular plates with single circular holes with and without stiffeners using physical experiments, and the ultimate capacity of stud sections with circular holes with and without stiffeners. Pennington Vann astutely observes the competing behavior of a hole's effect on in-plane stress distribution and bending stiffness; holes reduce bending stiffness and thus want to reduce the elastic buckling load, but they also force in-plane stresses away from the center of the plate which is most

prone to buckling and thus want to increase the buckling load. These observations played out in the finite element analyses. These studies found that elastic buckling capacity decreases as hole diameter increases until a point at which the plate behaves much like the unstiffened strip model of Kawai and Ohtsubo's research (1968) where elastic loads begin to increase. When the hole diameter is half of the plate width, the buckling load is equal to that of the plate without a hole and at no point elastic buckling of plates with holes is less than 90 percent of the no hole case. Physical testing confirmed this behavior.

Elastic buckling and ultimate post-buckling strength of plate elements with square and circular holes were examined by Yu and Davis (1971). Noted was that plates with square holes had lower elastic buckling loads than plates with circular holes, but post buckling strength was similar for circular holes with the same diameter as width of square holes. A clear distinction between uniform stress and uniform displacement approaches of past research examining the elastic buckling mode is made; for uniform displacement studies, large holes greatly stiffen plates while the opposite can be said for the uniform stress approach. The uniform stress approach provided more accurate approximations of the buckling coefficient in comparison to physical tests performed. The unstiffened strip model was revisited, writing design guide appropriate language for post buckling strength prediction of elements with holes that modified George Winter's effective width approach for elements without holes (Winter, 1947).

Noted by Chow and Narayanan (1984) is a perforation's general detrimental effect on ultimate strength of plates due to its effect on post buckling behavior. Studied by Chow and Narayanan were finite element models for circular and square holes placed with varying eccentricities on simply supported and clamped square plates subject to

uniaxial and biaxial compression and pure shear loadings. Physical testing using the inflection point method confirmed finite element models; error between the two was no greater than 10 percent. In uniaxial compression, testing for concentric holes found the same behavior present as Pennington Vann (1971). Eccentric holes had little effect on elastic buckling for hole widths less than or equal to a fifth of the uniaxially loaded plate, while larger holes began to reduce critical loads because they forced in-plane stresses back into portions of the plate more susceptible to buckling. Square holes, especially at larger widths, had a more detrimental effect on elastic buckling when compared to circular holes of similar diameter.

Mahendran, Shanmugam, and Richard Liew (1994) studied plates with single square holes within portions of the plates confined by stiffeners. These stiffeners can be seen as breaking up the plate into smaller rectangular simply supported plates with single square holes. Examined by the research was the combination of past research on elastic buckling coefficients of plates with holes, second order elastic post buckling using the redistribution of in-plane stresses in the deformed plate, and a rigid-plastic yield line analysis to predict the ultimate capacity of the stiffened plates. Theoretical predicted capacities were within 10 percent of physical test results.

Research was conducted by Moen and Schafer (2009b) in an effort to provide designers with a simple way of determining elastic buckling stress of long plates with holes simply supported on three or four sides. For cases simply supported on four sides, an approximate method was validated through examination of finite element models that stated plate buckling would either occur at either side of the unstiffened edges of holes (i.e., a simply supported plate on three sides of length equal to the length of the hole) or

in the gross plate between holes. For the former, an unstiffened plate buckling coefficient was explicitly found; for the latter, a classical solution to the plate buckling coefficient is used but may be conservatively taken as equal to 4, that of an infinitely long plate. By taking the minimum stress found by these methods, the critical elastic buckling load can be found. This formulation can predict the observed effect that sometimes holes may stiffen buckling such that buckling loads were greater than that of plates without holes. Observed in this research was a buckling mode featuring holes of smaller widths in stiffened elements (simply supported on four sides) where plate buckling occurred with holes located within buckling deformations. Treatment of this mode was not pursued. These approximate models were validated through finite element eigen-buckling analyses.

2.2. Members with discrete holes

Ortiz-Colberg (1981) performed stub column tests on sections with circular holes in an effort to refine past effective width methods involving holes (Yu and Davis, 1971) which did not account for internal stress distributions from cold work of forming of steel cross-sections. Noted in this study is that effective widths are affected by an interaction of perforation size, elemental slenderness, and material properties. Also studied by Ortiz-Colberg is the effect holes have on long column buckling, also known as global buckling. The cross-sections studied did not have a significant effect on global buckling (an average decrease in buckling capacity of nine percent) and including more holes in members did not necessarily decrease buckling loads. This was cited as a result of the most effective portions of the cross-section in the global buckling mode to be unaffected by holes located in the web.

Loov, in research done at the University of Calgary (1983), studied local buckling of wall stud sections of varying depth with circular and rectangular web perforations. His efforts examined modifications to the effective width approach to account for the unstiffened portions of the web at the location of holes. Similar tests were carried out by Miller and Pekoz (1994) which studied stub columns with rectangular holes of varying size to expand applicability and improve upon methods developed by others (Yu and Davis, 1971; Ortiz-Colberg, 1981). This study saw reductions in strength of up to ten percent due to perforations and confirms use of an effective width method that states the ineffective portion of a plate to be at least the width of the perforation.

Moen and Schafer, through a series of extensive studies, examined elastic buckling and strength prediction of columns with discrete holes (Moen and Schafer, 2009a; Moen and Schafer, 2011). For elastic local and distortional buckling, approximate finite strip methods are developed and validated with finite element eigen-buckling analyses. Local buckling prediction extends the observed buckling modes of elastic plate buckling with holes (Moen and Schafer, 2009b) to local buckling of the cross-section. Unstiffened strip buckling at the locations of holes can be determined through a finite strip analysis and is compared to buckling of the undisturbed cross-section between holes; whichever load is the lowest controls local buckling of the column. Distortional buckling prediction uses a reduced web thickness of finite strip models to simulate loss in transverse web bending stiffness due to the presence of holes. The critical distortional buckling load including the influence of holes ($P_{crd,h}$) is taken at the distortional buckled half-wavelength of the undisturbed section ($L_{crd,nh}$) as holes were not observed to affect lengths of deformations. Elastic buckling prediction of global buckling modes (modes

where the critical buckling half-wavelength is equal to the member length, $L_{cr}=L$) is done through modifying classical buckling equations to account for the influence of holes. For flexural buckling, a weighted average moment of inertia is used. This approach conspicuously overpredicts buckling loads and is a result of the method's inability to account for local instabilities in the cross-section (thin-walled behavior). The flexural-torsional buckling prediction method is less prone to this rigid-body error and uses a weighted average approach for all properties except the torsional warping constant. Instead, the net section torsional warping constant is used as warping shear stresses were observed to be disturbed at the location of the hole. Strength of sections with holes was addressed through modifying the DSM to account for their influence on elastic buckling parameters used in slenderness calculations, limiting capacity to the net section yielding capacity ($P_{y,net}$), and defining an inelastic buckling region on the local, distortional, and global buckling curves.

2.3. Members with periodic perforations

Tested by Hancock (1984) were rack type sections with and without perforation patterns. The focus of this study was distortional buckling and it found that slenderness of this mode, calculated using the squash load and elastic properties from finite strip analysis, was a good predictor of strength. This formed the basis for what was to become the Direct Strength Method. Hancock's prediction of distortional buckling including perforations was to determine buckling stress based on the gross section and then use the net cross-sectional area to calculate distortional capacity.

Research led by Rhodes investigated the effects of circular and slotted perforation patterns in stub column tests. Examination of circular perforations (Rhodes and

Schneider, 1994) found that local buckling loads depended on the location of perforations within the cross-section: perforations near the stiffer junctions of elements reduced loads more than those located more toward the center of elements. This research found that holes reduced capacity less than the reduction of net cross-sectional area and recommends a modification to the effective width method similar to the concept confirmed by Miller and Pekoz (1994). Slotted perforations were studied to determine the effects of perforation length on local buckling that could not be observed in the research on circular perforations (Rhodes and Macdonald, 1996). It was found that perforation length does in fact affect local buckling capacity which the effective width approach does not account for. Proposed is using the worst case capacity obtained by the effective width method and a method that examines column strip buckling – where perforations cause portions of cross-sectional elements to have two free edges and buckle like columns.

Pu and a team of researchers reexamined the column strip buckling phenomenon through testing of stub columns with rectangular perforations (Pu et al., 1999). This research found that the effective length of the column strip was slightly longer than the length of perforations. A modified Perry-Robertson approach to column buckling was developed for this local buckling mode that considered anisotropy of the material.

Local and distortional buckling of wall studs with long slit perforation patterns used for thermal barrier applications in Nordic countries were examined numerically and experimentally by Kesti (2000). Treatment of perforations in local buckling is done through a reduced thickness of the disturbed portion of elements and is calculated by $t_r=t(\sigma_{cr,h}/\sigma_{cr,nh})^{0.5}$, where t is the thickness of the unperforated section and $\sigma_{cr,h}$ and $\sigma_{cr,nh}$ are the critical buckling stresses of the perforated and unperforated element respectively.

Since the slit patterns of the research did not vary perforation size or spacing, a single reduction factor of $(\sigma_{cr,h}/\sigma_{cr,nh})^{0.5}=0.72$ is presented based on finite element studies. This reduced thickness is then used in finite strip or general beam theory analysis to determing the critical elastic local buckling load. That perforations in local buckling were treated with a reduced thickness implies only a mode where plate deformations contain perforations was observed and not column strip or unstiffened strip buckling. Distortional buckling is modeled through a reduced thickness applied to the perforated portion of the web that based on the reduction in perpendicular bending caused by perforations. This reduction is stated as $t_r=t(\sigma_{cr,bending,h}/\sigma_{cr,bending,nh})^{0.333}$ and found through finite element modeling to be equal to $0.39t$ and is used in finite strip or general beam theory analysis to predict critical elastic distortional buckling.

Within Chapter 4 of Sarawit's doctoral thesis (2003) is an examination of local buckling of axially loaded plates with perforation patterns and global buckling of axially loaded rack sections with perforation patterns. It was found through finite element modeling that elastic flexural-torsional buckling including perforations can be approximated through use of classical equations using either the average or weighted average section properties, as results from both were nearly the same. This is due to the longitudinal spacing of perforations causing the total length of the gross and net sections to be approximately equal. The local buckling mode observed in the finite element analyses of plates with perforations was the same as the one observed by Kesti (2000) – plate deformations containing perforations and not column or unstiffened strip buckling. A reduction in the plate buckling coefficient is given for the particular perforation pattern

studied, but explicit recommendations are not given for the prediction of elastic local buckling of members with perforations.

Casafont has led a team of researchers in finding elastic buckling prediction methods using finite strip models to predict the influence of perforation patterns in pallet rack sections (Casafont et al., 2012). These methods apply stress at member ends mimicking the stress at the net section, apply reduced thicknesses at the location of perforations to form reduced thickness strips along the member, and were calibrated with finite element models that forced deformations in pure sinusoidal shapes. The reduced thickness used in the local buckling prediction method was found to be dependent on longitudinal and transverse perforation pattern properties and the depth of member flanges. That a reduced thickness is used for local buckling signifies only the prediction of plate buckling with perforations to be present and not column or unstiffened strip buckling. The researchers acknowledge the fact that local buckling prediction was not adequate. For distortional buckling, a similar reduced thickness equation to the one developed by Moen and Schafer (2009a) is recommended and provides accurate but slightly conservative results. It was noted that accuracy could be improved by considering perforation pattern properties in the transverse direction. Global buckling reduced thicknesses were directly related to the ratio of the longitudinal length of the unperforated section between perforations to the longitudinal perforation spacing, more or less a continuation of a weighted average property approach. The global buckling model, when applied to flexural and torsional-flexural buckling was an accurate predictor of critical global buckling loads.

CHAPTER 3. FINITE STRIP ELASTIC BUCKLING SOLUTIONS FOR THIN-WALLED METAL COLUMNS WITH PERFORATION PATTERNS

3.1. Abstract

Approximate finite strip eigen-buckling solutions are introduced for local, distortional, flexural, and flexural-torsional elastic buckling of a thin-walled metal column with perforation patterns. These methods are developed to support a calculation-based strength prediction approach for steel pallet rack columns employing the American Iron and Steel Institute's Direct Strength Method; however they are generally posed and could be useful in structural studies of thin-walled thermal or acoustical members made of steel, aluminum, or other metals. The critical elastic global buckling load including perforations is calculated by reducing the finite strip buckling load of the cross-section without perforations using the weighted average of the net and gross cross-sectional moment of inertia along the length of the member for flexural (Euler) buckling, and for flexural-torsional buckling, using the weighted average of both the torsional warping and St. Venant torsional constants. For local buckling, a Rayleigh-Ritz energy solution leads to a reduced thickness stiffened element equation that simulates the influence of decreased longitudinal and transverse plate bending stiffness caused by perforation patterns. The cross-section with these reduced thicknesses is input into a finite strip analysis program to calculate the critical elastic local buckling load. Local buckling at a perforation is also treated with a net section finite strip analysis. For distortional buckling, a reduced thickness equation is derived for the web of an open cross-section to simulate the reduction in its transverse bending stiffness caused by perforation patterns. The approximate elastic buckling methods are validated with a database of 1282 thin

shell finite element eigen-buckling models considering five common pallet rack cross-sections, 36 perforation dimension combinations, and twelve perforation spacing combinations.

3.2. Introduction

Vertical steel pallet rack columns have perforation patterns punched continuously along their length to accommodate horizontal storage rack shelving (Fig. 1) and these perforations decrease a rack column's axial capacity. In the U.S., the Rack Manufacturer's Institute (RMI) predicts the strength decrease with the Q factor method (RMI, 2012), an empirical approach where stub column tests quantify decreased local buckling capacity from the perforations. The European Committee for Standardization (CEN) implements a similar test method to derive an effective cross-sectional area (CEN, 2009). Both approaches treat local buckling, however they do not provide specific methods for addressing perforation patterns and their influence on distortional and global buckling limit states. A calculation-based method that considers all buckling limit states would improve the structural reliability of rack columns and reduce or eliminate the need for testing when new storage rack systems are introduced.

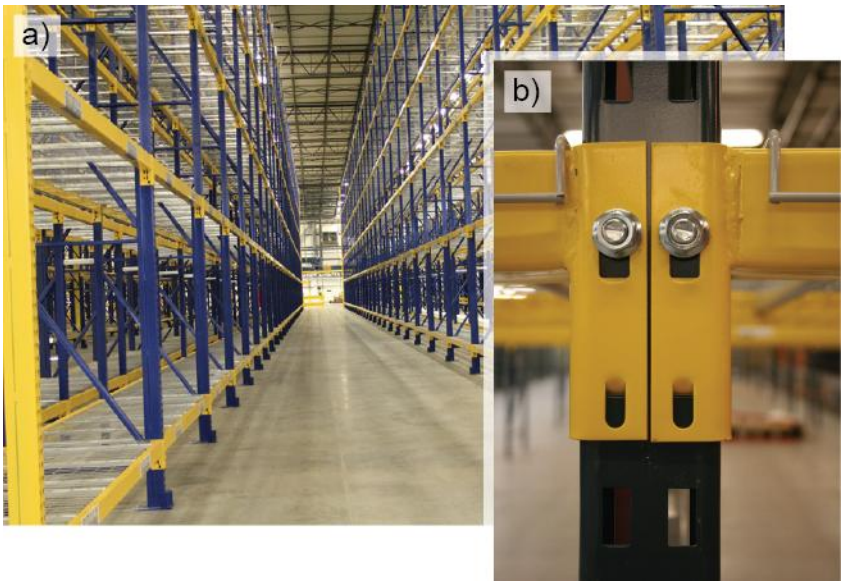

Fig. 1 Storage rack (a) assembly; (b) perforated rack column with shelf connection (UNARCO, 2012)

Efforts to improve rack column strength prediction are ongoing (Casafont et al., 2012) with a focus on the American Iron and Steel Institute's (AISI) Direct Strength Method (DSM) (AISI, 2007; Schafer, 2008). Nominal column strength with the DSM is calculated as the minimum of local, distortional, and global buckling strength, i.e., $P_n=\min(P_{n\ell}, P_{nd}, P_{ne})$. Limit state strengths are obtained from design equations that accept cross-section and global slenderness parameters as inputs, i.e., $\lambda_c=(P_y/P_{cre})^{0.5}$, $\lambda_\ell=(P_y/P_{cr\ell})^{0.5}$, and $\lambda_d=(P_y/P_{crd})^{0.5}$, where the column squash load $P_y=A_gF_y$, A_g is the gross column cross-sectional area, F_y is the steel yield stress, and the local distortional, and global critical elastic buckling loads are $P_{cr\ell}$, P_{crd}, and P_{cre} respectively. Elastic buckling loads are obtained from a signature curve generated with finite strip eigen-buckling analysis software, e.g., CUFSM (Li and Schafer, 2010), CFS (RSG Software, Inc., 2013), or THIN-WALL (Papangelis and Hancock, 1995).

Precedent for using the DSM to predict capacity of thin-walled members with perforations was established recently by a multi-year study (Moen and Schafer, 2009c) that demonstrated the DSM's viability both experimentally (Moen and Schafer, 2011; Moen et al., 2013) and computationally (Moen and Schafer, 2011) for cold-formed steel wall studs and floor joists with evenly spaced discrete perforations. The method is implemented in AISI S100-12 North American Specification for the Design of Cold-Formed Steel Structural Members, Appendix 1 (AISI, 2012). Nominal column strengths are obtained using the same DSM equations for columns without perforations, however, P_{cre}, $P_{cr\ell}$, and P_{crd} are calculated including perforations with finite strip analysis and modifications to classical plate and member stability equations (Moen and Schafer, 2009b; Moen and Schafer, 2009a). Inelastic buckling at a net section is treated with an equation transition to the net section capacity, P_{ynet}. It is hypothesized that this overall approach is applicable to any thin-walled metal column with perforation patterns if the critical elastic local, distortional, and global buckling loads are calculated considering the specific perforation layout.

In this manuscript, approximate finite strip methods are summarized and validated for cross-sectional and global elastic buckling loads of thin-walled columns with perforations patterns. A thin-shell finite element eigen-buckling database constructed with over 1200 models shows how perforation quantity, spacing, and size affect buckling loads and mode shapes. Then finite strip eigen-buckling analysis methods are introduced for calculating $P_{cr\ell}$, P_{crd}, and P_{cre} considering perforation patterns. Although the research motivation is cold-formed steel racks, mechanics underlying the methods are general, making them potentially applicable to perforated hot-rolled steel rack columns, slit steel

thermal studs (Kesti, 2000), acoustic cold-formed steel decks (Degtyarev and Degtyareva, 2012), and even marine engineering applications such as ship decks (Suneel Kumar et al. 2009).

3.3. Finite element parameter studies – thin-walled columns with perforation patterns

3.3.1. Elastic buckling database development

Finite element eigen-buckling analyses were conducted using the commercial software ABAQUS (Dassault Systèmes, 2011) to examine perforation pattern effects on elastic local, distortional, and global buckling loads and mode shapes, and to develop a database used later in the manuscript when validating the finite strip methods. The database includes cross-section types, thicknesses, perforation patterns, and unbraced column lengths common to cold-formed steel storage racks.

Five cross-section shapes were considered in this study (Fig. 2 and Table 1) with base metal thicknesses of 1.8 mm, 2.0 mm, and 2.5 mm. The shapes are consistent with other rack member studies (Casafont et al., 2012; Sarawit, 2003). Perforation dimension nomenclature is introduced in Fig. 3, and dimension ranges are provided in Table 2 and Table 3. Two column lengths are evaluated, $2.5L_{crd,nh}$ and $4L_{crd,nh}$, where $L_{crd,nh}$ is the distortional buckling half-wavelength for an unperforated member calculated with CUFSM.

Table 1 Centerline cross-section dimensions

Shape	h_o (mm)	b_o (mm)	D (mm)	θ (deg)	b_2 (mm)	D_2 (mm)
1	72	36	18	-	-	-
2	72	72	18	-	-	-
3	72	36	13.4	63.4	30	12
4	72	90	21.2	45	39	15
5	108	30	17.5	59.0	33	15

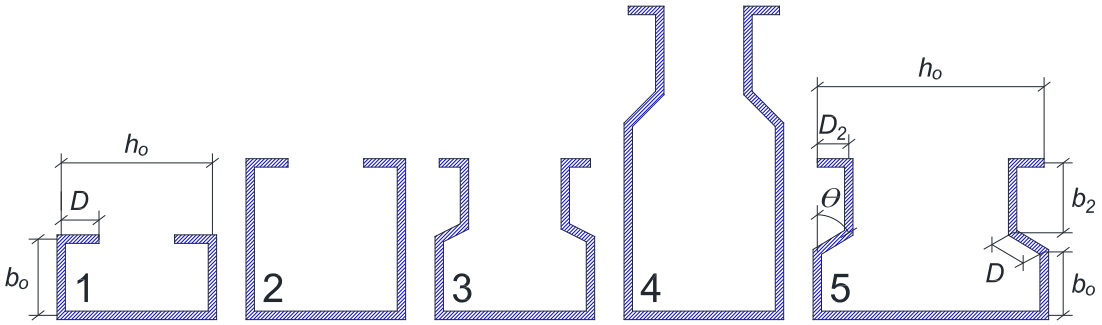

Fig. 2 Centerline cross-section dimension nomenclature

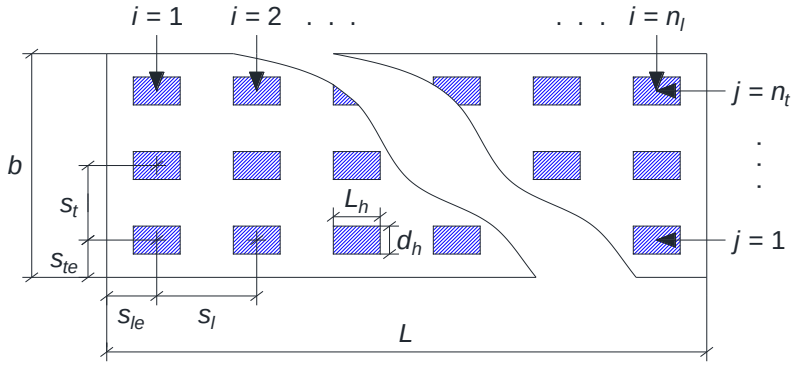

Fig. 3 Perforation pattern nomenclature for a cross-section element. Note that $b=h_o$ in this manuscript because only web holes were considered.

Table 2 Perforation schedule – longitudinal perforation dimensions and corresponding spacings

Longitudinal Dimension		Longitudinal Spacing (h_o/s_l)	
L_h/h_o	Name	Full Data Set	Rack Data Set
0.375	A	1, 1.5	1.5
0.313	B	1, 1.5	1.5
0.25	C	1, 1.5, 2	1.5
0.188	D	1, 1.5, 2	dimensions not used
0.125	E	1, 1.5, 2, 3	
0.094	F	1, 1.5, 2, 3	

Table 3 Perforation schedule – transverse perforation dimensions and corresponding spacings

Transverse Dimension		Transverse Spacing (n_t)	
d_h/h_o	Name	Full Data Set	Rack Data Set
0.375	A	1	dimensions not used
0.313	B	1	
0.25	C	1, 2	
0.188	D	1, 2	2
0.125	E	1, 2, 3	2
0.094	F	1, 2, 3	2

Perforation pattern combinations considered in the database are assigned two-letter combinations that represent perforation length, width, and spacing. To illustrate a sample combination, consider the model where shape=3 (see Fig. 2), L=2.5$L_{crd,nh}$, and t=1.8 mm with the perforation combination "*CE*". This "*CE*" combination represents a pattern in which the perforation length L_h="*C*", or L_h=0.25h_o, and the perforation width d_h="*E*", or 0.125h_o (see Fig. 3, Table 2, and Table 3). Corresponding to these dimensions, the longitudinal perforation spacing is varied (Table 2, $L_{cr\ell}/s_l$=1, 1.5 and 2) as well as the transverse perforation spacing (Table 3, n_t=1, 2, and 3), resulting in a total of 9 permutations. The model name for h_o/s_l=1.5 and n_t=2 is S3_L2-5_T1-8_NL1-5_NT2_CE;

names for other models follow this convention. Variable combinations for all 1282 columns in the database are summarized in Table 4. The complete elastic buckling database is archived in digital format and freely available for download at Virginia Tech (Smith, 2013).

Table 4 Column schedule

t (mm)	$L/L_{crd,nh}$	Shape 1	2	3	4	5
1.8	2.5	FF	AA	DD	CC	EE
		AB, BA	AC, CA	AD, DA	AE, EA	AF, FA
		CD, DC	BE, EB	BF, FB	BD, DB	BC, CB
		EF, FE	DF, FD	CE, EC	CF, FC	DE, ED
	4	DD	FF	CC	EE	BB
		AF, FA	AB, BA	AC, CA	AD, DA	AE, EA
		BD, DB	CF, FC	BE, EB	BC, CB	CD, DC
		CE, EC	DE, ED	DF, FD	EF, FE	BF, FB
2	2.5	AA	CC	EE	BB	FF
		AC, CA	AD, DA	AE, EA	AF, FA	AB, BA
		BF, FB	BC, CB	BD, DB	BE, EB	CE, EC
		DE, ED	EF, FE	CF, FC	CD, DC	DF, FD
	4	EE	DD	BB	AA	CC
		AE, EA	AF, FA	AB, BA	AC, CA	AD, DA
		BC, CB	BD, DB	CD, DC	BF, FB	BE, EB
		DF, FD	CE, EC	EF, FE	DE, ED	CF, FC
2.5	2.5	BB	EE	AA	FF	DD
		AD, DA	AE, EA	AF, FA	AB, BA	AC, CA
		BE, EB	BF, FB	BC, CB	CE, EC	BD, DB
		CF, FC	CD, DC	DE, ED	DF, FD	EF, FE
	4	CC	BB	FF	DD	AA
		AC, CA	AB, BA	AD, DA	AF, FA	AE, EA
		BF, FB	CD, DC	BE, EB	BD, DB	BC, CB
		DE, ED	EF, FE	CF, FC	CE, EC	DF, FD

3.3.2. Modeling protocol and boundary conditions

Finite element models were generated using custom Matlab (Mathworks, 2012) code written by the authors. Models feature thin-shell S9R5 elements with a maximum

aspect ratio of 4:1 consistent with the second author's validated modeling protocol (Moen, 2008). Cross-sections were modeled with sharp corners. Material properties considered are typical of cold-formed steel, with Young's modulus E=203.4 GPa and Poisson's ratio μ=0.30. Column end boundary conditions are pinned-warping free (Fig. 4). Consistent nodal loads that consider the S9R5 quadratic shape function (Schafer, 1997) were used to apply a uniform stress to the member ends.

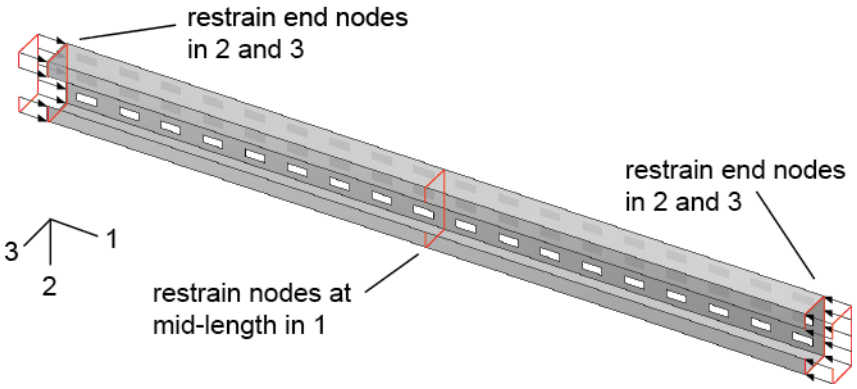

Fig. 4 Finite element model loading and boundary conditions

3.3.3. Modal identification methods

The lowest local, symmetric distortional, asymmetric distortional, flexural, and flexural-torsional buckling modes were identified visually for each of the 1282 finite element eigen-buckling models. In most cases the buckling mode could be found using the critical elastic buckling load and buckled half-wavelengths provided by an initial finite strip analysis in CUFSM excluding holes as a guide. Sometimes modes would mix as perforations caused critical elastic buckling loads of different modes to be near one another. In these cases, maximum relative displacements in a buckling mode aided the modal classification. For example, in Fig. 5, model S1_L2-5_T2-5_NL1_NT3_DE has critical elastic local and distortional buckling loads that are nearly equal – $P_{cr\ell,h}$=435.54

kN and $P_{crd,h}$=434.83 kN. The buckling mode shown in Fig. 5a is identified as being distortional buckling because half-waves similar in length to $L_{crd,nh}$=360 mm are dominant, while the mode in Fig. 5b is identified as local buckling because half-waves of similar length to $L_{cr\ell,nh}$=57 mm are dominant.

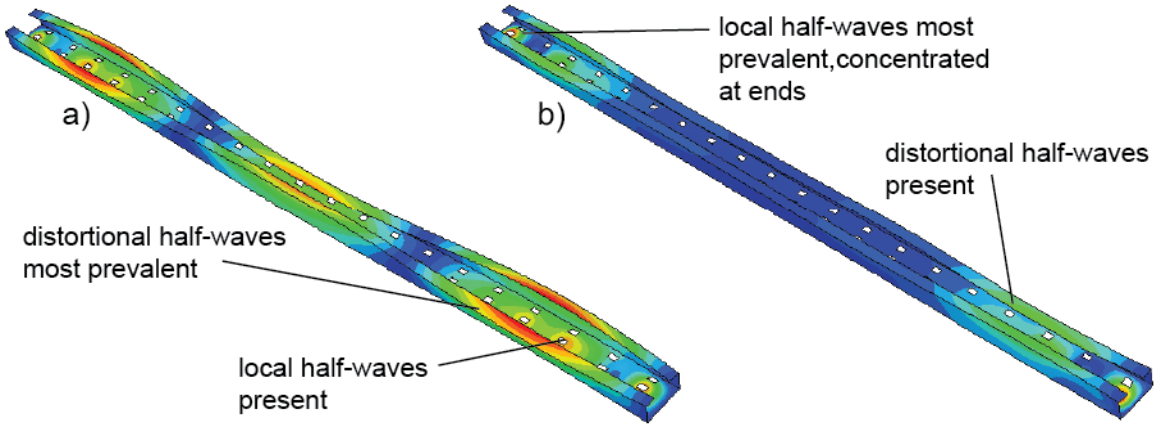

Fig. 5 Elastic (a) distortional and (b) local buckling identified using maximum relative mode shape displacements for model S1_L2-5_T2-5_NL1_NT3_DE

3.3.4. Influence of perforation patterns on elastic buckling loads

Perforation patterns typically decreased the buckling loads as shown in Table 5. Flexural-torsional buckling ($P_{cre,ft,h}$) in Fig. 6a was the least sensitive mode because only web perforations were considered in this study and the flanges contribute most to the torsional rigidity. Local buckling ($P_{cr\ell,h}$) in Fig. 6b and flexural buckling ($P_{cre,f,h}$) in Fig. 6e were the most sensitive, with reductions in elastic buckling loads of approximately 10 percent when compared to columns without perforations. Specific reasons for these sensitivities are provided in the following sections.

Table 5 Perforation pattern influence on critical elastic buckling loads

Mode n	Flexural-Torsional Buckling 1252	Flexural Buckling 1128	Distortional Buckling 1252	Local Buckling 1252
	$(P_{cr,h}/P_{cr,nh})_{ABAQUS}$			
Min	0.83[a]	0.72[b]	0.58[c]	0.48[d]
Max	1.00	0.99	1.04[e]	1.25[f]
Mean	0.97	0.92	0.95	0.91
COV	0.03	0.05	0.06	0.12

[a]S5_L2-5_T2-5_NL1-5_NT2_AC, [b]S2_L2-5_T2-5_NL1-5_NT3_AE, [c]S5_L4_T1-8_NL1_NT3_AE, [d]S5_L2-5_T2-5_NL1-5_NT2_AC, [e]S1_L2-5_T1-8_NL1_NT1_BA, [f]S5_L4_T1-8_NL1_NT1_EA

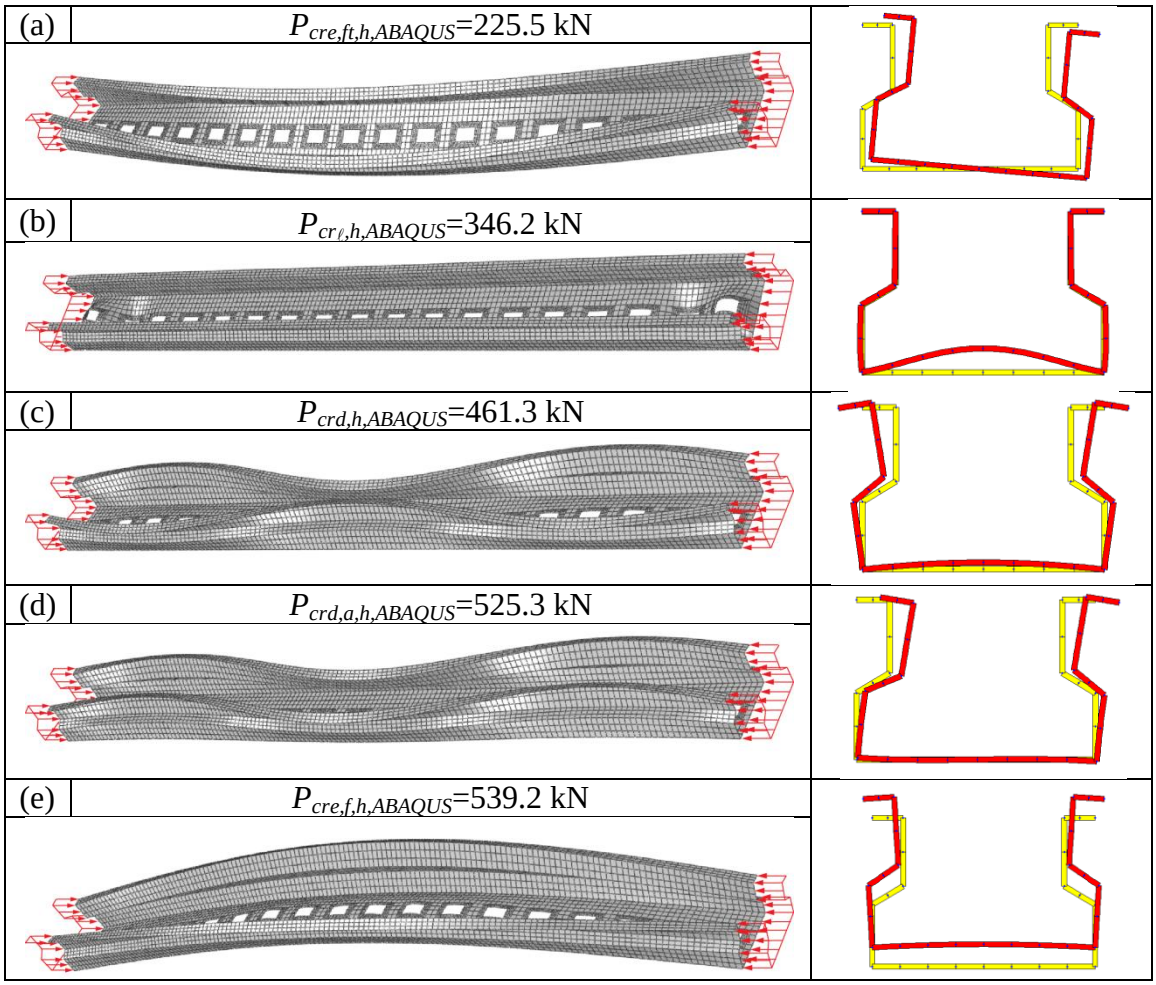

Fig. 6 Elastic buckling modes for model S5_L2-5_T2-5_NL1-5_NT1_BD: (a) flexural-torsional buckling, (b) local buckling, (c) symmetric distortional buckling, (d) asymmetric distortional buckling, and (e) flexural buckling with coupled long wave distortional buckling caused by perforations

3.3.4.1. Local buckling observations for columns with perforation patterns

Critical elastic local buckling loads reduce the most when there is more than one perforation across the web width as shown in Fig. 7c and Fig.7d. Removing web material near the web-flange juncture causes larger losses in transverse web membrane and bending stiffness when compared to a single perforation in a half-wave, see Fig.7a and Fig. 7b. Transverse plate stiffness (and buckling load) is reduced more by perforations when the longer dimension is oriented along the column length; compare $L_h/d_h \geq 1$ in Fig. 7b to $L_h/d_h < 1$ in Fig. 7a. The local buckling load is higher than the unperforated case in Fig. 7a because of wavelength stiffening (Moen and Schafer, 2009b) where the half-wave shape changes to fit between perforations. Unstiffened strip buckling on either side of a perforation (Pennington Vann, 1971; Yu and Davis, 1971) (Fig. 7b) and Euler strip buckling between perforations (Fig. 7c) are also observed; this net section buckling deformation reduces column capacity in tests (Moen and Schafer, 2008).

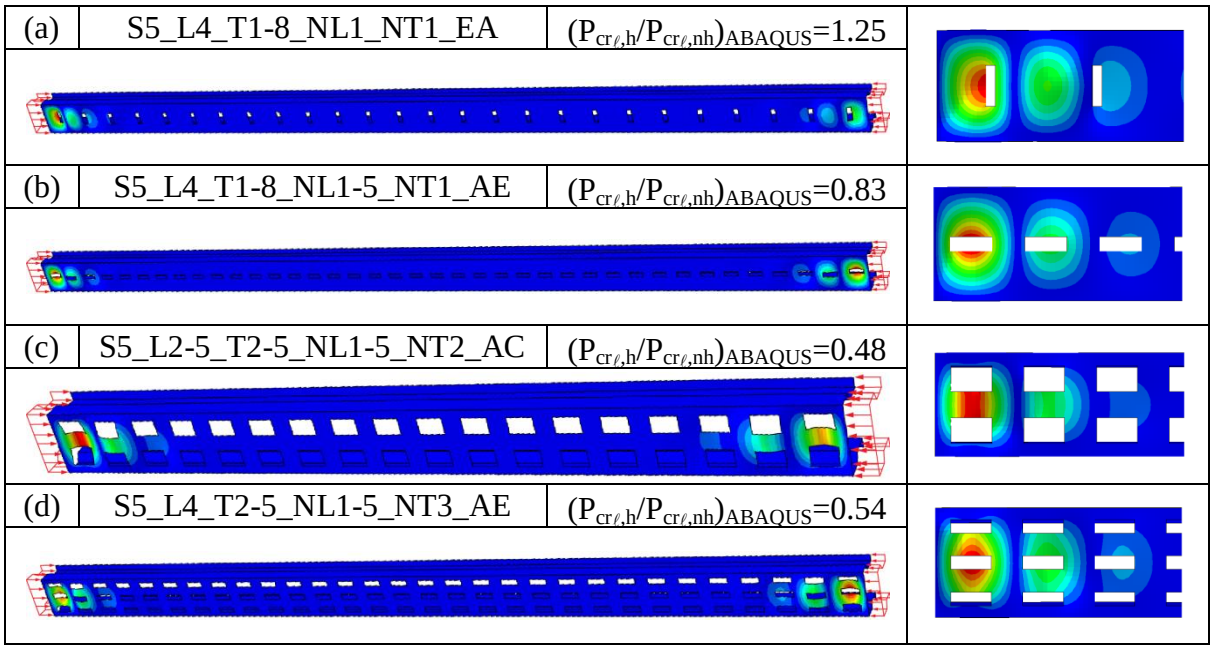

Fig. 7 Local buckling and perforation patterns: (a) n_t=1 with wavelength stiffening, (b) n_t=1 with unstiffened strip buckling, (c) n_t=2 with Euler strip buckling, and (d) n_t=3

3.3.4.2. Distortional buckling observations for columns with perforation patterns

Perforation patterns always decreased the critical elastic distortional buckling load and increased the distortional buckling half-wavelength in this study. Distortional buckling is restrained flexural-torsional buckling of the compressed flanges, where the restraint on the flanges comes from transverse web bending stiffness. When perforations are added to the web, transverse web bending stiffness decreases, reducing the distortional buckling load. The most severe reduction in buckling load is caused by more than one transverse perforation, i.e., n_t>1, see $P_{cr,h}/P_{cr,nh}$=0.58 for model S5_L4_T1-8_NL1_NT3_AE in Table 5. The half-wavelength increases as web bending stiffness decreases from perforations, just as the buckled half-wavelength for a column on an elastic foundation increases when the spring stiffness tends to zero.

The critical elastic distortional buckling load reported in the database is the lowest of the symmetric (Fig. 6c) and asymmetric (Fig. 6d) modes. Local buckling and

symmetric distortional buckling interacted most frequently in the finite element models with t=1.8 mm. This interaction was rarely observed for asymmetric distortional buckling (Fig. 6d) because transverse double web curvature prevents local buckling half-waves from forming. Asymmetric distortional buckling governed over symmetric distortional buckling in approximately 30 percent of the models in the database.

3.3.4.3. Global buckling observations for columns with perforation patterns

The lowest critical elastic buckling load for rack sections in this study was the flexural-torsional mode (Fig. 6a), and since $P_{cre,ft}$ was always much lower than $P_{cr\ell}$ and P_{crd}, interaction with cross-sectional modes was not observed. Weak axis flexural bucking coupled with a long wave distortional buckling mode in most of the models (Fig. 6e), i.e., the cross-section opens along the column length because transverse bending stiffness is reduced by the perforation patterns. The most severe reduction in the weak axis flexure buckling load results from more than one transverse perforation and closely spaced perforations longitudinally, see model S2_L2-5_T2-5_NL1-5_NT3_AE in Table 5 where $P_{cr,h}/P_{cr,nh}$=0.72. Finite strip analysis methods that consider the influence of perforation patterns are introduced in the following sections, starting with global buckling.

3.4. Global buckling of thin-walled metal columns with perforation patterns

The results in Table 5 and past research on thin-walled metal columns with discrete holes (Moen and Schafer, 2011; Ortiz-Colberg, 1981) and perforation patterns (Casafont et al., 2012; Sarawit, 2003) confirm that the critical elastic global buckling load, P_{cre}, always decreases because of the reduction in cross-section moment of inertia,

I, and torsional constants, J and C_w, along the column length. The following sections introduce methods for quantifying this reduction for columns with perforation patterns based on a weighted average approach previously derived from a Rayleigh-Ritz energy solution (Moen and Schafer, 2009a).

3.4.1. Global flexural buckling

3.4.1.1. Critical elastic flexural buckling load prediction

The critical elastic flexural (Euler) buckling load including the influence of perforation patterns is approximated as

$$P_{cre} = P_{cre,f,nh} \frac{I_{avg}}{I_g} \tag{1}$$

where

$$I_{avg} = \frac{I_g L_g + I_{net} L_{net}}{L}. \tag{2}$$

The critical elastic flexural buckling load without perforations, $P_{cre,f,nh}$, is calculated with finite strip analysis or the classical equation $P_{cre,f,nh}=\pi^2 EI_g/L^2$, and I_{net} and I_g are the net and gross cross-section moments of inertia. The net section length along the column is $L_{net}=n_l L_h$, i.e., the number of longitudinal perforations multiplied by the perforation length, and the length of gross cross-section is $L_g=L-L_{net}$. Note that calculating $P_{cre,f,nh}$ for a thin-walled section with a finite strip analysis is more accurate than the classical equations which overpredict the buckling load because of the rigid cross-section assumption (Moen and Schafer, 2009a; Ádány and Schafer, 2006).

3.4.1.2. Finite element verification for flexural column buckling considering perforation patterns

Finite element eigen-buckling ($P_{cre,f,ABAQUS}$) to approximate method (P_{cre}) results for flexural buckling of rack type sections and all sections are plotted in Fig. 8. The *x*-axis is the ratio of web planar net area, $A_{web,net}$, to web planar gross area, $A_{web,g}$, where $A_{web,net}=(Lh_o-n_l n_t L_h d_h)$ and $A_{web,g}=Lh_o$. The finite element-to-predicted statistics confirm the viability of the approach, with a COV of 0.03 over 1282 models. The finite element-to-predicted mean is slightly unconservative (mean of 0.96, see Fig. 8 legend). This bias could be improved with future research that incorporates long wave distortional buckling cross-section deformations caused by perforation patterns (see Fig. 6e) in the finite strip analysis.

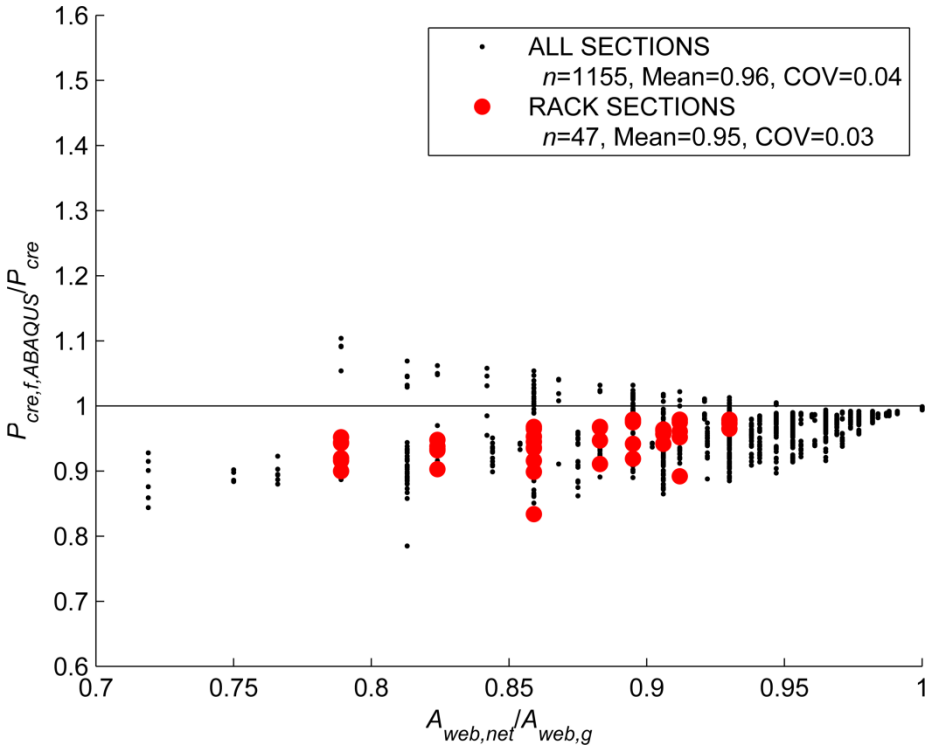

Fig. 8 Flexural buckling finite element to predicted results for P_{cre} calculated using Eq. (1) and $P_{cre,f,nh}$ calculated with CUFSM

3.4.2. Global flexural-torsional buckling

3.4.2.1. Torsional properties of thin-walled metal columns with perforation patterns

Previous research by the second author demonstrated that the weighted average approach employed for flexural buckling can be extended to flexural-torsional buckling for columns with discrete holes, except the warping torsion constant, C_w, should be that of the net section, $C_{w,net}$, because warping torsion shear stresses are disrupted at a perforation (Moen and Schafer, 2009a). A similar torsional constant study is summarized here to quantify how, on average, the St. Venant and warping torsion constants are affected by perforation patterns along the length of a thin-walled metal column.

The boundary and loading conditions for the torsion study are described in Fig. 9. A unit twist, β_o, is applied to one end of a thin-walled metal column, the other end being twist fixed and both ends free to warp. These boundary conditions produce a linear change in the angle of twist, β, along the member from which the column St. Venant torsion constant, J, including perforation patterns, can be calculated using the classical differential equation for uniform torsion $T_o=GJ(d\beta/dz)$ (Timoshenko and Gere, 1961). Once J is calculated, another finite element analysis is performed where a unit twist is applied to the column, but this time the end with the unit rotation, β_o, is also warping fixed. The angle of twist along the column is now nonlinear, and C_w can be calculated, including the perforation patterns, from the differential equation for nonuniform torsion $T_o=GJ(d\beta/dz)-EC_w(d^3B/dz^3)$. The torsion study was conducted on 34 models summarized in Table 6, and the results are compared to proposed approximate calculation methods in the following paragraphs.

Table 6 Torsion study models

Model	Shape	$L/L_{crd,nh}$	t	h_o/s_l	n_t	L_h	d_h
S3_L2-5_T2-5_NL1-5_NT1_AA	3	2.5	2.5	1.5	1	A	A
S4_L2-5_T1-8_NL1_NT1_BB	4	2.5	1.8	1	1	B	B
S3_L2-5_T2_NL2_NT2_CC	3	2.5	2	2	2	C	C
S1_L4_T2-5_NL1-5_NT1_DD	1	4	2.5	1.5	1	D	D
S5_L2_T2_NL3_NT1_EE	5	2	2	3	1	E	E
S3_L2-5_T1-8_NL1_NT2_FF	3	2.5	1.8	1	2	F	F
S5_L4_T1-8_NL1_NT1_AB	5	4	1.8	1	1	A	B
S2_L3_T2-5_NL1-5_NT1_AC	2	3	2.5	1.5	1	A	C
S4_L4_T2-5_NL1_NT2_AD	4	4	2.5	1	2	A	D
S1_L2-5_T2_NL1-5_NT3_AE	1	2.5	2	1.5	3	A	E
S1_L4_T2_NL1_NT1_AF	1	4	2	1	1	A	F
S4_L4_T1-8_NL1-5_NT2_BC	4	4	1.8	1.5	2	B	C
S2_L3_T2-5_NL1_NT2_BD	2	3	2.5	1	2	B	D
S5_L2-5_T1-8_NL1-5_NT2_BE	5	2.5	1.8	1.5	2	B	E
S3_L5_T2-5_NL1-5_NT2_BF	3	5	2.5	1.5	2	B	F
S1_L4_T2_NL1_NT1_CD	1	4	2	1	1	C	D
S2_L2_T2_NL2_NT3_CE	2	2	2	2	3	C	E
S5_L4_T1-8_NL1-5_NT1_CF	5	4	1.8	1.5	1	C	F
S4_L4_T2_NL2_NT2_DE	4	4	2	2	2	D	E
S3_L2-5_T1-8_NL1_NT1_DF	3	2.5	1.8	1	1	D	F
S1_L4-5_T2-5_NL3_NT3_EF	1	4.5	2.5	3	3	E	F
S3_L2-5_T1-8_NL1_NT1_BA	3	2.5	1.8	1	1	B	A
S5_L4_T2_NL2_NT1_CA	5	4	2	2	1	C	A
S2_L3-5_T2-5_NL1_NT1_DA	2	3.5	2.5	1	1	D	A
S4_L2-5_T2-5_NL1_NT1_EA	4	2.5	2.5	1	1	E	A
S2_L2_T1-8_NL2_NT1_FA	2	2	1.8	2	1	F	A
S5_L2-5_T1-8_NL1_NT1_DB	5	2.5	1.8	1	1	D	B
S4_L4_T2-5_NL3_NT1_EB	4	4	2.5	3	1	E	B
S3_L4_T2_NL1-5_NT1_FB	3	4	2	1.5	1	F	B
S2_L3-5_T2-5_NL1-5_NT1_DC	2	3.5	2.5	1.5	1	D	C
S3_L2-5_T1-8_NL2_NT2_EC	3	2.5	1.8	2	2	E	C
S1_L4_T1-8_NL1_NT1_FC	1	4	1.8	1	1	F	C
S2_L3-5_T2-5_NL1-5_NT1_FD	2	3.5	2.5	1.5	1	F	D
S5_L4_T2_NL1-5_NT3_FE	5	4	2	1.5	3	F	E

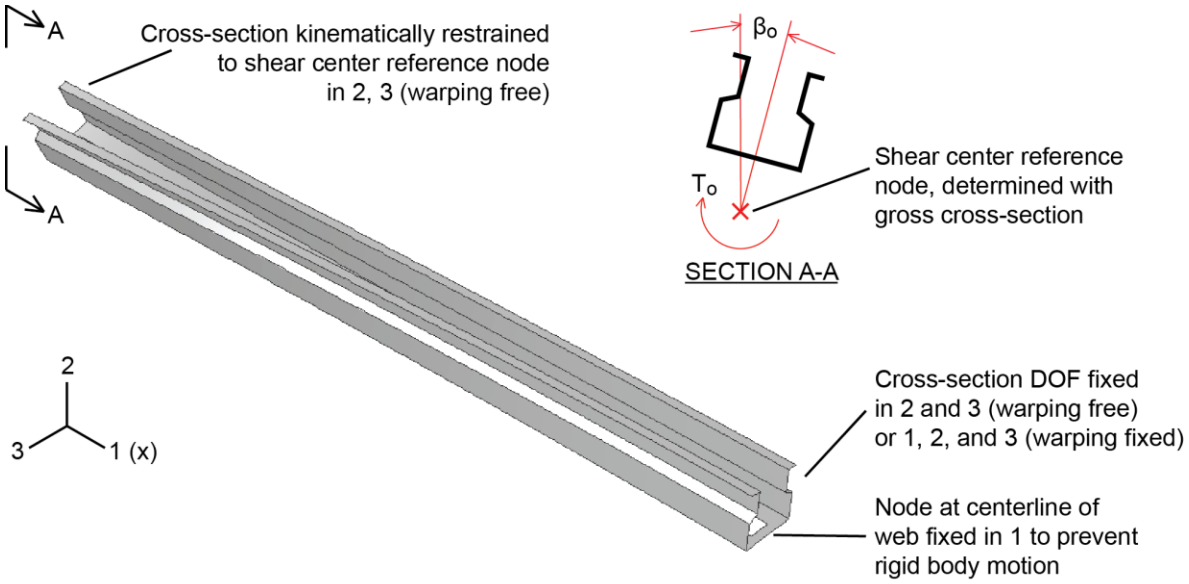

Fig. 9 Warping study boundary and loading conditions

The weighted average St. Venant torsional constant, J_{avg}, calculated in a form consistent with Eq. (2), is demonstrated to be a viable approach when compared to results from the finite element torsion study (J_{ABAQUS}) in Fig. 10. The finite element-to-predicted statistics confirm that Eq. (2) is accurate for one perforation transversely, i.e., n_t=1 (n=21, Mean=1.03, COV=0.02) and also for multiple perforations, i.e., n_t>1 (n=13, Mean=1.01, COV=0.05).

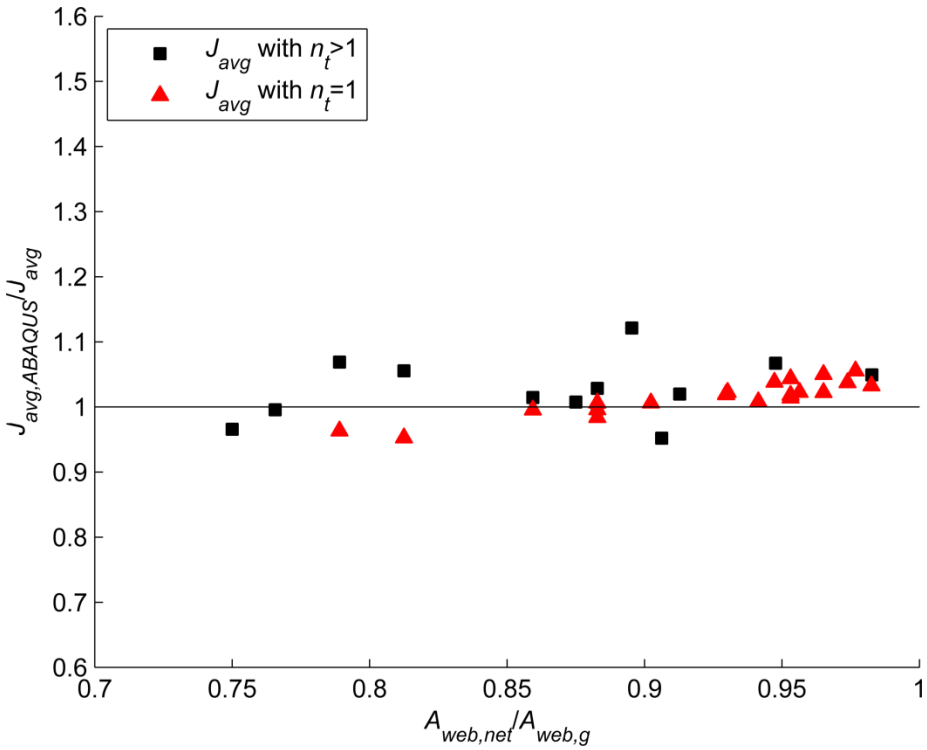

Fig. 10 Comparison of finite element to weighted average approximations for the St. Venant torsional constant, J_{avg}, calculated consistent with Eq. (2)

For warping torsion including perforation patterns, the net section constant, $C_{w,net}$, determined with a section property calculator in CUFSM by setting the thickness at perforations to zero, is a viable predictor of C_w for the columns with n_t=1 (n=21, Mean=1.05, COV=0.06) and when n_t>1 (n=13, Mean=1.15, COV=0.04). The weighted average warping torsion constant, $C_{w,avg}$, is more accurate for n_t>1 (n=13, Mean=1.03, COV=0.03), however for n_t=1 $C_{w,avg}$ become unconservative as discrete perforations take up more of the web, i.e., as $A_{web,net}/A_{web,g}$ decreases, supporting the current recommendation of using $C_{w,net}$ for evenly spaced discrete perforations [15], i.e., when n_t=1.

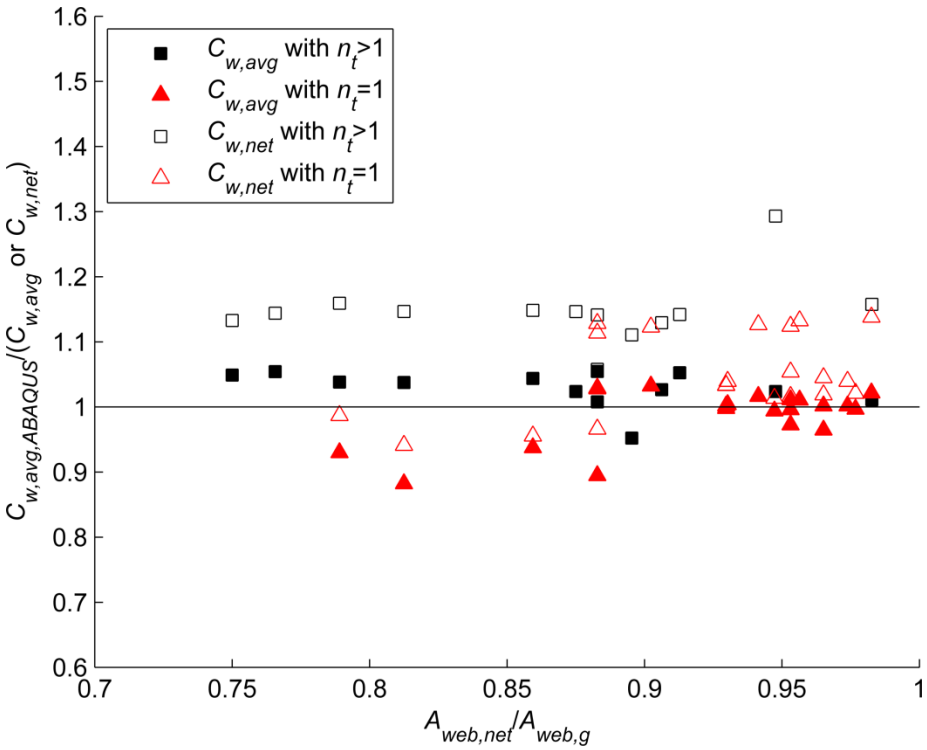

Fig. 11 Comparison of finite element predictions and weighted average $C_{w,avg}$ and net section $C_{w,net}$ for columns with perforation patterns

Why is $C_{w,avg}$ more accurate for members with web perforation patterns (n_t>1) and $C_{w,net}$ more appropriate for web discrete holes (n_t=1)? The answer lies in the warping shear stress distribution around the cross-section that defines C_w (Lue et al., 2007). Warping shear stresses are plotted in Fig. 12 along a column web twisted at one end with β_o=1 radian where boundary conditions are consistent with Fig. 9, and the twist fixed end is also warping fixed. The member cross-section shape is 3 (see Fig. 2), $L/L_{crd,nh}$=2.5, t=2.0 mm, h_o/s_l=1.5, L_h=0.25h_o, d_h=0.125h_o, and the number of transverse web perforations (n_t) varies from 1 to 3.

Web warping shear stresses vary nonlinearly in Fig. 12 for a member without perforations. When a single perforation is added at the center of the web (Fig. 12a), the shear stress decreases to zero in the net section where the web material is removed. For

net sections with n_t=2 (Fig. 12b) and n_t=3 (Fig. 12c), the shear stresses again converge to zero at the perforations but spike higher between perforations as the net section is still required to carry the warping portion of the applied torsion.

The warping shear stresses are also affected in the gross section adjacent to a net section, with higher stress magnitudes observed at the perforations to compensate for the removed web material. The variations in the warping shear stress are more severe as n_t increases, compare Fig. 12a to Fig. 12c. The results confirm that perforations interrupt warping shear stresses in a net section, and that the warping shear stresses in a gross section also vary when perforations are nearby.

The weighted average $C_{w,avg}$ is accurate when n_t>1 because the net section between perforations and the gross section adjacent to perforations develop warping resistance on average of $C_{w,net}$ and $C_{w,g}$ respectively based on the observed stress peaks in Fig. 12b and Fig. 12c. However, for single discrete holes (n_t=1), the cross-section cannot develop stress peaks adjacent to the perforation (see Fig. 12a), even in the gross cross-section, which means that warping resistance is derived primarily from the net section, especially as perforations remove more material from the web, i.e., $A_{web,net}/A_{web,g}$<0.85. These conclusions are implemented in a flexural-torsional buckling prediction method presented in the next section.

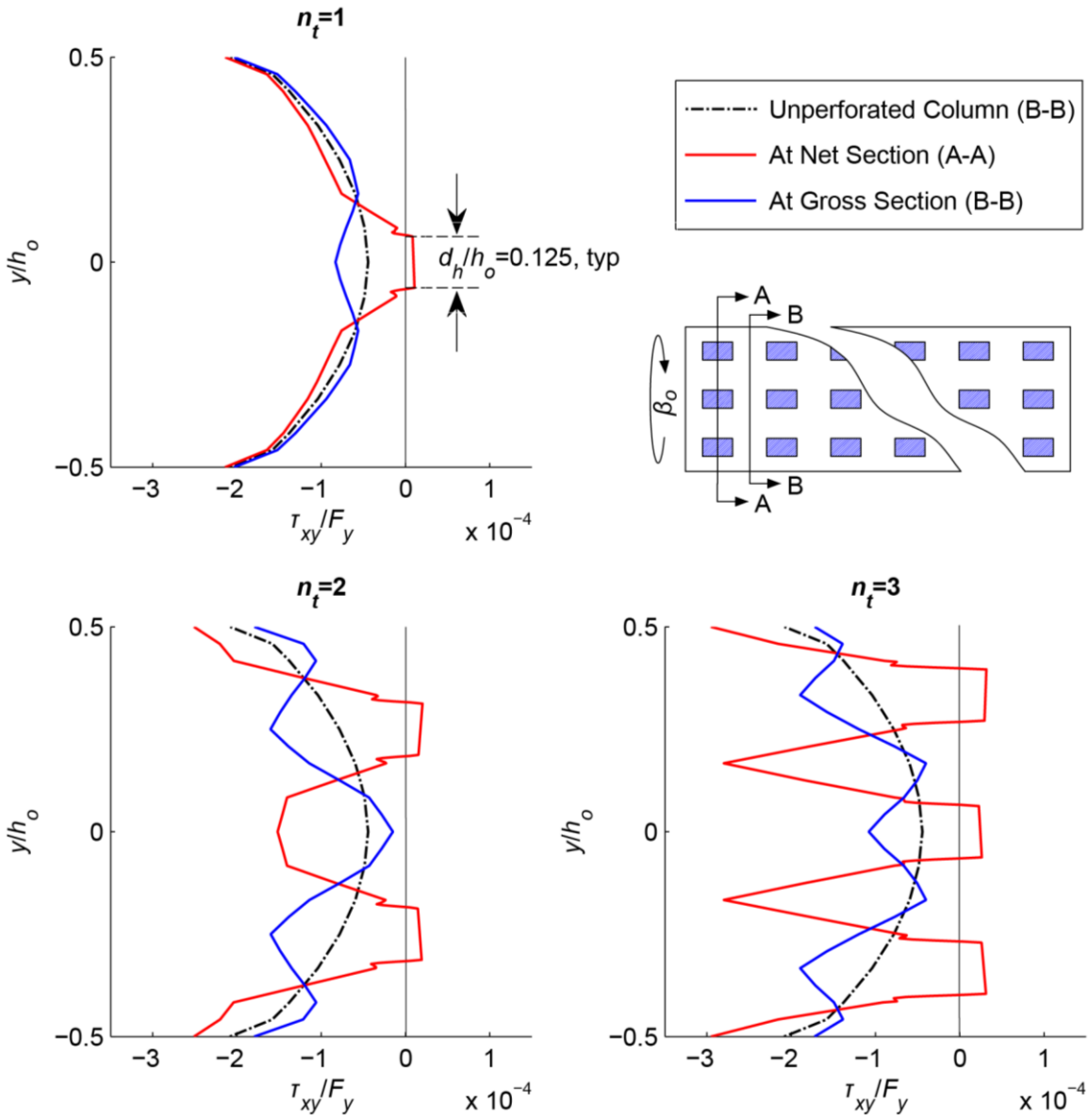

Fig. 12 Web warping shear stresses for (a) n_t=1, (b) n_t=2, and (c) n_t=3. The warping stresses are normalized to material yield stress of F_y=345 MPa.

3.4.2.2. Critical elastic flexural-torsional buckling load prediction

The critical elastic buckling load for flexural-torsional buckling including the influence of perforation patterns, P_{cre}, is approximated with an extension of the weighted average approach to the classical cubic column buckling equation (Timoshenko and Gere, 1961)

$$P_{cre} = \frac{A_g}{2\beta_h}\left[\left(\sigma_{ex,h} + \sigma_{t,h}\right) - \sqrt{\left(\sigma_{ex,h} + \sigma_{t,h}\right)^2 - 4\beta_h \sigma_{ex,h}\sigma_{t,h}}\right] \quad (3)$$

where

$$\beta_h = 1 - \left(\frac{x_{o,avg}}{r_{o,avg}}\right)^2 \quad (4)$$

$$\sigma_{ex,h} = \frac{\pi^2 E I_{x,avg}}{A_g\left(K_x L_x\right)^2} \quad (5)$$

$$\sigma_{t,h} = \frac{1}{A_g r_{o,avg}^2}\left[GJ_{avg} + \frac{\pi^2 E C_w}{\left(K_t L_t\right)^2}\right] \quad (6)$$

and C_w is equal to $C_{w,net}$ when n_t=1 and is equal to $C_{w,avg}$ for all other cases.

The elastic modulus is E, the shear modulus is G, and K_xL_x, and K_tL_t are the effective column lengths about the x centroidal axis and torsional axis respectively. The x distance from the centroid to the shear center for the weighted cross-section is $x_{o,avg}$ calculated in the same way as Eq. (2). The weighted average radius of gyration about the shear center is calculated using $r_{o,avg}=(r_{x,avg}^2+r_{y,avg}^2+x_{o,avg}^2)^{0.5}$ where $r_{x,avg}$ and $r_{y,avg}$ are the weighted average radii of gyration about the centroidal axes calculated using $r_{x,avg}=(I_{x,avg}/A_{avg})^{0.5}$ and $r_{y,avg}=(I_{y,avg}/A_{avg})^{0.5}$. The weighted average moments of inertia about the centroidal axes are $I_{x,avg}$ and $I_{y,avg}$ and A_{avg} is the weighted average area of the cross-section. The weighted average area A_{avg} should not be substituted for the gross cross-section area A_g in Eq. (3) through Eq. (6) because A_g accounts for the conversion of stress to force at the column ends.

The net section properties required to calculate $x_{o,avg}$, $I_{x,avg}$, $I_{y,avg}$, A_{avg}, J_{avg}, and $C_{w,avg}$ can be determined with the section property calculator in CUFSM by setting the element thickness to zero at the perforation locations in the cross-section. All weighted average properties are calculated in the same manner as Eq. (2).

A simpler finite strip approach for calculating P_{cre} is also proposed as an alternative to Eq. (3). In this method, the reduced buckling load is calculated with weighted average ratios of the St. Venant and warping torsion constants

$$P_{cre} = P_{cre,\,ft,nh}\,\frac{J_{avg}}{J_g}\,\frac{C_w}{C_{w,g}} \tag{7}$$

where $P_{cre,ft,nh}$ is the critical elastic flexural-torsional buckling load of the unperforated shape calculated with finite strip analysis and C_w is equal to $C_{w,net}$ when n_t=1 and is equal to $C_{w,avg}$ for all other cases. The parameters J_g and $C_{w,g}$ are the gross section St. Venant and warping torsion constants, and J_{avg} and $C_{w,avg}$ are the weighted average St. Venant and warping torsion constant calculated in the same manner as Eq. (2).

3.4.2.3. Finite element verification for flexural-torsional column buckling considering perforation patterns

Flexural-torsional buckling prediction results using Eq. (3) through Eq. (6) (weighted average classical solution) and Eq. (7) (finite strip approach) are shown in Fig. 13 and Fig. 14 for the 54 rack models and all 1282 models in the elastic buckling database. Both the modified classic cubic buckling equation (Fig. 13) and finite strip approach (Fig. 14) are accurate predictors of global elastic buckling, with finite element-to-predicted ratios near 1.0 and a COV less than 0.03. The classical weighted average solution is more general and applicable even when many large perforations are present, whereas Eq. (7) has only been validated for the cross-sections and perforation patterns ($A_{web,net}/A_{web,g} \geq 0.72$) considered in this study.

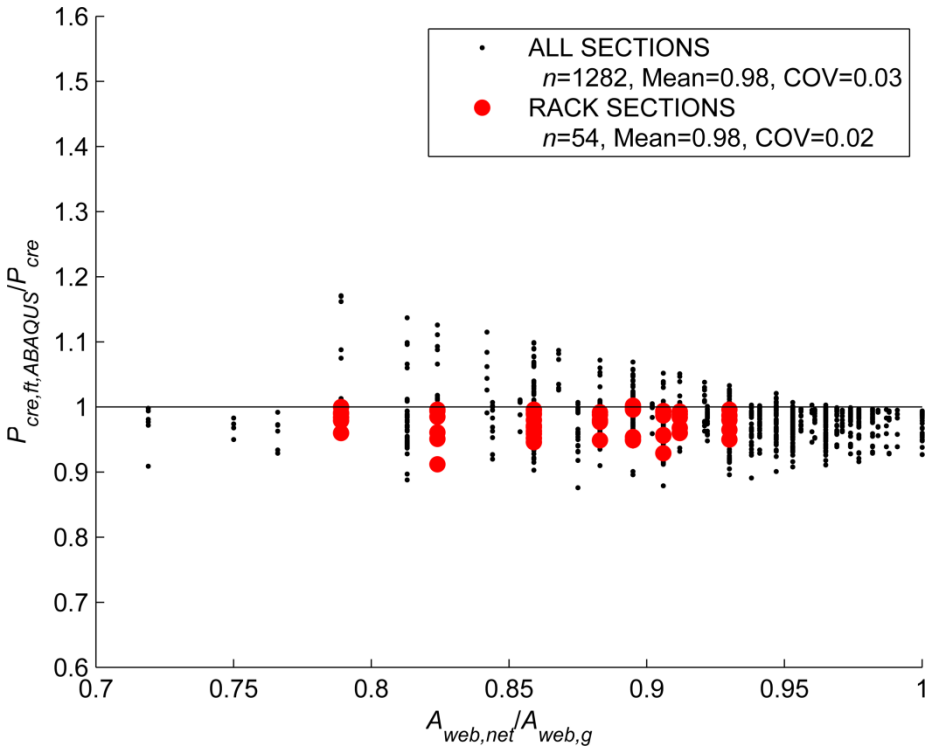

Fig. 13 Flexural-torsional buckling ABAQUS to predicted results of P_{cre} calculated using the weighted average classical equations, Eq. (3) through Eq. (6)

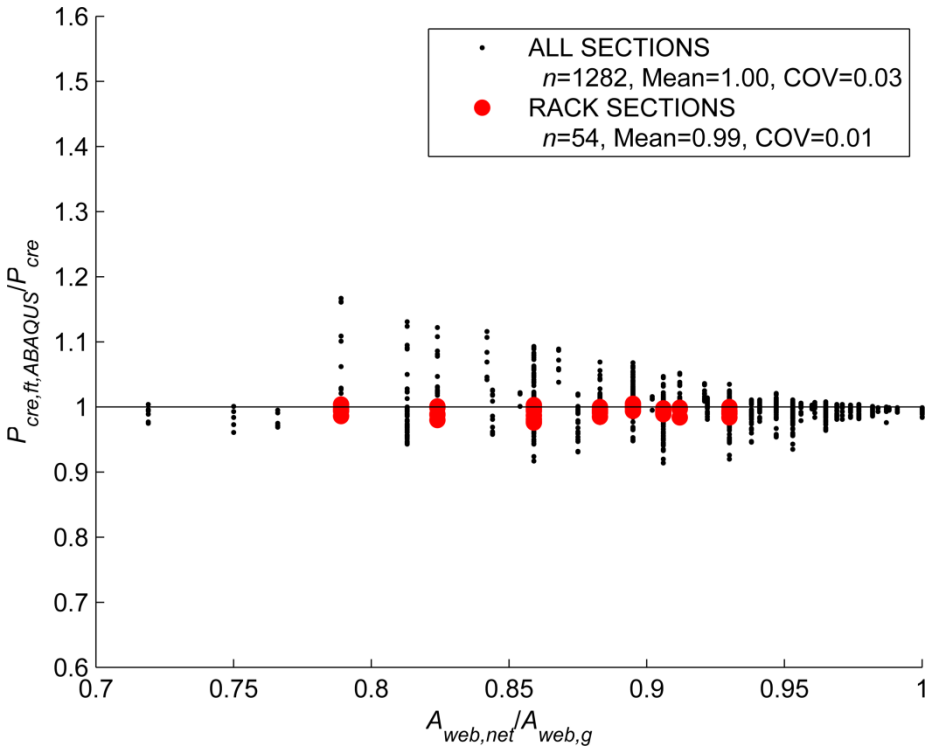

Fig. 14 Flexural-torsional buckling ABAQUS to predicted results of P_{cre} calculated using Eq. (7) and $P_{cre,ft,nh}$ found in CUFSM

3.5. Distortional buckling of thin-walled metal columns with perforation patterns

Elastic distortional buckling is a mode associated with open cross-sections with stiffened flanges in which the flange and stiffener buckle together in restrained flexural-torsional buckling. There are two types of distortional buckling – symmetric and asymmetric. Symmetric distortional buckling occurs when flange and stiffener elements buckle away or towards each other but are restrained by the web, resulting in single curvature of the web and an opening and closing of the cross-section (Fig. 6c). Asymmetric distortional buckling occurs when the flanges buckle in the same direction, resulting in the web bending in double curvature (Fig. 6d). Deformation in these modes is governed by the rotational restraint of the web – the stiffer the web is, the less the flanges will rotate relative to the cross-section. The critical elastic distortional buckling load is taken as the minimum of symmetric and asymmetric distortional buckling modes.

When perforations are present, the transverse web stiffness is degraded, increasing distortional buckling deformation and decreasing the elastic buckling load (Moen et al., 2013, Moen and Schafer, 2009a, Hancock, 1984). Existing methods for predicting this decrease in the distortional buckling load are based on reducing the web thickness to simulate the loss in transverse web stiffness from discrete holes in wall studs (Moen and Schafer, 2009a), thermal slits in wall studs (Kesti, 2000), and perforation patterns in rack sections (Casafont et al., 2012). This web stiffness degradation is quantified for perforation patterns in the following section.

3.5.1. Loss of transverse web bending stiffness due to perforation patterns

A finite element study was conducted to characterize the reduction in transverse web bending stiffness caused by perforation patterns. An imposed rotation varying in

magnitude proportional to a half sine wave was imposed to mimic the web deformation during distortional buckling. Transverse web rotational stiffness is calculated along the plate length using the imposed rotations and the moments caused by these rotations.

The perforations patterns considered in this study are similar to that of Section A-HDR in (Sarawit, 2003). The plate width is h_o=76 mm, L=600 mm (equal to the distortional buckling half-wavelength of the shape without perforations), t=2.16 mm. Perforation dimensions are rectangular and based on the bounds of perforations in (Sarawit, 2003) – L_h/h_o=0.36, d_h/h_o=0.24 (similar to the "*AC*" perforation combination described in Table 2, Table 3, and Table 4). Three perforation arrangements were examined – patterns with one and two transverse perforations spaced longitudinally at h_o/s_l=1.5 and a single row of two transverse perforations. Boundary conditions for this finite element plate model are shown in Fig. 15, E=203.4 GPa, μ=0.30, and the plate is meshed with ABAQUS S9R5 thin shell elements.

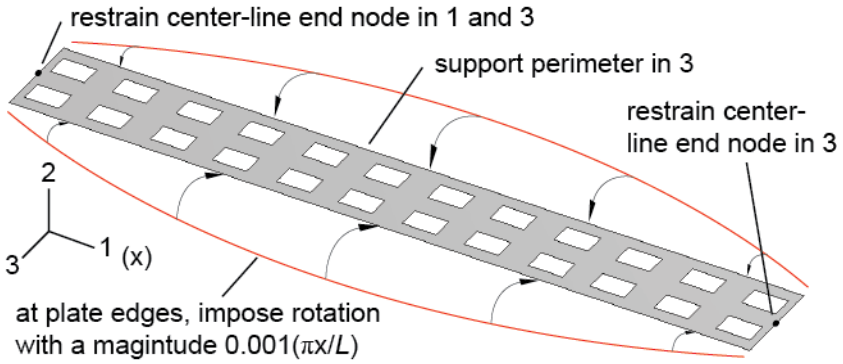

Fig. 15 Web rotational restraint boundary and loading conditions

The study results in Fig. 16 demonstrate that the presence of perforation patterns decreases the plate bending stiffness along the length of a distortional buckling half-wave. The stiffness reduces rapidly and locally for single row of perforations (Plate A in

Fig. 16) which is consistent with (Moen and Schafer, 2009a). For perforation patterns, the web stiffness oscillates about an average value (Plates B and C in Fig. 16) and the web stiffness for Plate C where n_t=2 is reduced about twice as much when compared to Plate B where n_t=1.

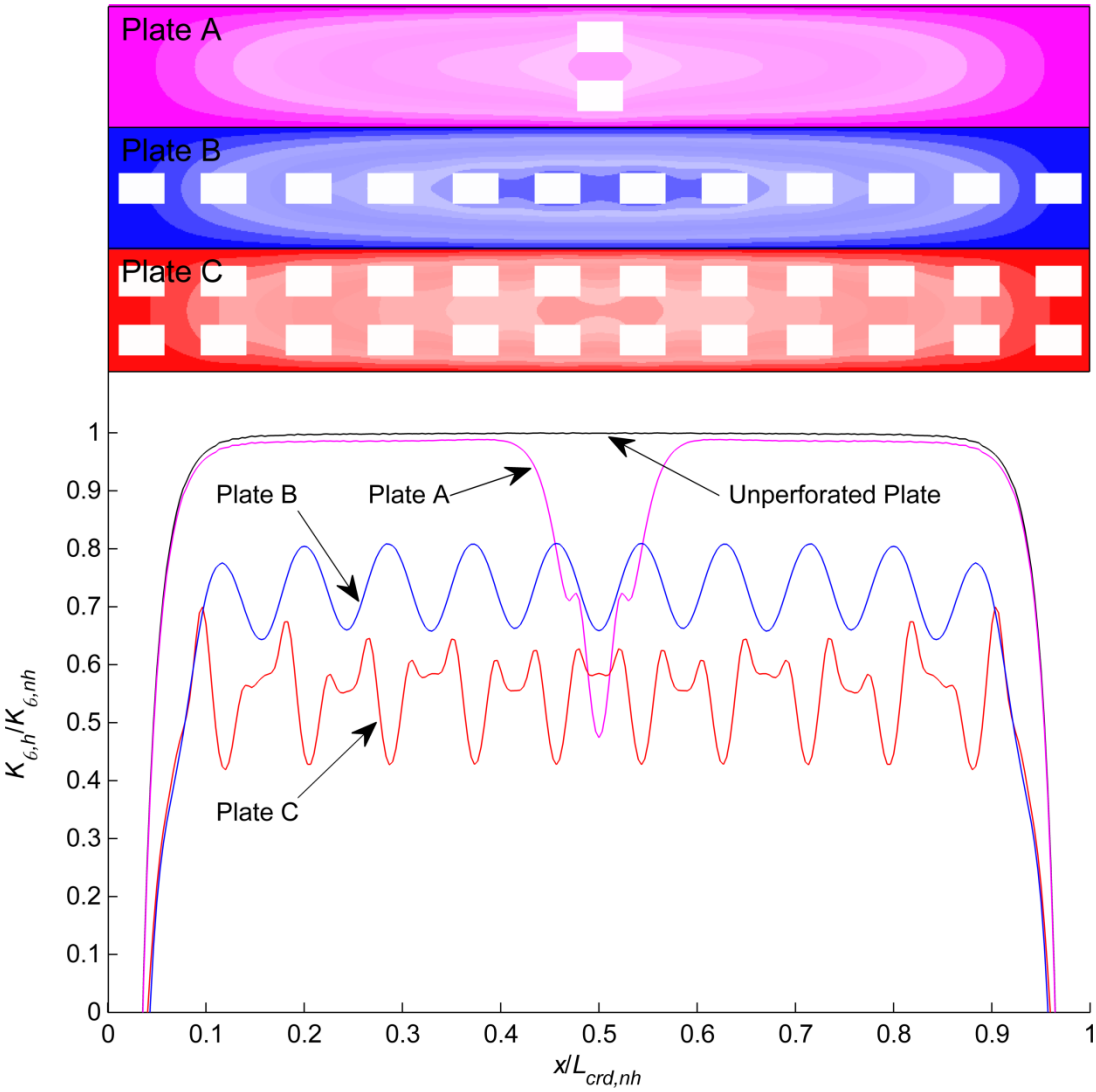

Fig. 16 Transverse rotational stiffness of web plates with periodic perforations

The loss in transverse bending stiffness from perforation patterns can be defined as a ratio of the average transverse rotational stiffness of perforated ($K_{\theta,h}$) to unperforated web plates ($K_{\theta,nh}$)

$$\frac{K_{\theta,h}}{K_{\theta,nh}} \propto \frac{D_h}{D} = \frac{\frac{Et_r^{\,3}}{12\left(1-\mu^2\right)}}{\frac{Et^3}{12\left(1-\mu^2\right)}} = \frac{t_r^{\,3}}{t^3}. \tag{8}$$

A reduced web thickness equation for distortional buckling is derived by rearranging Eq. (8)

$$t_r = t\left(\frac{K_{\theta,h}}{K_{\theta,nh}}\right)^{\frac{1}{3}}. \tag{9}$$

It is hypothesized that the transverse web rotational stiffness due to perforation patterns is proportional to the ratio of the web planar net area, $A_{web,net}=(Lh_o-n_l n_t L_h d_h)$, to the web planar gross area, $A_{web,g}=Lh_o$, i.e.,

$$K_{\theta,h} = \left(\frac{A_{web,net}}{A_{web,g}}\right) K_{\theta,nh}. \tag{10}$$

The reduced web thickness for approximating P_{crd} including perforation patterns is obtained by substituting Eq. (10) into Eq. (9); this method is presented and validated in the following sections.

3.5.2. Critical elastic distortional buckling load prediction

The critical elastic distortional buckling load including the influence of web perforation patterns, P_{crd}, is approximated in a finite strip analysis by reducing the thickness of the cross-section web to

$$t_r = t\left(\frac{A_{web,net}}{A_{web,g}}\right)^{\frac{1}{3}}. \tag{11}$$

A finite strip reference stress is calculated using a unit compressive load applied to the modified cross-sectional geometry. The critical elastic distortional buckling load including the influence of perforations, P_{crd}, is taken as the minimum buckling load on the distortional buckling branch of the elastic buckling curve. The distortional buckling half-wavelength from the reduced thickness analysis, $L_{crd,h}$, will be longer than $L_{crd,nh}$.

3.5.3. Finite element verification for distortional buckling considering perforation patterns

The finite element to predicted ratio statistics and trends for distortional buckling in Fig. 17 confirm the viability of the reduced thickness finite strip approach, with a mean around 1.0 and a COV=0.09 for all sections and 0.08 for rack sections. The scatter in Fig. 17 comes from local-distortional buckling interaction in the finite element eigen-buckling analyses caused by perforation patterns.

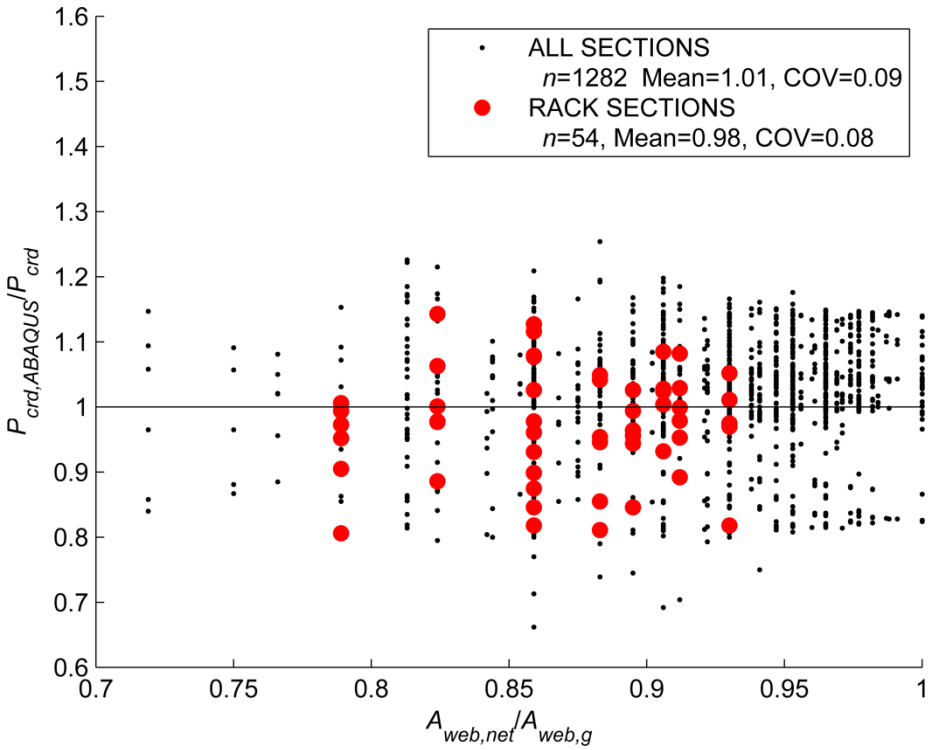

Fig. 17 Distortional buckling ABAQUS to predicted results of P_{crd} calculated using Eq. (11) and CUFSM

3.6. Local buckling of thin-walled steel columns with perforation patterns

Local buckling of thin-walled members with discrete holes typically occurs as unstiffened strip buckling at a perforation or as half-waves forming between perforations (Moen and Schafer, 2009a). However, for thin-walled members with perforation patterns like those present in pallet racks, full local buckling half-waves can also be accommodated by the network of plate material remaining after the perforations are punched (see Fig. 7d). Euler strip buckling between two perforations (Fig. 7c) and unstiffened strip buckling (Fig. 7b) are also possible. The proposed finite strip approximate methods for treating these cases are described in the following sections.

3.6.1. Rayleigh-Ritz energy solution for stiffened element local buckling with perforation patterns

It is hypothesized that a reduced thickness can be derived to represent the decreased critical elastic buckling stress of a stiffened element (i.e., a uniaxially loaded simply-supported plate) caused by perforation patterns, i.e.,

$$\sigma_{cr,h} = \frac{\pi^2 E t^2}{12(1-\mu^2)b^2} k_h = \frac{\pi^2 E t_r^{\,2}}{12(1-\mu^2)b^2} k_{nh} \rightarrow t_r = t\left(\frac{k_h}{k_{nh}}\right)^{\frac{1}{2}} \tag{12}$$

where $\sigma_{cr,h}$ is the buckling stress including perforations and k_{nh} and k_h are the plate buckling coefficients for a plate without and with perforation patterns respectively (note that k_{nh}=4.0 for an infinitely long stiffened element).

An equation for k_h considering perforation patterns is needed to solve for t_r in Eq. (12). To obtain this equation, a Rayleigh-Ritz plate buckling energy solution is employed where the variation in total potential energy of the plate is zero, representing equilibrium in the buckled configuration, i.e.,

$$\delta(U_{nh} - U_h + W) = 0\,. \tag{13}$$

The elastic strain energy of the stiffened element without holes is U_{nh} and W is the external work resulting from a uniform traction load, N_{cr}. To account for the presence of perforation patterns, strain energy at the location of perforations, U_h, is subtracted from the strain energy of the corresponding unperforated plate, U_{nh}. The energy terms are expressed as

$$W = \frac{N_{cr}}{2}\int_0^b\int_0^L \left(\frac{\partial w}{\partial x}\right)^2 dxdy \tag{14}$$

$$U_{nh} = \frac{D}{2}\int_0^b\int_0^L \left[\left(\frac{\partial^2 w}{\partial x^2}\right)^2 + \left(\frac{\partial^2 w}{\partial y^2}\right)^2 + 2\mu\left(\frac{\partial^2 w}{\partial x^2}\right)\left(\frac{\partial^2 w}{\partial y^2}\right) + 2(1-\mu)\left(\frac{\partial^2 w}{\partial x \partial y}\right)^2\right] dxdy \tag{15}$$

$$U_h = \frac{D}{2}\sum_{j=1}^{n_t}\sum_{i=1}^{n_l}\int_{LO_t}^{HI_t}\int_{LO_l}^{HI_l}\left[\left(\frac{\partial^2 w}{\partial x^2}\right)^2 + \left(\frac{\partial^2 w}{\partial y^2}\right)^2 + 2\mu\left(\frac{\partial^2 w}{\partial x^2}\right)\left(\frac{\partial^2 w}{\partial y^2}\right) + 2(1-\mu)\left(\frac{\partial^2 w}{\partial x \partial y}\right)^2\right]dxdy \quad (16)$$

where b is the stiffened element width and the element's flexural rigidity is

$$D = \frac{Et^3}{12(1-\mu^2)}, \quad (17)$$

and integration limits for the strain energy at perforations are

$$LO_l = s_l(i-1) + s_{le} - \frac{L_h}{2} \quad (18)$$

$$HI_l = s_l(i-1) + s_{le} + \frac{L_h}{2} \quad (19)$$

$$LO_t = s_t(j-1) + s_{te} - \frac{d_h}{2} \quad (20)$$

$$HI_t = s_t(j-1) + s_{te} + \frac{d_h}{2} \quad (21)$$

The out-of-plane buckled shape, w, is represented as a double Fourier series where m and n are the number of longitudinal and transverse half-waves in a series term respectively (Chajes, 1974)

$$w = \sum_{m=1}^{\infty}\sum_{n=1}^{\infty} A_{m,n} \sin\frac{m\pi x}{L}\sin\frac{n\pi y}{b}. \quad (22)$$

The critical elastic local buckling solution is obtained by taking the partial derivatives of the total potential energy relative to the constant coefficients of the Fourier series, resulting in

$$N_{cr} = \frac{\pi^2 D}{b^2}k_h, \quad (23)$$

where the plate buckling coefficient including perforations is

$$k_h = \left(\frac{m^2 b^2}{L^2} + \frac{n^4 L^2}{m^2 b^2} \right) \left[1 - \sum_{j=1}^{n_t} \sum_{i=1}^{n_l} \left[\frac{\left(L_h - \alpha X_i \right)\left(d_h - \beta Y_j \right)}{Lb} \right] \right] \cdots$$
$$+ 2n^2 \left[1 - \sum_{j=1}^{n_t} \sum_{i=1}^{n_l} \left[\frac{\left(L_h + \alpha X_i \right)\left(d_h + \beta Y_j \right) - 2\mu \left(L_h \alpha Y_j + d_h \beta X_i \right)}{Lb} \right] \right]. \quad (24)$$

The longitudinal and transverse positions of an individual perforation relative to a buckled half-wave are accounted for by X_i and Y_j respectively. The terms α and β are perforation dimension modification factors that account for the size of the perforation relative to the size of buckled deformations. These factors are written as

$$X_i = \cos\left(\frac{2\pi m}{L} \left[s_l \left(i - 1 \right) + s_{le} \right] \right) \quad (25)$$

$$Y_j = \cos\left(\frac{2\pi m}{b} \left[s_t \left(j - 1 \right) + s_{te} \right] \right) \quad (26)$$

$$\alpha = \frac{L}{\pi m} \sin\left(\frac{\pi L_h m}{L} \right) \quad (27)$$

$$\beta = \frac{b}{\pi n} \sin\left(\frac{\pi d_h n}{b} \right). \quad (28)$$

Solving Eq. (24) is tedious, requiring the numbers of longitudinal and transverse half-waves (m and n) that produce the lowest value of k_h to be found by iteration. Eq. (24) can be simplified with several assumptions and observations.

To minimize k_h, the number of transverse buckled half-waves, n, will always be equal to one. If the longitudinal perforation spacing is assumed constant, then it is equal to length of the plate divided by the number of longitudinal perforations, i.e., $s_l=L/n_l$, and thus the longitudinal perforation centerline-to-edge spacing is equal to half the center-to-center spacing, i.e., $s_{le}=s_l/2$. By assuming a constant transverse perforation spacing ($s_t=b/n_t$ and $s_{te}=s_t/2$), both longitudinal and transverse spacing terms can be expressed

through the single variables n_l and n_t. It is assumed that the classical unperforated plate solution for number of longitudinal half-waves is applicable, i.e., $m=L/b$.

The combination of these assumptions leads to a single solution of k_h, replacing the summation operands with the number of longitudinal and transverse perforations (n_l and n_t)

$$k_h = 4\left[1 - \frac{n_l n_t \left(L_h d_h - \mu d_h \alpha X - \mu L_h \beta Y + \alpha X \beta Y\right)}{Lb}\right] \tag{29}$$

where

$$X = \begin{cases} -1 & if \quad \frac{n_l b}{L} = 1/1, 1/3, 1/5, \ldots \\ 1 & if \quad \frac{n_l b}{L} = 1/2, 1/4, 1/6, \ldots \\ 0 & if \quad \frac{n_l b}{L} \neq 1/1, 1/2, 1/3, \ldots \end{cases} \tag{30}$$

$$Y = \begin{cases} -1 & if \quad n_t = 1 \\ 0 & if \quad n_t \neq 1 \end{cases} \tag{31}$$

and α and β can be simplified by substituting $m=L/b$ and $n=1$ into Eq. (27) and Eq. (28). The average effect of an individual perforation's position on local buckling is represented by X and Y, and the terms $n_l n_t X$ or $n_l n_t Y$ contain the cumulative effect of the perforation pattern's position relative to the plate's buckled configuration. To further simplify the solution, it is recommended that X=-1 and Y=-1 which conservatively assumes that strain energy is always removed from the plate no matter the location within a half-wave.

3.6.2. Finite strip treatment of Euler and unstiffened strip local buckling modes

The proposed net section finite strip method predicts column strip and unstiffened strip buckling for sections with perforation patterns with the same approach validated for discrete perforations in (Moen and Schafer, 2009a). The net cross-section is input into

finite strip software using single zero thickness elements at the locations of perforations (Fig. 18a). A reference stress calculated with a compressive unit load (Fig. 18b) is applied. The critical elastic local buckling load of the net section, $P_{cr\ell h}$, equals the minimum load on the signature curve for $L_{cr\ell,h} \leq L_h$, i.e., $P_{cr\ell h}$ is the lowest load that causes buckling within the length of a single perforation which can be unstiffened strip buckling (Fig. 19a) or Euler buckling of a strip between perforations (Fig. 19b).

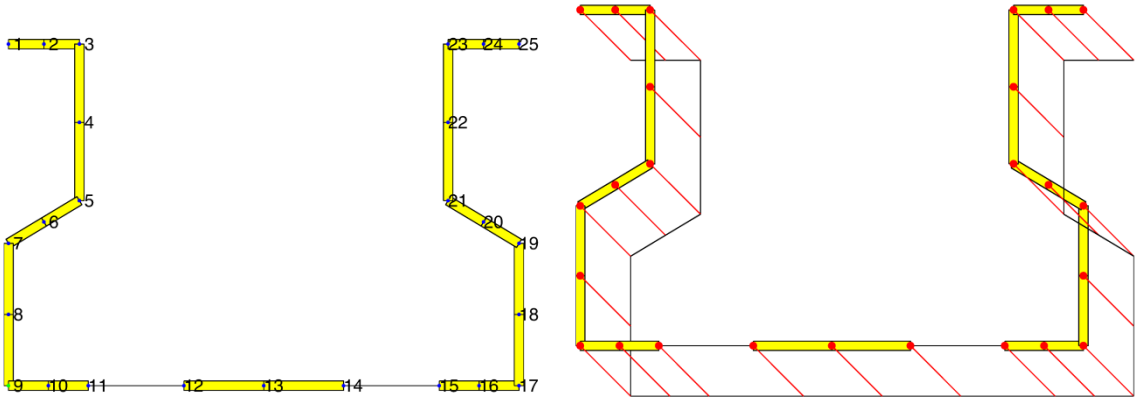

Fig. 18 Section S5_L4_T2_NL_1-5_NT1_AD (a) node and element and (b) stress inputs for sub-elemental local buckling analysis using CUFSM

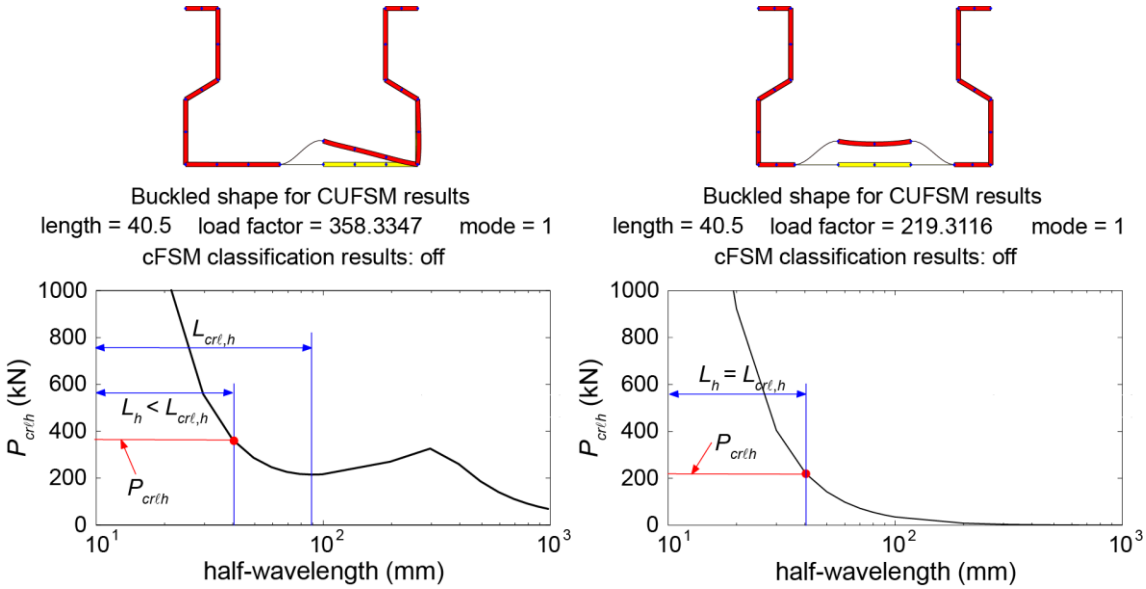

Fig. 19 Net Section finite strip analysis for (a) member S5_L4_T2_NL_1-5_NT1_AD, $P_{cr\ell h}$=358.3 kN at $L_{cr\ell,h}$=L_h=40.5 mm showing unstiffened strip buckling; (b) for member S5_L4_T2_NL_1-5_NT1_AD, $P_{cr\ell h}$=219.3 kN, $L_{cr\ell,h}$=L_h=40.5 mm showing Euler strip buckling

3.6.3. Critical elastic local buckling load prediction

The critical elastic local buckling load including the influence of perforation patterns, $P_{cr\ell}$, is taken as the minimum of

$$P_{cr\ell} = \min(P_{cr\ell tr}, P_{cr\ell h}) \tag{32}$$

where $P_{cr\ell tr}$ is the local buckling load including perforation patterns and $P_{cr\ell h}$ is the local buckling load for modes at or between perforations. The local buckling load $P_{cr\ell tr}$ is approximated in a finite strip analysis by reducing the thickness of each stiffened element in a cross-section containing perforation patterns to

$$t_r = t\left[1 - \frac{n_l n_t \left(L_h d_h + \mu d_h \alpha + \mu L_h \beta + \alpha\beta\right)}{Lb}\right]^{\frac{1}{2}} \tag{33}$$

where μ is Poisson's ratio and the longitudinal and transverse perforation dimension modification factors are α and β and are approximated with Eq. (27) and Eq. (28)

assuming $m=L/b$ and n=1. A finite strip reference stress is calculated using a unit compressive load applied to the modified cross-section and the elemental $P_{cr\ell tr}$ is taken as the minimum buckling load on the local buckling branch of the elastic buckling curve. The buckling load at a perforation, $P_{cr\ell h}$, is calculated with the method described in Section 5.2, i.e., the lowest load on the signature buckling curve for $L_{cr\ell,h} \leq L_h$.

3.6.4. Finite element verification for local buckling considering perforation patterns

The finite element to predicted statistics and trends in Fig. 20 confirm the viability of the local buckling approach for rack sections (mean of 0.98, COV of 0.05, n=54) and for all columns considered in this study (mean of 1.05, COV of 0.11, n=1282). The local buckling load for the net section ($P_{cr\ell h}$) was always higher than $P_{cr\ell tr}$ which is consistent with the local buckling finite element parameter study in Section 2.4.1. The energy solution for $P_{cr\ell tr}$ becomes increasingly conservative as $A_{web,net}/A_{web,g}$ decreases.

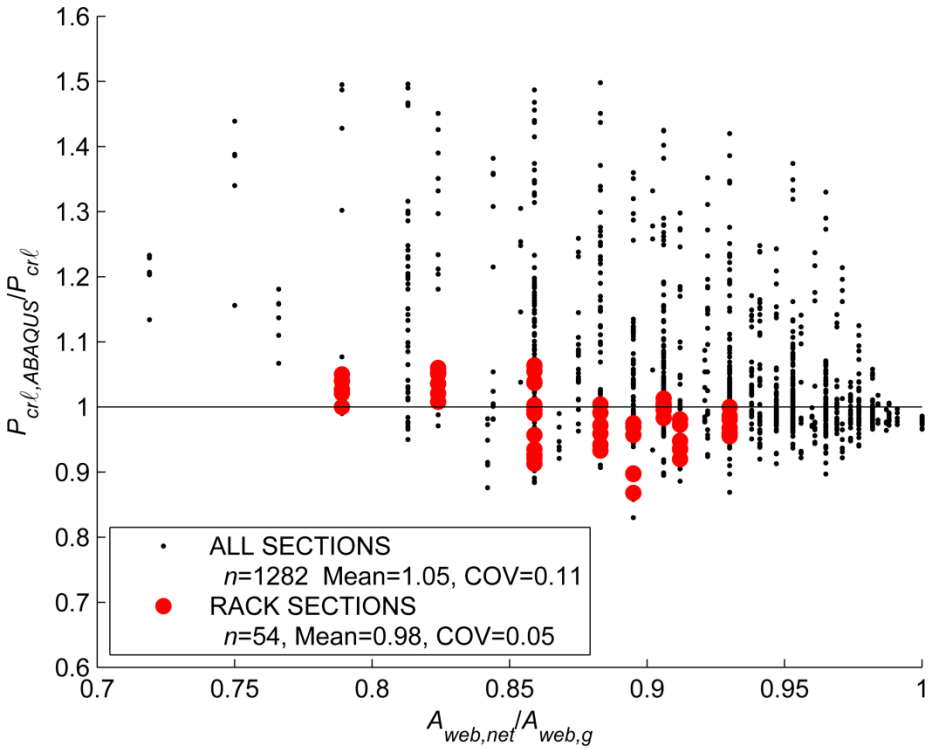

Fig. 20 Local buckling ABAQUS to predicted results of $P_{cr\ell}$ calculated using the minimum of the elemental buckling mode, found using Eq. (33) and CUFSM, and the sub-elemental buckling mode, found using the net section in CUFSM

3.7. Conclusions

Approximate finite strip calculation methods are introduced and validated for critical elastic global, distortional, and local buckling loads of thin-walled metal columns with perforation patterns like those in cold-formed steel pallet racks. For global flexural buckling, the column Euler buckling load without perforations is obtained from finite strip analysis or classical equations and then reduced with the weighted average of the net and gross-cross section moment of inertia. The flexural-torsional buckling load also decreases when perforation patterns are present, and this decrease is predicted with the weighted average of the St. Venant and warping torsion constants because perforation patterns are found to disrupt the warping shear stress distribution at a net section and in a gross section adjacent to a net section.

Perforation patterns reduce the plate bending stiffness of elements in a cross-section, and this reduction is taken into account for both local and distortional buckling with a reduced thickness in the finite strip analysis. Engineering expressions are derived for calculating the reduced thickness considering perforation dimensions and transverse and longitudinal spacing in a cross-sectional element. For local buckling, the reduced thickness is calculated with a plate buckling coefficient derived with a Rayleigh-Ritz energy solution that considers the influence of perforations. Local buckling within a single perforation is also evaluated with a net section finite strip analysis. For distortional buckling of a thin-walled open cross-section, decreased transverse web bending stiffness from perforations is simulated in a finite strip analysis with a reduced thickness calculated using the ratio of web planar net and gross areas. Viability of the finite strip methods is confirmed with a database of over 1200 thin shell finite element eigen-buckling analyses. This research will support an upcoming specification ballot to extend the American Iron and Steel Institute's Direct Strength Method for cold-formed steel member design to pallet rack columns with perforation patterns.

CHAPTER 4. CONCLUSIONS

4.1. Summary

The research presented in this document describes approximate methods to predict elastic buckling of pallet rack sections including the influence of perforation patterns using finite strip software. These methods are validated with a database of 1282 finite element models featuring shapes typical of pallet rack columns with a wide array of perforation patterns.

Global flexural buckling uses an approach that relates reduction in buckling capacity to a ratio of the weighted average to gross moment of inertia. It is noted that rack sections with this buckling mode may be subject to long wave distortional-global interaction which is not accounted for by the flexural buckling prediction method. Two approximate methods are presented for global flexural-torsional buckling. The first is a modified classical buckling equation method that uses weighted average cross-sectional properties to approximate the influence of perforation patterns. The second is a simplified method that relates reduction in flexural-torsional buckling to the ratios of weighted average to gross St. Venant torsional and warping torsional constants. Distortional buckling prediction uses a reduced web thickness that relates the reduction in web rotational stiffness due to perforations to the ratio of web planar net to gross areas. Contrary to previous research on discrete holes (Moen and Schafer, 2009a), perforation patterns are observed to increase the distortional buckling half-wavelength which is taken into account in the prediction method. Prediction of local buckling only validates a method in which holes are located within elemental buckled half-waves; cross-sectional elements with perforation sizes or spacings outside of the scope of this research may

experience other types of local buckling modes. The local buckling prediction method relates a reduction in elemental thickness to the reduction in the plate buckling coefficient due to perforations. While observed in models, this method cannot account for plate stiffening due to perforations as the plate buckling coefficient can only be reduced when perforations are present.

4.2. Future Research

The next step to be taken is to examine pallet rack column strength prediction accuracy of the Direct Strength Method when used in conjunction with the elastic buckling prediction methods of this research. Presented in Appendix A is modifications to current language of the American Iron and Steel Institute's North American Specification for the Design of Cold-Formed Steel Structural Members and commentary for the specification is presented in Appendix B. Appendix C outlines a design example that showcasing how modifications to the code language might be implemented by comparing strengths predicted with the Direct Strength Method to axial capacity of a rack cross-section tested by Koen at the University of Sydney (Koen, 2008). This example brings to light several topics that future research should address:

- At what perforation sizes and spacings should unstiffened strip and column strip buckling modes be considered and how prediction methods should address these modes
- How web stiffeners affect the implementation of local and distortional prediction methods

- If the lower bound on distortional buckling half-wavelength of three times the greatest outside dimension should be modified due to an observed short wave distortional buckling mode
- How rack bracing affects effective lengths in the *x*, *z*, and torsional axes

Additionally, this manuscript raises other points that should be examined in future research:

- How observed long wave distortional-global buckling interaction should be treated
- How stiffening of elements subject to local buckling due to perforation patterns should be addressed
- If the simplified flexural-torsional buckling prediction method is applicable to other cross-sections besides those typical of pallet racks.
- If the distortional buckling prediction method is applicable for cross-sections with flange perforations
- At what point does sub-elemental local buckling (unstiffened strip and column strip modes) control over local buckling modes captured through a reduced thickness approach

Buckling of members with perforation patterns is a complex phenomenon and further research into the topic can further enhance the collective understanding of its behavior and the prediction of its strength.

REFERENCES

Ádány, S. and Schafer, B.W. (2006) 'Buckling mode decomposition of single-branched open cross-section members via finite strip method: Application and examples', *Thin-Walled Structures*, vol. 44, no. 5, May, pp. 585-600.

AISI (2007) *North-American Specification for the Design of Cold-Formed Steel Structural Members. S100-2007*, American Iron and Steel Institute and Canadian Standards Association.

AISI (2012) *North-American Specification for the Design of Cold-Formed Steel Structural Members. S100-2012*, American Iron and Steel Institute and Canadian Standards Association.

Casafont, M., Pastor, M., Bonada, J., Roure, F. and Pekoz, T. (2012) 'Linear buckling analysis of perforated steel storage rack columns with the Finite Strip Method', *Thin-Walled Structures*, vol. 61, pp. 71-85.

CEN (2009) *Steel static storage systems - Ajustable pallet racking systems - Prinicples for structural design. EN15512:2009*, European Committee for Standardization.

Chajes, A. (1974) 'Chapter 6 - Buckling of Plates', in *Principles of Structural Stability Theory*, Englewood Cliffs, NJ: Prentice Hall.

Chow, F.Y. and Narayanan, R. (1984) 'Buckling of plates containing openings', Seventh International Specialty Conference on Cold-Formed Steel Structures, St. Louis, MO, 39-53.

Dassault Systèmes (2011) *Abaqus/CAE 6.11-2*, Providence, RI.

Degtyarev, V.V. and Degtyareva, N.V. (2012) 'Elastic stability of univormly compressed plates perforated in triangular patterns', *Thin-Walled Structures*, vol. 52, pp. 165-173.

Hancock, G.J. (1984) 'Distortional buckling of steel storage rack columns', Proceedings of the Seventh International Specialty Conference on Cold-Formed Steel Structures, St. Louis, MO, 345-373.

Kawai, T. and Ohtsubo, H. (1968) 'A Method of Solution for the Complicated Buckling Problems of Elastic Plates with Combined Use of Rayleigh-Ritz's Procedure in the Finite Element Method', Proceedings of the Second Conference on Matrix Methods in Structural Mechanics, Wright-Patterson Air Force Base, OH, 967-994.

Kesti, J. (2000) *Local and distortional buckling of perforated steel wall studs*, Report TKK-TER-19: Laboratory of Steel Structures, Helsinki University of Technology.

Koen, D.J. (2008) *Structural Capacity of Light Gauge Steel Storage Rack Uprights*, Sydney, Austrailia: Masters Thesis, University of Sydney.

Levy, S., Woolley, R.M. and Kroll, W.D. (1947) 'Instability of Simply Supported Square Plate With Reinforced Circular Hole in Edge Compression', *Journal of Research of the National Bureau of Standards*, vol. 39, pp. 571-577.

Li, Z. and Schafer, B.W. (2010) 'Buckling analysis of cold-formed steel members with general boundary conditionas using CUFSM: conventional and constrained finite strip methods', Proceedings of the 20th International Specialty Conference on Cold-Formed Steel Structures, St. Louis, MO.

Loov, R. (1983) 'Local buckling capacity of C-shaped cold-formed steel sections with punched webs', *Canadian Journal of Civil Engineering*, vol. 11, no. 1, pp. 1-7.

Lue, D.M., Liu, J.-L. and C-H, L. (2007) 'Numerical Evaluation on Warping Constants of General Cold-Formed Steel Open Sections', *International Journal of Steel Structures*, vol. 07, no. 04, pp. 297-309.

Mahendran, M., Shanmugam, N.E. and Richard Liew, J.Y. (1994) 'Strength of stiffened plates with openings', Twelfth International Specialty Conference on Cold-Formed Steel Structures, St. Louis, MO.

Mathworks (2012) *Matlab 7.14.0.739 (R2012a)*, MathWorks, Inc.

Miller, T.H. and Pekoz, T. (1994) 'Unstiffened Strip Approach for Perforated Wall Studs', *Journal of Structrual Engineering*, vol. 120, no. 1, pp. 410-421.

Moen, C.D. (2008) *Direct Strength Design of Cold-Formed Steel Members with Perforations*, Baltimore, MD: Ph.D. Thesis, Johns Hopikins University.

Moen, C.D. and Schafer, B.W. (2008) 'Experiments on cold-formed steel columns with holes', *Thin-Walled Structures*, vol. 46, pp. 1164-1182.

Moen, C.D. and Schafer, B.W. (2009a) 'Elastic buckling of cold-formed steel columns and beams with holes', *Engineering Structures*, vol. 31, no. 12, pp. 2812-2824.

Moen, C.D. and Schafer, B.W. (2009b) 'Elastic buckling of thin plates with holes in compression or bending', *Thin-Walled Structures*, vol. 47, no. 12, pp. 1597-1607.

Moen, C.D. and Schafer, B.W. (2009c) *Direct Strength design of cold-formed steel members with perforations*, Washington, DC 20036: American Iron and Steel Institute, Committee on Specifications for the Design of Cold-Formed Steel Structural Members.

Moen, C.D. and Schafer, B.W. (2011) 'Direct Strength Method for Design of Cold-Formed Steel Columns with Holes', *Journal of Structural Engineering*, vol. 137, no. 5, pp. 559-570.

Moen, C.D., Schudlich, A. and von der Heyden, A. (2013) 'Experiments on cold-formed steel joists with unstiffened web holes', *Journal of Structural Engineering*, vol. 139, no. SPECIAL ISSUE: Cold-Formed Steel Structures, pp. 695-704.

Ortiz-Colberg, R.A. (1981) *The Load Carrying Capacity of Perforated Cold-Formed Steel Columns*, Ithaca, NY: Masters Thesis, Cornell University.

Papangelis, J.P. and Hancock, G.J. (1995) 'Computer Analysis of Thin-walled Structural Members', *Computers & Structures*, vol. 56, no. 1, pp. 157-176.

Pennington Vann, W. (1971) 'Compressive buckling of perforated plate elements', First Specialty Conference on Cold-Formed Steel Structures, Rolla, MO, 52-57.

Pu, Y., Godley, M.H.R., Beale, R.G. and Lau, H.H. (1999) 'Prediction of Ultimate Capacity of Perforated Lipped Channels', *Journal of Structural Engineering*, vol. 125, no. 5, pp. 510-514.

Rhodes, J. and Macdonald, M. (1996) 'The Effects of Perforation Length on the Behaviour of Perforated Elements in Compression', Proceedings of the Thirteenth International Specialty Conference on Cold-Formed Steel Structures, St. Louis, MO.

Rhodes, J. and Schneider, F.D. (1994) 'The Compressional Behaviour of Perforated Elements', Proceedings of the Twelfth International Specialty Conference on Cold-Formed Steel Structures, St. Louis, MO.

RMI (2012) *Specification for the Design, Testing and Utilization of Industrial Steel Storage Racks, MH16.1-2012*, Charlotte, NC, USA: Rack Manufacturers Institute.

RSG Software, Inc. (2013) *CFS Version 7.0*, [Online], Available: http://www.rsgsoftware.com/ [28 May 2013].

Sarawit, A.T. (2003) *Cold-formed steel frame and beam-column design*, Ithaca, NY: Ph. D. thesis, Cornell University.

Schafer, B.W. (1997) *Cold-formed steel behavior and design: analytical and numerical modeling of elements and members with longitudinal stiffeners*, Ithaca, NY: Ph.D. Thesis, Cornell University.

Schafer, B.W. (2008) 'Review: the Direct Strength Method of cold-formed steel member design', *Journal of Constructional Steel Research*, vol. 64, no. 7-8, pp. 776-778.

Schlack Jr., A.L. (1964) 'Elastic Stability of Pierced Square Plates', *Experimental Mechanics*, pp. 167-172.

Smith, F.H. (2013) *Elastic Buckling Database for Thin-Walled Metal Columns with Perforation Patterns*, June, [Online], Available: http://vtechworks.lib.vt.edu/.

Smith, F.H. and Moen, C.D. (2013) 'Elastic buckling prediction of cold-formed steel columns with periodic perforations', Proceedings of the Annual Stability Conference, Structural Stability Research Council, St. Louis, MO.

Suneel Kumar, M., Alagusundaramoorthy, P. and Sundaravadivelu, R. (2009) 'Ultimate strength of stiffened plates with a square opening under axial and out-of-plane loads', *Engineering Structures*, vol. 31, no. 11, Nov, pp. pp. 2568-2579.

Timoshenko, S.P. and Gere, J.M. (1961) *Theory of elastic stability*, 2nd edition, New York: McGraw-Hill.

UNARCO (2012) *Pallet Rack Photo Gallery*, [Online], Available: www.unarcorack.com [15 Jan. 2013].

Winter, G. (1947) 'Strength of Thin Steel Cmopression Flanges', *Transactions, American Society of Civil Engineers*, vol. 112, pp. pp. 527-554.

Yu, W.W. and Davis, C.S. (1971) 'Buckling behavior and post-buckling strength of perforated stiffened compression elements', Proceedings of the First Specialty Conference on Cold-Formed Steel Structures, Rolla, MO, 58-64.

APPENDIX A. MODIFICATIONS TO AISI S100 SPECIFICATION

APPENDIX 1: Design of Cold-Formed Steel Structural Members Using the Direct Strength Method

1.1 General Provisions

1.1.1 Applicability

The provisions of this Appendix shall be permitted to be used to determine the nominal axial (P_n) and flexural (M_n) strengths [resistances] of *cold-formed steel members*. Sections 1.2.1 and 1.2.2 present a method applicable to all cold-formed steel columns and beams. Those members meeting the criteria of Section 1.1.1.1 for columns and Section 1.1.1.2 for beams have been pre-qualified for use, and the calibrated *safety factor*, Ω, and *resistance factor*, ϕ, given in 1.2.1 and 1.2.2 shall be permitted to apply. The use of the provisions of Sections 1.2.1 and 1.2.2 for other columns and beams shall be permitted, but the standard Ω and ϕ factors for *rational engineering analysis* (Section A1.2(b) of the main *Specification*) shall apply. The main *Specification* refers to Chapters A through G, Appendices A and B, and Appendix 2 of the *North American Specification for the Design of Cold-Formed Steel Structural Members*.

Currently, the Direct Strength Method provides no explicit provisions for members in tension, shear, combined bending and shear, *web crippling*, combined bending and web crippling, or combined axial load and bending (beam-columns). Further, no provisions are given for structural assemblies or *connections* and *joints*. As detailed in main *Specification*, Section A1.2, the provisions of the main *Specification*, when applicable, shall be used for all cases listed above.

It shall be permitted to substitute the *nominal strengths* [*resistances*], resistance factors, and safety factors from this Appendix for the corresponding values in Sections C3.1, C4.1.1, C4.1.2, C4.1.3, C4.1.4, D6.1.1, and D6.1.2 of the main *Specification*.

For members or situations to which the main *Specification* is not applicable, the Direct Strength Method of this Appendix shall be permitted to be used, as applicable. The usage of the Direct Strength Method shall be subjected to the same provisions as any other rational engineering analysis procedure, as detailed in Section A1.2(b) of the main *Specification*:

(1) applicable provisions of the main *Specification* shall be followed when they exist, and

(2) increased safety factors, Ω, and reduced resistance factors, ϕ, shall be employed for strength when rational engineering analysis is conducted.

1.1.1.1 Pre-qualified Columns

~~Unperforated c~~Columns that fall within the geometric and material limitations given in Table 1.1.1-1 shall be permitted to be designed using the *safety factor*, Ω, and *resistance factor*, ϕ, defined in Section 1.2.1~~.~~ and shall be permitted to be either with or without holes or perforation patterns. There shall be no limitations on the size, shape and spacing of ~~the~~ holes or patterns.

Columns which fall outside the geometric and material limitations of Table 1.1.1-1 shall be permitted to still use the Ω or ϕ of Section 1.2.1 if through the use of Chapter F of the main *Specification*, the predicted ϕ from Chapter F provides an equal or higher ϕ (equal or higher level of reliability) to that of Section 1.2.1. In the use of Chapter F, the professional factor, P, shall be the test-to-predicted ratio where the prediction is that of the Direct Strength Method

expressions of Section 1.2.1, P_m is the mean of P_t and V_p the coefficient of variation of P. At least three tests shall be conducted. If V_p is less than or equal to 15%, C_p shall be permitted to be set to 1.0.

Table 1.1.1-1
Limits for Pre-qualified Columns*

Lipped C-Sections Simple Lips: Title: 1112_a.FH5 Creator: FreeHand 5.0 Preview: This EPS picture with a preview inc Comment: Complex Lips: 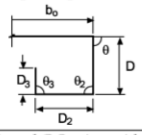	For all C-sections: $h_o/t < 472$ $b_o/t < 159$ $4 < D/t < 33$ $0.7 < h_o/b_o < 5.0$ $0.05 < D/b_o < 0.41$ $\theta = 90°$ $E/F_y > 340$ [$F_y < 86$ ksi (593 MPa or 6050 kg/cm²)] For C-sections with complex lips: $D_2/t < 34$ $D_2/D < 2$ $D_3/t < 34$ $D_3/D_2 < 1$ Note: a) θ_2 is permitted to vary (D_2 lip is permitted to angle inward, outward, etc.) b) θ_3 is permitted to vary (D_3 lip is permitted to angle up, down, etc.)
Lipped C-Section with Web Stiffener(s) Title: 1112_b.FH5 Creator: FreeHand 5.0 Preview: This EPS pictu with a preview i Comment:	For one or two intermediate stiffeners: $h_o/t < 489$ $b_o/t < 160$ $6 < D/t < 33$ $1.3 < h_o/b_o < 2.7$ $0.05 < D/b_o < 0.41$ $E/F_y > 340$ [$F_y < 86$ ksi (593 MPa or 6050 kg/cm²)]
Z-Section Title: 1112_c.FH5 Creator: FreeHand 5.0 Preview: This EPS picture wa with a preview includ Comment:	$h_o/t < 137$ $b_o/t < 56$ $0 < D/t < 36$ $1.5 < h_o/b_o < 2.7$ $0.00 < D/b_o < 0.73$ $\theta = 50°$ $E/F_y > 590$ [$F_y < 50$ ksi (345 MPa or 3520 kg/cm²)]
Rack Upright Title: 1112_d.FH5 Creator: FreeHand 5.0 Preview: This EPS picture was not saved	See C-Section with Complex Lips
Hat Title: 1112_e.FH5 Creator: FreeHand 5.0 Preview: This EPS picture	$h_o/t < 50$ $b_o/t < 43$ $4 < D/t < 6$ $1.0 < h_o/b_o < 1.2$ $D/b_o = 0.13$ $E/F_y > 428$ [$F_y < 69$ ksi (476 MPa or 4850 kg/cm²)]

Note: * $r/t < 10$, where r is the centerline bend radius
b_o = overall width; D =overall lip depth; t = base metal *thickness*; h_o = overall depth

1.1.1.2 Pre-qualified Beams

~~Unperforated b~~Beams without hole(s) that fall within the geometric and material limitations given in Table 1.1.1-2 shall be permitted to be designed using the *safety factor*, Ω, and *resistance factor*, ϕ, defined in Section 1.2.2.

Beams which fall outside the geometric and material limitations of Table 1.1.1-2 shall be permitted to still use the Ω or ϕ of Section 1.2.1 if through the use of Chapter F of the main *Specification* the predicted ϕ from Chapter F provides an equal or higher ϕ (equal or higher level of reliability) to that of Section 1.2.1. In the use of Chapter F, the professional factor, P, shall be the test-to-predicted ratio where the prediction is that of the Direct Strength Method expressions of Section 1.2.2, P_m is the mean of P and V_P the coefficient of variation of P. At least three tests shall be conducted. If V_P is less than or equal to 15% then C_P is permitted to be set to 1.0.

Table 1.1.1-2
Limitations for Pre-qualified Beams*

C-Sections Simple Lips: Title: 1112_a.FH5 Creator: FreeHand 5.0 Preview: This EPS picture with a preview inc Comment: Complex Lips: 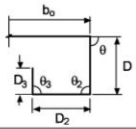	For all C-sections $h_o/t < 321$ $b_o/t < 75$ $0 < D/t < 34$ $1.5 < h_o/b_o < 17.0$ $0 < D/b_o < 0.70$ $44° < \theta < 90°$ $E/F_y > 421$ [$F_y < 70$ ksi (483 MPa or 4920 kg/cm²)] For C-sections with complex lips: $D_2/t < 34$ $D_2/D < 2$ $D_3/t < 34$ $D_3/D_2 < 1$ Note: a) θ_2 is permitted to vary (D_2 lip is permitted to angle inward or outward) b) θ_3 is permitted to vary (D_3 lip is permitted to angle up or down).
Lipped C-Sections with Web Stiffener Title: 1112_b.FH5 Creator: FreeHand 5.0 Preview: This EPS pictu with a preview i Comment:	$h_o/t < 358$ $b_o/t < 58$ $14 < D/t < 17$ $5.5 < h_o/b_o < 11.7$ $0.27 < D/b_o < 0.56$ $\theta = 90°$ $E/F_y > 578$ [$F_y < 51$ ksi (352 MPa or 3590 kg/cm²)]

(Continued)

Table 1.1.1-2
Limitations for Pre-qualified Beams (Continued)

Z-Sections Simple Lips: Title: 1112_c.FH5 Creator: FreeHand 5.0 Preview: This EPS picture wa with a preview includ Comment: Complex Lips: 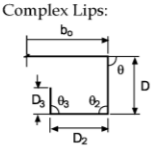	For all Z-sections: $h_o/t < 183$ $b_o/t < 71$ $10 < D/t < 16$ $2.5 < h_o/b_o < 4.1$ $0.15 < D/b_o < 0.34$ $36° < \theta < 90°$ $E/F_y > 440$ [$F_y < 67$ ksi (462 MPa or 4710 kg/cm²)] For Z-sections with complex lips: $D_2/t < 34$ $D_2/D < 2$ $D_3/t < 34$ $D_3/D_2 < 1$ Note: a) θ_2 is permitted to vary (D_2 lip is permitted to is permitted to angle inward, outward, etc.) b) θ_3 is permitted to vary (D_3 lip is permitted to angle up, down, etc.)
Hats (Decks) with Stiffened Flange in Compression Title: 1112_f.FH5 Creator: FreeHand 5.0 Preview: This EPS picture was not	$h_o/t < 97$ $b_o/t < 467$ $0 < d_s/t < 26$ (d_s =Depth of stiffener) $0.14 < h_o/b_o < 0.87$ $0.88 < b_o/b_t < 5.4$ $0 < n \le 4$ (n = Number of compression flange stiffeners) $E/F_y > 492$ [$F_y < 60$ ksi (414 MPa or 4220 kg/cm²)]
Trapezoids (Decks) with Stiffened Flange in Compression Title: 1112_g.FH5 Creator: FreeHand 5.0 Preview: This EPS picture was not saved with a preview included in it.	$h_o/t < 203$ $b_o/t < 231$ $0.42 < (h_o/\sin\theta)/b_o < 1.91$ $1.10 < b_o/b_t < 3.38$ $0 < n_c \le 2$ (n_c = Number of compression flange stiffeners) $0 < n_w \le 2$ (n_w = Number of web stiffeners and/or folds) $0 < n_t \le 2$ (n_t = Number of tension flange stiffeners) $52° < \theta < 84°$ (θ = Angle between web and horizontal plane) $E/F_y > 310$ [$F_y < 95$ ksi (655 MPa or 6680 kg/cm²)]

Note:
* $r/t < 10$, where r is the centerline bend radius.
See Section 1.1.1.1 for definitions of other variables given in Table 1.1.1-2.

1.1.2 Elastic Buckling

Analysis shall be used for the determination of the elastic *buckling loads* and/or moments used in this Appendix. For columns, this includes the *local*, *distortional*, and overall *buckling* loads ($P_{cr\ell}$, P_{crd}, and P_{cre} of Section 1.2.1). For beams, this includes the local, distortional, and overall buckling moments ($M_{cr\ell}$, M_{crd}, and M_{cre} of Section 1.2.2). In some cases, for a given column or beam, all three modes do not exist. In such cases, the non-existent mode shall be

ignored in the calculations of Sections 1.2.1 and 1.2.2. The commentary to this Appendix provides guidance on appropriate analysis procedures for elastic buckling determination, including the calculation of elastic buckling properties for columns and beams with hole(s) and columns with perforation patterns.

1.1.3 Serviceability Determination

The bending deflection at any moment, M, due to *nominal loads* shall be permitted to be determined by reducing the gross moment of inertia, I_g, to an effective moment of inertia for deflection, as given in Eq. 1.1.3-1:

$$I_{eff} = I_g(M_d/M) \le I_g \qquad (Eq.\ 1.1.3\text{-}1)$$

where

M_d = Nominal flexural strength [resistance], M_n, defined in Section 1.2.2, but with M_y replaced by M in all equations of Section 1.2.2

M = Moment due to nominal loads [specified loads] on member to be considered ($M \le M_y$)

1.2 Members

1.2.1 Column Design

The *nominal axial strength* [*resistance*], P_n, shall be the minimum of P_{ne}, $P_{n\ell}$, and P_{nd} as given in Sections 1.2.1.1 to 1.2.1.3. For columns meeting the geometric and material criteria of Section 1.1.1.1, Ω_c and ϕ_c shall be as follows:

Ω_c = 1.80 (*ASD*)

ϕ_c = 0.85 (*LRFD*)

= 0.80 (*LSD*)

For all other columns, Ω and ϕ of the main *Specification*, Section A1.2(b), shall apply. The *available strength* [*factored resistance*] shall be determined in accordance with applicable method in Section A4, A5, or A6 of the main *Specification*.

1.2.1.1 Flexural, Torsional, or Flexural-Torsional Buckling

1.2.1.1.1 Columns without Holes

The *nominal axial strength* [*resistance*], P_{ne}, for *flexural*, *torsional*, or *flexural-torsional buckling* shall be calculated in accordance with the following:

(a) For $\lambda_c \le 1.5$

$$P_{ne} = \left(0.658^{\lambda_c^2}\right)P_y \qquad (Eq.\ 1.2.1\text{-}1)$$

(b) For $\lambda_c > 1.5$

$$P_{ne} = \left(\frac{0.877}{\lambda_c^2}\right)P_y \qquad (Eq.\ 1.2.1\text{-}2)$$

where

$$\lambda_c = \sqrt{P_y/P_{cre}} \qquad (Eq.\ 1.2.1\text{-}3)$$

Formatted: Font: Italic
Formatted: Font: Italic
Formatted: Normal
Formatted: Right: 0"
Formatted: head3
Formatted: Font: Italic
Formatted: Font: Italic
Formatted: Font: Italic
Formatted: Font: Italic
Formatted: Font: Italic
Formatted: eq 3 text, Tab stops: Not at 1.5" + 1.58" + 1.67"

where

$P_y = A_g F_y$ (*Eq.* 1.2.1-4)

P_{cre} = Minimum of the critical elastic column buckling load in *flexural*, *torsional*, or *flexural-torsional buckling* determined by analysis in accordance with Section 1.1.2

1.2.1.1.2 Columns with Hole(s) or Perforation Patterns

The *nominal axial strength* [*resistance*], P_{ne}, for *flexural*, *torsional*, or *flexural-torsional buckling* of columns with hole(s) shall be calculated in accordance with Section 1.2.1.1.1, except P_{cre} shall be determined including the influence of hole(s) or perforation patterns.

1.2.1.2 Local Buckling

1.2.1.2.1 Columns without Holes

The *nominal axial strength* [*resistance*], $P_{n\ell}$, for *local buckling* shall be calculated in accordance with the following:

(a) For $\lambda_\ell \le 0.776$

$P_{n\ell} = P_{ne}$ (*Eq.* 1.2.1-5)

(b) For $\lambda_\ell > 0.776$

$$P_{n\ell} = \left[1 - 0.15\left(\frac{P_{cr\ell}}{P_{ne}}\right)^{0.4}\right]\left(\frac{P_{cr\ell}}{P_{ne}}\right)^{0.4} P_{ne} \quad \text{(Eq. 1.2.1-6)}$$

where

$\lambda_\ell = \sqrt{P_{ne}/P_{cr\ell}}$ (*Eq.* 1.2.1-7)

P_{ne} = A value as defined in Section 1.2.1.1.1

$P_{cr\ell}$ = Critical elastic local column buckling *load* determined by analysis in accordance with Section 1.1.2

1.2.1.2.2 Columns with Hole(s) or Perforation Patterns

The *nominal axial strength* [*resistance*], $P_{n\ell}$, for *local buckling* of columns with hole(s) shall be calculated in accordance with Section 1.2.1.2.1, except $P_{cr\ell}$ shall be determined including the influence of hole(s) or perforation patterns and:

$P_{n\ell} \le P_{ynet}$ (*Eq.* 1.2.1-8)

where

$P_{ynet} = A_{net} F_y$ (*Eq.* 1.2.1-9)

A_{net} = Net area of section at the location of a hole or least net area at a line of perforations

1.2.1.3 Distortional Buckling

1.2.1.3.1 Columns without Holes

The *nominal axial strength* [resistance], P_{nd}, for *distortional buckling* shall be calculated in

Formatted: Normal, Indent: Left: 0", First line: 0"
Formatted: Font: Italic
Formatted: Font: Italic
Formatted: Font: Italic
Formatted: Font: Italic
Formatted: Font: Italic
Formatted: head3
Formatted: Font: Italic
Formatted: Font: Italic
Formatted: Font: Symbol
Formatted: Normal, Tab stops: Not at 1.08"
Formatted: text3
Formatted: Font: Italic
Formatted: Font: Italic
Formatted: Font: 9 pt, Lowered by 2 pt
Formatted: Font: 9 pt, Lowered by 2 pt
Formatted: eq 3, Right: 0", Tab stops: Not at 4.25" + 4.81"
Formatted: Indent: Left: 0.67", Tab stops: 0.75", Left + Not at 0.69"
Formatted: Font: 9 pt, Lowered by 2 pt
Formatted: Indent: Left: 0", Hanging: 1.25", Tab stops: 0.63", Left
Formatted: Indent: Left: 0", First line: 0", Tab stops: 0.63", Left
Formatted: head3
Formatted: Font: Italic

accordance with the following:

(a) For $\lambda_d \le 0.561$

$$P_{nd} = P_y \qquad \text{(Eq. 1.2.1-8}\sout{10}\text{)}$$

(b) For $\lambda_d > 0.561$

$$P_{nd} = \left(1 - 0.25\left(\frac{P_{crd}}{P_y}\right)^{0.6}\right)\left(\frac{P_{crd}}{P_y}\right)^{0.6} P_y \qquad \text{(Eq. 1.2.1-9}\sout{11}\text{)}$$

where

$$\lambda_d = \sqrt{P_y / P_{crd}} \qquad \text{(Eq. 1.2.1-}\sout{10}\text{12)}$$

where

P_y = A value as given in Eq. 1.2.1-4

P_{crd} = Critical elastic distortional column buckling *load* determined by analysis in accordance with Section 1.1.2

1.2.1.3.2 Columns with Hole(s) or Perforation Patterns

The *nominal axial strength [resistance]*, P_{nd}, for *distortional buckling* of columns with hole(s) shall be calculated in accordance with Section 1.2.1.3.1, except P_{crd} shall be determined including the influence of hole(s) or perforation patterns, and ~~section~~if $\lambda_d \le \lambda_{d2}$ then:

(a) For $\lambda_d \le \lambda_{d1}$

$$P_{nd} = P_{ynet} \qquad \text{(Eq. 1.2.1-13)}$$

(b) For $\lambda_{d1} < \lambda_d \le \lambda_{d2}$

$$P_{nd} = P_{ynet} - \left(\frac{P_{ynet} - P_{d2}}{\lambda_{d2} - \lambda_{d1}}\right)(\lambda_d - \lambda_{d1}) \qquad \text{(Eq. 1.2.1-14)}$$

where

$$\lambda_d = \sqrt{P_y / P_{crd}} \qquad \text{(Eq. 1.2.1-16}\sout{5}\text{)}$$

$$\lambda_{d1} = 0.561(P_{ynet} / P_y) \qquad \text{(Eq. 1.2.1-15}\sout{6}\text{)}$$

$$\lambda_{d2} = 0.561\left(14\left(P_y / P_{ynet}\right)^{0.4} - 13\right) \qquad \text{(Eq. 1.2.1-16}\sout{7}\text{)}$$

$$P_{d2} = \left(1 - 0.25(1/\lambda_{d2})^{1.2}\right)(1/\lambda_{d2})^{1.2} P_y \qquad \text{(Eq. 1.2.1-17}\sout{8}\text{)}$$

P_y = A value as given in Eq. 1.2.1-4

P_{ynet} = A value as given in Eq. 1.2.1-9

Formatted: Font: Italic
Formatted: Font: Italic
Formatted: Font: Italic
Formatted: Font: 10 pt, Lowered by 5 pt
Formatted: Lowered by 15 pt
Formatted: Font: 8 pt, Lowered by 8 pt
Formatted: Not Highlight
Formatted: Not Highlight

APPENDIX B. MODIFICATION TO AISI S100 COMMENTARY

COMMENTARY

APPENDIX 1: COMMENTARY ON APPENDIX 1 DESIGN OF COLD-FORMED STEEL STRUCTURAL MEMBERS USING THE DIRECT STRENGTH METHOD

1.1 GENERAL PROVISIONS

1.1.1 Applicability

The Direct Strength Method of Appendix 1 is an alternative procedure for determining the strength [resistance] and stiffness of cold-formed steel members (beams and columns). The reliability of Appendix 1 is insured by using calibrated safety factor, Ω, and resistance factor, ϕ, within set geometric limits, and conservative Ω and ϕ for other configurations. The applicability of Appendix 1 to all beams and columns implies that in some situations competing methods may exist for strength determination of a member: the main *Specification** and Appendix 1. In this situation there is no preferred method. Either method may be used to determine the strength [resistance]. The fact that one method may give a greater or lower strength [resistance] prediction in a given situation does not imply an increased accuracy for either method. The Ω and ϕ factors are designed to insure that both methods reach their target reliability.

The method of Appendix 1 provides solutions for beams and columns only, but these solutions must be combined with the regular provisions of the main *Specification* to cover other cases: shear, beam-columns, etc. For example, an application to purlin design was completed using the provisions of this Appendix for the bending strength, and then those calculations were augmented by shear, and shear and bending interaction calculations, in line with the main *Specification* (Quispe and Hancock, 2002). Further, beam-columns may be conservatively examined using the provisions of the main *Specification*, by replacing the beam and column design strength [factored resistance] with the provisions of this Appendix, or beam-columns may be analyzed using the actual stress state (Schafer, 2002b).

Direct Strength design provisions for columns with holes and beams with holes were developed between 2006 and 2011. ~~The pre-qualified columns and beams only include members without perforations (punchouts). For members with holes, Members with perforations generally may be designed by the main *Specification*. For perforated members not covered by the *Specification* one may want to consider a rational analysis method, which partially employs the methods of this Appendix. The key issue in such a rational analysis is~~ the ~~accurate~~ determination of the elastic local, distortional, and global buckling loads ~~(or moments) for the member with~~including the influence of the ~~perforation~~holes~~.~~ can be obtained with ~~N~~numerical (e.g., finite element) analysis where the ~~holes~~ holes are explicitly considered or with the approximate methods provided in this Commentary. Additionally, provisions to account for the influence of perforation patterns on elastic buckling are provided in this Commentary. ~~is one option in this case.~~The approximate methods utilize the finite strip method and hand solutions derived from modifications to classical stability solutions, and are general enough to accommodate the hole sizes, shapes, and spacings common in industry. Refer to Moen and Schafer (2010a) for a design example of a cold-formed steel column with holes and Moen and Schafer (2010b) for a design example of a cold-formed steel joist with holes.

Note:

* The *North American Specification for the Design of Cold-Formed Steel Structural Members*, Chapters A

through G and Appendices A and B and Appendix 2, is herein referred to as the main *Specification*.

1.1.1.1 Pre-qualified Columns

An extensive amount of testing has been performed on concentrically loaded, pin-ended, cold-formed steel columns (Kwon and Hancock, 1992; Lau and Hancock, 1987; Loughlan, 1979; Miller and Peköz, 1994; Mulligan, 1983; Polyzois et al., 1993; Thomasson, 1978). Data from these researchers were compiled and used for calibration of the Direct Strength Method. The geometric limitations listed in Appendix 1 are based on these experiments. In 2006 the pre-qualified category of Lipped C-Section and Rack Upright were merged, as a rack upright is a C-section with a complex stiffener. In addition, the complex stiffener limits from the original Rack Upright category were relaxed to match those found for C-section beams with complex stiffeners (Schafer, et al., 2006).

It is intended that as more cross-sections are verified for use in the Direct Strength Method, these tables and sections will be augmented. Companies with proprietary sections may wish to perform their own testing and follow Chapter F of the main *Specification* to justify the use of the pre-qualified Ω and ϕ factors for a particular cross-section. When such testing is performed the provisions of *Specification* Section 1.1.1.1 provide some relief from the sample size correction factor, C_P, of *Specification* Chapter F. Based on the existing data the largest observed V_P for the pre-qualified categories is 15% (Schafer 2006, 2008). Therefore, as long as the tested section, over at least three tests, exhibits a $V_P < 15\%$ then the section is assumed to be similar to the much larger database of tested sections used to calibrate the Direct Strength Method and the correction for small sample sizes C_P is not required and therefore is set to 1.0. If the ϕ generated from *Specification* Chapter F is higher than that of Section 1.2.1 of Appendix 1, this is evidence that the section behaves as a pre-qualified section. It is not anticipated that member testing is necessarily required for all relevant limit states: local, distortional and global buckling. An engineer may only require testing to reflect a single common condition for the member, with a minimum of three tests in that condition. However, beams and columns should be treated as separate entities. A manufacturer who cannot establish a common condition for a product may choose to perform testing in each of the limit states to ensure reliable performance in any condition. Engineering judgment is required. Note that for the purposes of this section, the test results in *Specification* Chapter F are replaced by test to predicted ratios. The prediction is that of the Direct Strength Method (this Appendix) using the actual material and cross-sectional properties from the tests. The P_m parameter, taken as equal to one in *Specification* Chapter F, is taken instead as the mean of the test-to-predicted ratios, and V_P is the accompanying coefficient of variation.

Alternatively, member geometries that are not pre-qualified may still use the method of Appendix 1, but with the increased Ω and reduced ϕ factors consistent with any rational analysis method as prescribed in A1.2 of the main *Specification*.

1.1.1.2 Pre-qualified Beams

An extensive amount of testing has been performed on laterally braced beams (Cohen, 1987; Ellifritt et al., 1997; LaBoube and Yu, 1978; Moreyara, 1993; Phung and Yu, 1978; Rogers, 1995; Schardt and Schrade, 1982; Schuster, 1992; Shan et al., 1994; Willis and Wallace, 1990) and on hats and decks (Acharya and Schuster, 1998; Bernard, 1993; Desmond, 1977; Höglund, 1980; König, 1978; Papazian et al., 1994). Data from these researchers were compiled and used

for calibration of the Direct Strength Method. The geometric limitations listed in the Appendix are based on the experiments performed by these researchers. The original geometric limits were extended to cover C- and Z-section beams with complex lip stiffeners based on the work of Schafer et al. (2006). For rounded edge stiffeners or other edge stiffeners that do not meet the geometric criteria either for pre-qualified simple, or complex, stiffeners one may still use the method of Appendix 1, but instead with the rational analysis Ω and ϕ factors prescribed in A1.2 of the main *Specification*. See the note on pre-qualified columns for further commentary on members which do not meet the pre-qualified geometric limits.

For beams that do not meet the material and geometric requirements defined by the pre-qualified categories, similar to column design, provisions are provided to potentially permit those members to use the Ω and ϕ factors of the pre-qualified members by using *Specification* Chapter F as discussed in detail in commentary section 1.1.1.1 above.

Users of this Appendix should be aware that pre-qualified beams with large flat width-to-thickness ratios in the compression flange will be conservatively predicted by the method of this Appendix when compared to the main *Specification* (Schafer and Peköz, 1998). However, the same beam with small longitudinal stiffeners in the compression flange will be well predicted using this Appendix.

1.1.2 Elastic Buckling

The elastic buckling load is the load in which the equilibrium of the member is neutral between two alternative states: buckled and straight. Thin-walled cold-formed steel members have at least 3 relevant elastic buckling modes: local, distortional, and global (Figure C-1.1.2-1). The global buckling mode includes flexural, torsional, or flexural-torsional buckling for columns, and lateral-torsional buckling for beams. Traditionally, the main *Specification* has only addressed local and global buckling. Further, the main *Specification*'s approach to local buckling is to conceptualize the member as a collection of "elements" and investigate local buckling of each element separately.

The method of this Appendix provides a means to incorporate all three relevant buckling modes into the design process. Further, all buckling modes are determined for the member as a whole rather than element by element. This insures that compatibility and equilibrium are maintained at element junctures. Consider, as an example, the lipped C-Section shown in pure compression in Figure C-1.1.2-1(a). The member's local elastic buckling load from the analysis is:

$P_{cr\ell}$ = 0.12 x 48.42 kips = 5.81 kips (25.84 kN).

The column has a gross area (A_g) of 0.881 in^2 (568.4 mm^2), therefore,

$f_{cr\ell} = P_{cr\ell}/A_g$ = 6.59 ksi (45.44 MPa)

The main *Specification* determines a plate buckling coefficient, k, for each element, then f_{cr}, and finally the effective width. The centerline dimensions (ignoring corner radii) are h = 8.94 in. (227.1 mm), b = 2.44 in. (62.00 mm), d = 0.744 in. (18.88 mm), and t = 0.059 in. (1.499 mm), the critical buckling stress, f_{cr} of each element as determined from the main *Specification*:

lip: k = 0.43, $f_{cr\ell\text{-lip}} = 0.43[\pi^2E/(12(1-\mu^2))](t/d)^2$ = 72.1 ksi (497 MPa)

flange: k = 4, $f_{cr\ell\text{-flange}} = 4.0[\pi^2E/(12(1-\mu^2))](t/b)^2$ = 62.4 ksi (430 MPa)

web: k = 4, $f_{cr\ell\text{-web}} = 4.0[\pi^2E/(12(1-\mu^2))](t/h)^2$ = 4.6 ksi (32.0 MPa)

Each element predicts a different buckling stress, even though the member is a connected

group. These differences in the buckling stress are ignored in the main *Specification*. The high flange and lip buckling stresses have little relevance given the low web buckling stress. The finite strip analysis, which includes the interaction amongst the elements, shows that the flange aids the web significantly in local buckling, increasing the web buckling stress from 4.6 ksi (32.0 MPa) to 6.59 ksi (45.4 MPa), but the buckling stress in the flange and lip are much reduced due to the same interaction. Comparisons to the distortional buckling stress (f_{crd}) using k from B4.2 of the main *Specification* do no better (Schafer and Peköz, 1999; Schafer, 2002).

The method of this Appendix allows rational analysis to be used for determining the local, distortional and global buckling load or moment. Specific guidance on elastic buckling determination follows. Users are reminded that the strength of a member is not equivalent to the elastic buckling load (or moment) of the member. In fact the elastic buckling load can be lower than the actual strength, for slender members with considerable post-buckling reserve; or the elastic buckling load can be fictitiously high due to ignoring inelastic effects. Nonetheless, the elastic buckling load is a useful reference load for determining a member's slenderness and ultimately its strength.

Manual and numerical solutions for elastic buckling prediction are covered in the following sections. It is permissible to mix the manual and numerical methods; in some cases it is even advantageous. For example, numerical solutions for member local and distortional buckling are particularly convenient; however, unusual long column bracing conditions $(KL)_x \neq (KL)_y \neq (KL)_t$ may often be handled with less confusion using the traditional manual formulas. Use of the numerical solutions is generally encouraged, but verification with the manual solutions can aid in building confidence in the numerical solution.

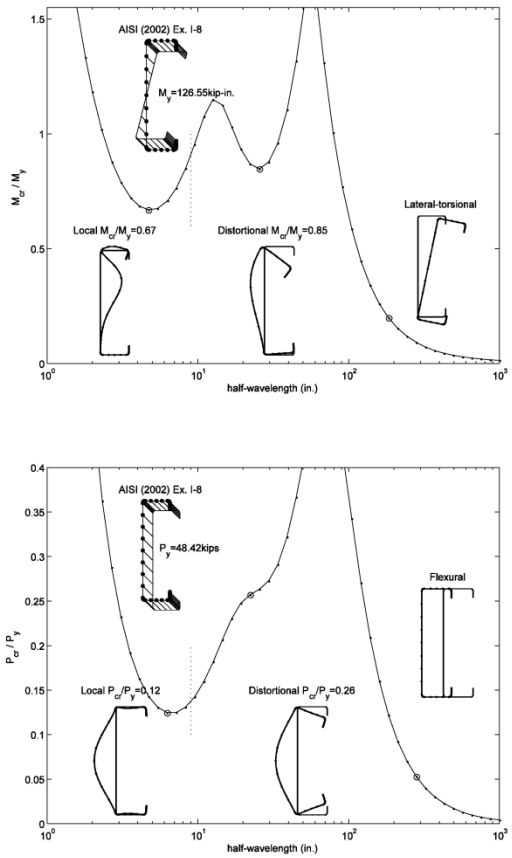

(a) 9CS2.5x059 of AISI 2002 Cold-Formed Steel Design Manual Example I-8

Figure C-1.1.2-1 Examples of Bending and Compression Elastic Buckling Analysis with Finite Strip Method

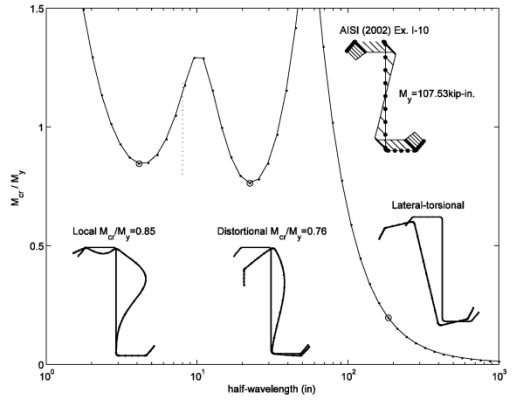

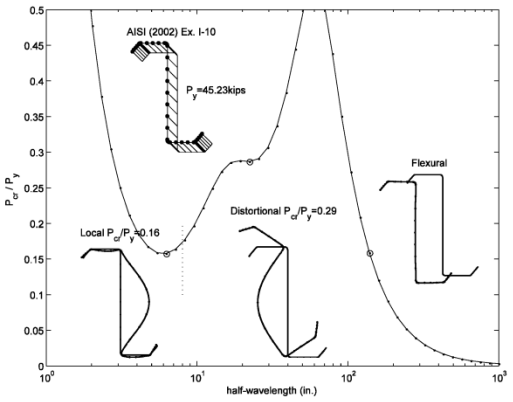

(b) 8ZS2.25x059 of AISI 2002 Cold-Formed Steel Design Manual Example I-10

Figure C-1.1.2-1 Examples of Bending and Compression Elastic Buckling Analysis with Finite Strip Method (cont.)

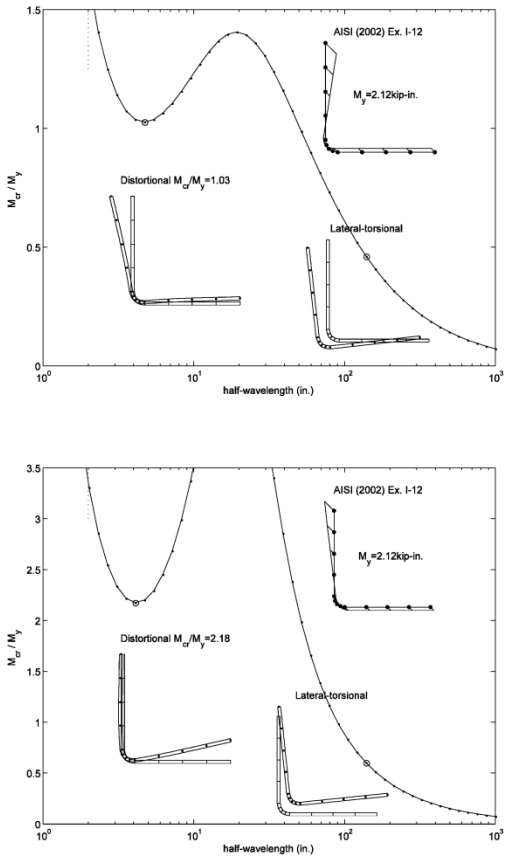

(c) 2LU2x060 of AISI 2002 Cold-Formed Steel Design Manual Example I-12

Figure C-1.1.2-1 Examples of Bending and Compression Elastic Buckling Analysis with Finite Strip Method (cont.)

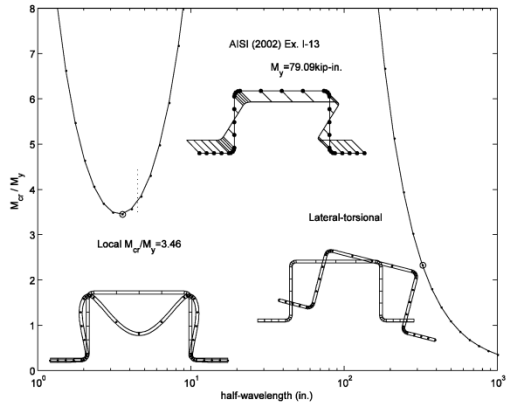

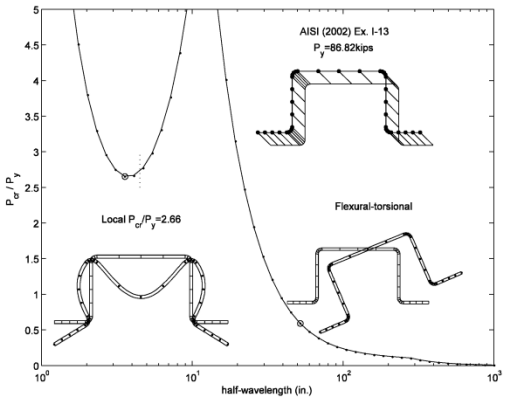

(d) 3HU4.5x135 of AISI 2002 Cold-Formed Steel Design Manual Example I-13

Figure C-1.1.2-1 Examples of Bending and Compression Elastic Buckling Analysis with Finite Strip Method (cont.)

1.1.2.1 Elastic Buckling - Numerical Solutions

A variety of numerical methods: finite element, finite differences, boundary element, generalized beam theory, finite strip analysis, and others, may provide accurate elastic buckling solutions for cold-formed steel beams and columns.

Traditional finite element analysis using thin plate or shell elements may be used for elastic buckling prediction. Due to the common practice of using polynomial shape functions, the number of elements required for reasonable accuracy can be significant. Finite element analysis books such as Cook et al. (1989) and Zienkiewicz and Taylor (1989, 1991) explain the basic theory; while a number of commercial implementations can provide accurate elastic buckling answers if implemented with care. Finite difference solutions for plate stability are implemented by Harik et al. (1991) and others. The boundary element method may also be used for elastic stability (Elzein, 1991).

Generalized beam theory, developed by Schardt (1989), extended by Davies et al. (1994) and implemented by Davies and Jiang (1996, 1998), and Silvestre and Camotim (2002a, 2002b) has been shown to be a useful tool for elastic stability analysis of cold-formed steel members. The ability to separate the different buckling modes makes the method especially amenable to design methods.

Finite strip analysis is a specialized variant of the finite element method. For elastic stability of cold-formed steel structures, it is one of the most efficient and popular methods. Cheung and Tham (1998) explains the basic theory while Hancock et al. (2001) and Schafer (1997) provide specific details for stability analysis with this method. Hancock and his researchers (see Hancock et al., 2001 for full references and descriptions) pioneered the use of finite strip analysis for stability of cold-formed steel members and convincingly demonstrated the important potential of finite strip analysis in both cold-formed steel design and behavior.

The Direct Strength Method of this Appendix emphasizes the use of finite strip analysis for elastic buckling determination. Finite strip analysis is a general tool that provides accurate elastic buckling solutions with a minimum of effort and time. Finite strip analysis, as implemented in conventional programs, does have limitations, the two most important ones are

- the model assumes the ends of the member are simply supported, and
- the cross-section may not vary along its length.

These limitations preclude some analysis from readily being used with the finite strip method, but despite these limitations the tool is useful, and a major advance over plate buckling solutions and plate buckling coefficients (k's) that only partially account for the important stability behavior of cold-formed steel members.

The American Iron and Steel Institute has sponsored research that, in part, has led to the development of the freely available program, CUFSM, which employs the finite strip method for elastic buckling determination of any cold-formed steel cross-section. The program is available at www.ce.jhu.edu/bschafer/cufsm and runs on any PC with Windows 9x, NT, 2000, XP. Tutorials and examples are available online at the same address.

1.1.2.1.1 Local Buckling via Finite Strip ($P_{crℓ}$, $M_{crℓ}$)

In the finite strip method, members are loaded with a reference stress distribution: pure compression for finding P_{cr}, and pure bending for finding M_{cr} (see Figure C-1.1.2-1).

Determination of the buckling mode requires consideration of the half-wavelength and mode shape of the member. Special attention is given to the half-wavelength and mode shape for local, distortional, and global buckling via finite strip analysis in the following sections.

Half-wavelength

Local buckling minima occur at half-wavelengths that are less than the largest characteristic dimension of the member under compressive stresses. For the examples of Figure C-1.1.2-1, this length has been demarcated with a short vertical dashed line. For instance, the largest out-to-out dimension for the lipped channel of Figure C-1.1.2-1 (a) is 9 in. (229 mm), therefore the cutoff for local buckling is at 9 in. (229 mm). Minima in the buckling curves that fall at half-wavelengths less than this length are considered as local buckling modes. Buckling modes occurring at longer lengths are either distortional or global in nature.

The criteria of limiting the half-wavelength for local buckling to less than the largest outside dimension under compressive stresses is based on the following. Local buckling of a simply supported plate in pure compression occurs in square waves, i.e., it has a half-wavelength that is equal to the plate width (the largest outside dimension). If any stress gradient exists on the plate, or any beneficial restraint is provided to the edges of the plate by other elements, the critical half-wavelength will be less than the width of the plate. Therefore, local buckling, with the potential for stable post-buckling response, is assumed to occur only when the critical half-wavelength is less than the largest potential "plate" (i.e., outside dimension with compressive stresses applied) in a member.

Mode shape

Local buckling involves significant distortion of the cross-section, but this distortion involves only rotation, not translation, at the fold lines of the member. The mode shapes for members with edge stiffened flanges such as those of the lipped cee or zee provide a direct comparison between the difference between local buckling and distortional buckling. Note the behavior at the flange/lip junction – for local buckling only rotation occurs, for distortional buckling translation occurs.

Discussion

Local buckling may be indistinct from distortional buckling in some members. For example, buckling of the unlipped angle may be considered as local buckling by the main *Specification*, but is considered as distortional buckling as shown in Figure C-1.1.2-1(c), because of the half-wavelength of the mode, and the characteristics of the mode shape. By the definitions of this Appendix, no local buckling mode exists for this member. Local buckling may be at half-wavelengths much less than the characteristic dimension if intermediate stiffeners are in place, or if the element undergoes large tension and small compressive stress.

Users may encounter situations where they would like to consider the potential for bracing to retard local buckling. Springs may be added to a numerical model to include the effect of external bracing. Care should be used if the bracing only provides support in one direction (such as a deck on a compression flange) as the increase of the local buckling strength is limited in such a case. In general, since local buckling occurs at short wavelengths, it is difficult to effectively retard this mode by external bracing. Changes to the geometry of the member (stiffeners, change of thickness, etc.) should be pursued

instead.

Members with holes

Researchers have observed that holes can change the local buckling mode shapes of thin plates and cold-formed steel columns and beams (Kumai, 1952; Schlack, Jr., 1964; Kawai and Ohtsubo, 1968; Vann 1971; Kesti, 2000; El-Sawy and Nazmy, 2001; Sarawit, 2003; Moen and Schafer, 2009a). A finite strip approximate method for predicting $P_{cr\ell}$ and $M_{cr\ell}$ including the influence of holes is described in Moen and Schafer (2009c). The method assumes that local buckling occurs as either buckling of the unstiffened strip(s) adjacent to a hole at the net section or as local buckling of the gross section between holes. This approach is an improvement over element-based methods because the interaction between the unstiffened strip and the connected cross-section is explicitly considered. For a column with holes:

$$P_{cr\ell} = \min(P_{cr\ell nh}, P_{cr\ell h}) \qquad \text{(C-1.1.2-1)}$$

where

$P_{cr\ell nh}$ = local buckling load of the gross section by a finite strip analysis

$P_{cr\ell h}$ = local buckling load of the net section by a finite strip analysis (e.g., in CUFSM), but restraining the deformations to local buckling and examining only those buckling half-wavelengths shorter than the length of the hole

To calculate $P_{cr\ell h}$, a finite strip analysis of the net section is performed as shown in Figure C-1.1.2-2. To ensure a consistent comparison of $P_{cr\ell h}$ and $P_{cr\ell nh}$, the reference stress used in the net section and gross section finite strip analyses should be calculated with the same reference load (e.g., 1 kip on the net section, 1 kip on the gross section).

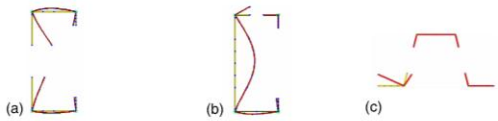

Figure C-1.1.2-2 Modeling a column net cross-section in the finite strip method (e.g., CUFSM): (a) C-section with a web hole, (b) C-section with a flange hole, (c) hat section with web holes

Eigen-buckling analysis of the restrained cross section results in an elastic buckling curve similar to Figure C-1.1.2-3, where the buckled half-wavelength at the minimum buckling load is $L_{cr\ell h}$. When the hole length, L_h, is less than $L_{cr\ell h}$, as shown in Figure C-1.1.2-3a, $P_{cr\ell h}$ is equal to the buckling load for a single half-wave forming over the length of the hole. (This case is common for circular and square holes, where L_h is less than the width of the cross-sectional element containing the hole.) If $L_h \geq L_{cr\ell h}$ (Figure C-1.1.2-3b), $P_{cr\ell h}$ is the minimum on the buckling curve, corresponding to a single half-have forming within the length of the hole. Note that use of the net cross-section for buckling half-wavelengths greater than L_h is conservative by failing to reflect the stiffness contributions of the gross section. Knowledge of the specific buckling half-wavelength of interest allows the finite strip method to be extended by utilizing the net section, but only for half-waves less than the length of the hole, L_h.

Formatted: Indent: Hanging: 0.1", Tab stops: 0.38", Left + Not at 0.42"
Formatted: text3, Indent: Left: 0", Tab stops: Not at 3.07" + 5.88"
Field Code Changed
Formatted
Formatted: eq 3 text, Indent: Left: 0.67", Hanging: 0.6", Tab stops: Not at 3.07" + 5.88"
Formatted
Formatted: Font: Book Antiqua
Formatted: text3, Tab stops: Not at 0.5" + 3.07" + 5.88"
Formatted
Formatted: Font: Franklin Gothic Demi, 10 pt
Formatted: Font: Book Antiqua, 11 pt
Formatted: Line spacing: single
Formatted: Indent: Left: 0.31", First line: 0.25", Line spacing: single, Tab stops: 0.25", Left
Formatted

The same approached described previously for columns is also applicable to beams, i.e., $M_{cr\ell} = \min(M_{cr\ell nh}, M_{cr\ell h})$. In this case, the applied reference stress in the finite strip analysis should represent as a moment, i.e., 1 kip-in. on the net section, 1 kip-in. on the gross section, see Moen and Schafer (2010b).

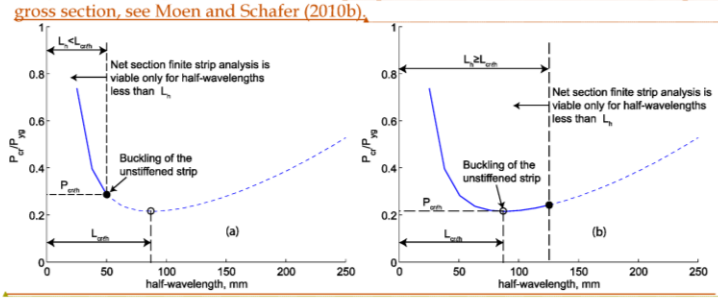

(a) Hole Length Less than $L_{cr\ell h}$ (b) Hole Length Greater Than $L_{cr\ell h}$

Figure C-1.1.2-3 Local Elastic Buckling Curve of Net Cross-Section

Columns with perforation patterns

Past research has suggested the inclusion of additional buckling modes in addition to the ones applicable to larger, discrete holes – Euler strip buckling of the material between perforations (Rhodes and Macdonald, 1996; Pu et al., 1999) and plate buckling where a network of material contains the full local buckling deformations (Kesti, 2000) – to accommodate the influence of perforation patterns on local buckling. Additionally, plate buckling between perforations longitudinally can be ignored as patterns are typically arranged with perforations in tightly spaced arrays. Smith and Moen (to appear) describe an approximate finite strip analysis method that accounts for elemental buckling, where perforations are located within local buckling half-wavelengths, through a reduced thickness of a perforated element, and sub-elemental buckling, where unstiffened strip or Euler strip buckling govern, through the same net section analysis described by Moen and Schafer (2009c). The reduced thickness method applies a unit load to the modified cross-section and takes the elastic local buckling load as the minimum in the local buckling branch of the modified cross-section's signature curve. The elastic local buckling load of a column including perforation patterns is:

$$P_{cr\ell} = \min(P_{cr\ell tr}, P_{cr\ell h}) \qquad \text{(C-1.1.2-2)}$$

where

$P_{cr\ell tr}$ = local buckling load of a modified section with reduced thicknesses as described in (C-1.1.2-3) applied to perforated elements

$P_{cr\ell h}$ = local buckling load of the net section by a finite strip analysis (e.g., in CUFSM), but restraining the deformations to local buckling and examining

Formatted: Not Superscript/ Subscript, Not Raised by / Lowered by

Formatted: Font: Book Antiqua, 11 pt, Not Superscript/ Subscript, Not Raised by / Lowered by

Formatted: Not Superscript/ Subscript, Not Raised by / Lowered by

Formatted: Font: Book Antiqua, 11 pt

Formatted: Font: Book Antiqua, 11 pt, Not Superscript/ Subscript, Not Raised by / Lowered by

Formatted: Line spacing: single

Formatted: figure, Left, Don't keep with next, Tab stops: 0.81", Left + 4", Left + Not at 3.07" + 5.88"

Field Code Changed

Formatted: Indent: Left: 0.67", Hanging: 0.58", Tab stops: Not at 1.17"

Formatted: Indent: Left: 0.58", Hanging: 0.67"

only those buckling half-wavelengths shorter than the length of the hole

and

$$t_r = t\left[1 - \frac{n_l n_t \left(L_h d_h + \mu d_h \alpha + \mu L_h \beta + \alpha\beta\right)}{Lb}\right]^{\frac{1}{2}} \qquad \text{(C-1.1.2-3)}$$

where

t = base metal thickness
n_l = number of longitudinal perforations
n_t = number of transverse perforations
L_h = longitudinal size of a perforation
d_h = transverse size of a perforation
μ = Poisson's ratio
α = longitudinal perforation size modification factor, found using (C-1.1.2-4)
β = transverse perforation size modification factor, found using (C-1.1.2-5)
L = length of the perforated element
b = width of the perforated element

and

$$\alpha = \frac{b}{\pi}\sin\left(\frac{\pi L_h}{b}\right) \qquad \text{(C-1.1.2-4)}$$

$$\beta = \frac{b}{\pi}\sin\left(\frac{\pi d_h}{b}\right) \qquad \text{(C-1.1.2-5)}$$

Field Code Changed

Formatted: Font: Book Antiqua, 11 pt, Not Raised by / Lowered by

Formatted: Font: Book Antiqua, 11 pt, Not Raised by / Lowered by

Formatted: Font: Book Antiqua, 11 pt, Not Raised by / Lowered by

Formatted: Font: Book Antiqua, 11 pt, Not Raised by / Lowered by

Field Code Changed

Field Code Changed

1.1.2.1.2 Distortional Buckling via Finite Strip (P_{crd}, M_{crd})

Half-wavelength

Distortional buckling occurs at a half-wavelength intermediate to local and global buckling modes, as shown in the figures given in C-1.1.2-1. The half-wavelength is typically several times larger than the largest characteristic dimension of the member. The half-wavelength is highly dependent on both the loading and the geometry.

Mode shape

Distortional buckling involves both translation and rotation at the fold line of a member. Distortional buckling involves distortion of one portion of the cross-section and predominately rigid response of a second portion. For instance, the edge stiffened flanges of the lipped cee and zee are primarily responding as one rigid piece while the web is distorting.

Discussion

Distortional buckling may be indistinct (without a minimum) even when local buckling and long half-wavelength (global) buckling are clear. The lipped cee and zee in bending show this basic behavior. For some members distortional buckling may not occur.

Bracing can be effective in retarding distortional buckling and boosting the strength [resistance] of a member. Continuous bracing may be modeled by adding a continuous spring in a finite strip model. For discrete bracing of distortional buckling, when the unbraced length is less than the critical distortional half-wavelength, best current practice is to use the buckling load (or moment) at the unbraced length. The key consideration for

distortional bracing is limiting the rotation at the compression flange/web juncture.

Members with holes

The distortional buckling loads P_{crd} and M_{crd} are, at least in part, dictated by the bending stiffness provided by the web of an open cross-section as it restrains the attached flange from rotating (see Figure C-1.1.2-1). If a hole with length L_h is introduced into the web of an open cross-section, the rotational restraint provided by the web is decreased, resulting in a lower critical distortional buckling load (Kesti, 2000; Moen and Schafer, 2009b). An approximate method for calculating P_{crd} and M_{crd} including the influence of unstiffened web holes has been developed by Moen and Schafer (2009c). To implement the method, first a finite strip analysis is performed with the gross cross-section to identify the distortional buckling half-wavelength, L_{crd}. Then, the web thickness is modified from t to t_r to simulate the reduction in bending stiffness caused by the presence of a web hole:

$$t_r = \left(1 - \frac{L_h}{L_{crd}}\right)^{1/3} t \qquad \text{(C-1.1.2-26)}$$

Note that the cross-section thickness is modified over the full depth of the web, not just at the location of the hole in the cross-section. The buckling load P_{crd} or M_{crd} (including the influence of holes) is obtained with another finite strip analysis of the modified cross-section performed just at L_{crd} of the gross cross-section with the reduced thickness. The second analysis is only conducted at L_{crd} as this is the only length for which the reduced thickness t_r has any relevance.

Columns with perforation patterns

Research by Smith and Moen (to appear) has found perforation patterns to reduce web rotational restraint along the entire length of a column. This effect increases distortional buckling half-wavelengths and decreases elastic distortional buckling loads. The influence of perforation patterns on distortional buckling is accounted by reducing the web thickness in finite strip analysis to:

$$t_r = \left(\frac{A_{web,net}}{A_{web,g}}\right)^{1/3} t \qquad \text{(C-1.1.2-7)}$$

where $A_{web,net}$ is the planar net area of the web and is equal to $Lh_o - n_l n_t L_h d_h$ and $A_{web,g}$ is the planar gross area of the web and is equal to Lh_o. A reference stress is calculated by applying a unit load to the modified cross-section. The distortional buckling half-wavelength L_{crdh} is associated with the minimum value of P_{crd} on the distortional buckling branch of the signature curve associated with the modified cross-section. This allows the half-wavelengths to increase to match observed elastic behavior of perforation patterns.

1.1.2.1.3 Global (Euler) Buckling via Finite Strip (P_{cre}, M_{cre})

Global bucking modes for columns include: flexural, torsional and flexural-torsional buckling. For beams bent about their strong-axis, lateral-torsional buckling is the global buckling mode of interest.

Half-wavelength

Global (or "Euler") buckling modes: flexural, torsional, or flexural-torsional for

Formatted: text3a-title, Indent: Left: 0"

Formatted: text3, Indent: Left: 0", First line: 0", Tab stops: Not at 0.5" + 3.07" + 5.88"

Formatted: Font: Book Antiqua, Not Superscript/ Subscript, Lowered by 2 pt

Formatted: Font: Book Antiqua, 11 pt, Not Superscript/ Subscript, Not Raised by / Lowered by

Formatted: Font: Book Antiqua, Not Superscript/ Subscript

Formatted: Font: Book Antiqua, 11 pt, Not Superscript/ Subscript, Not Raised by / Lowered by

Formatted: Font: Book Antiqua, Not Superscript/ Subscript

Formatted: Font: Book Antiqua, 11 pt, Not Superscript/ Subscript, Not Raised by / Lowered by

Formatted: Font: Book Antiqua, Not Superscript/ Subscript

Formatted: Font: Book Antiqua, 11 pt, Not Superscript/ Subscript, Not Raised by / Lowered by

Formatted: Font: Book Antiqua, Not Superscript/ Subscript

Formatted: Font: Book Antiqua, 11 pt, Not Superscript/ Subscript, Not Raised by / Lowered by

Formatted: eq 3, Indent: Left: 0", Tab stops: Not at 0.5" + 3.07" + 6.5"

Field Code Changed

Formatted: text3, Indent: Left: 0", Tab stops: Not at 0.5" + 3.07" + 5.88"

Formatted: text3, Indent: Left: 0", Tab stops: Not at 0.5" + 3.07" + 5.88"

Field Code Changed

Formatted: eq 3, Justified, Indent: Left: 0.31", Tab stops: 0.88", Left + Not at 0.5" + 3.07" + 5.88"

columns, lateral-torsional for beams, occur as the minimum mode at long half-wavelengths.

Mode Shape

Global buckling modes involve translation (flexure) and/or rotation (torsion) of the entire cross-section. No distortion exists in any of the elements in the long half-wavelength buckling modes.

Discussion

Flexural and distortional buckling may interact at relatively long half-wavelengths making it difficult to determine long column modes at certain intermediate to long lengths. When long column end conditions are not simply supported, or when they are dissimilar for flexure and torsion, higher modes are needed for determining the appropriate buckling load. By examining higher modes in a finite strip analysis, distinct flexural and flexural-torsional modes may be identified. Based on the boundary conditions, the effective length, KL, for a given mode can be determined. With KL known, then P_{cre} (or M_{cre}) for that mode may be read directly from the finite strip at a half-wavelength of KL by using the curve corresponding to the appropriate mode. For beams, C_b of the main *Specification* may be employed to account for the moment gradient. Mixed flexural and torsional boundary conditions may not be directly treated. Alternatively, traditional manual solutions may be used for global buckling modes with different bracing conditions.

Columns with perforation patterns

Approximations for flexural and flexural-torsional buckling have been described by Smith and Moen (to appear). Flexural buckling is taken as P_{cre} from the unperforated section found in finite strip software and is multiplied by the ratio of the weighted average moment of inertia, I_{avg}, determined with Eq. C1-1.1.2-16, to the gross moment of inertia, I_g. This method does not account for flexural and long-wave distortional buckling modal mixing and may become unconservative as perforations aggregate in web elements.

For flexural-torsional buckling, P_{cre} of the unperforated section found in finite strip software is multiplied by the ratio of weighted average to gross cross-sectional St. Venant torsion constant, J_{avg} and J_g respectively, and the ratio of weighted average to gross cross-sectional warping torsion constant, C_{wavg} and C_{wg} respectively. The weighted average cross-sectional properties, J_{avg} and C_{wavg}, are determined in the same manner as Eq. C1-1.1.2-16. This method has only been validated for cross-sections typical of pallet rack uprights and may not be applicable to other shapes.

Elastic Buckling – Manual Solutions

Local buckling

Manual solutions for member local buckling rely on the use of element plate buckling coefficients, as given below.

For columns,

$$P_{cr\ell} = A_g f_{cr\ell} \qquad \text{(C-1.1.2}$$

where

A_g = gross area

$f_{cr\ell}$ = local buckling stress

Formatted: Font: Book Antiqua, 11 pt, Italic, Not Superscript/ Subscript, Not Raised by / Lowered by

Formatted: eq 2 text

For beams,

$M_{cr\ell} = S_g f_{cr\ell}$

where

S_g = gross section modulus to the extreme compression fiber

$f_{cr\ell}$ = local buckling stress at the extreme compression fiber

and

$$f_{cr\ell} = k\frac{\pi^2 E}{12(1-\mu^2)}\left(\frac{t}{w}\right)^2 \qquad \text{(C-1.1.2-3105)}$$

where

E = Young's Modulus

μ = Poisson's ratio

t = element thickness

w = element flat width

k = element (plate) buckling coefficient. Local plate buckling coefficients for an isolated element may be predicted through use of commentary Table C-B2-1. Schafer and Peköz (1999) present additional expressions for stiffened and unstiffened elements under a stress gradient. Elastic local buckling of a member may be conservatively approximated by using the minimum of the local buckling stress of the elements, which make up the member. However, using the minimum element solution and ignoring interaction may be excessively conservative for predicting member local buckling. To alleviate this, hand methods that account for the interaction of two elements are available. Solutions include two stiffened or edge stiffened elements (a flange and a web) under a variety of loading cases Schafer (2001, 2002); and local buckling of an edge stiffened element, including lip/flange interaction (Schafer and Peköz, 1999).

Elements with holes

Moen and Schafer (2009a) provides approximations for $f_{cr\ell}$ including the influence of discrete unstiffened hole(s), for stiffened and unstiffened elements in uniaxial compression, and stiffened elements under a stress gradient. The approximations include a conversion of the buckling stress at the net section to that of the gross section to allow for direct implementation with Eq. C-1.1.2-83 and Eq. C-1.1.2-94.

Elements with perforation patterns

Smith and Moen (to appear) have determined an approximate plate buckling coefficient for stiffened elements including the influence of perforation patterns. This coefficient, k_h, may be substituted in the stead of k in Eq. C-1.1.2-12 to manually predict elastic buckling of plates with perforation patterns.

Distortional Buckling

Distortional buckling of members with edge stiffened flanges may also be predicted by manual solutions. Unfortunately, the complicated interaction that occurs between the edge stiffened flange and the web leads to cumbersome and lengthy formulas.

For columns,

$P_{crd} = A_g f_{crd}$ (C-1.1.2-3116)

Formatted: eq 2 text

Formatted: Indent: Left: 0.5", Hanging: 0.5"

Formatted: Indent: Hanging: 0.67"

Formatted: Indent: Left: 0.5", Hanging: 0.5", Tab stops: 2.46", Left + Not at 1.17"

Formatted: text3a-title, Indent: Left: 0"

Formatted: Font: Book Antiqua, 11 pt, Not Superscript/ Subscript, Not Raised by / Lowered by

Formatted: Font: Book Antiqua, 11 pt, Not Superscript/ Subscript, Not Raised by / Lowered by

Formatted: Font: Book Antiqua, Not Superscript/ Subscript

Formatted: Not Superscript/ Subscript

Formatted: Font: Book Antiqua, 11 pt, Not Superscript/ Subscript, Not Raised by / Lowered by

Formatted: text3

Formatted: text3

Formatted: Indent: Left: 0", First line: 0"

A_g = gross area of the member
f_{crd} = distortional buckling stress (see below)

For beams,

$M_{crd} = S_f f_{crd}$ (C-1.1.2-4127)

S_f = gross section modulus to the extreme compression fiber
f_{crd} = distortional buckling stress at the extreme compression fiber. Solutions and design aids for f_{crd} are available for beams (Hancock et al., 1996; Hancock, 1997; Schafer and Peköz, 1999) and for columns (Lau and Hancock, 1987; Schafer 2002). Design aids for flanges with unusual edge stiffeners (e.g., Bambach et al., 1998) or flexural members with a longitudinal stiffener in the web (Schafer, 1997) are also available. See the *Commentary* on the Main *Specification* Sections C3.1.4 and C4.2 for additional information.

Members with holes or perforation patterns

The modified web thickness, t_r, in Eq. C-1.1.2-62 or C-1.1.2-7 can be used directly with the hand methods in *Specification* Section C3.1.4 and *Specification* Section C4.2 to approximate the influence of unstiffened web holes on P_{crd} and M_{crd}. For beams, t_r replaces t in *Specification* Eq. C3.1.4-142 (elastic stiffness contribution of the web) and *Specification* Eq. C.3.1.4-164 (geometric stiffness contribution of the web). For beams, t_r replaces t in Eq. C.4.2-911 and Eq. C.4.2.-120.

Global Buckling

Global buckling of members is calculated in the main *Specification*. Therefore, for both beams and columns, extensive closed-form expressions are already available and may be used for manual calculation. See the *Commentary* to main *Specification* Sections C4 and C3 for additional details.

For columns,

$P_{cre} = A_g f_{cre}$ (C-1.1.2-1385)

A_g = gross area of the member
f_{cre} = minimum of the elastic critical flexural, torsional, or flexural-torsional buckling stress. f_{cre} is equal to F_e of Section C4 of the main *Specification*. The hand methods presented in *Specification* Sections C4.1.1 through C4.1.4 provide all necessary formula. Note, Section C4.1.4 specifically addresses the long-standing practice that F_e (or f_{cre}) may be calculated by rational analysis. Rational analysis hand solutions to long column buckling are available - see the *Commentary* for main *Specification* Section C4.1.4 as well as Yu (2000) or Hancock et al. (2001). The hand calculations may be quite lengthy, particular if member properties x_o and C_w are unknown.

For beams,

$M_{cre} = S_f f_{cre}$ (C-1.1.2-6914)

S_f = gross section modulus to the extreme compression fiber
f_{cre} = elastic critical lateral-torsional buckling stress. f_{cre} is equal to F_e of main *Specification* Section C3.1.2.1 for open cross-section members and C3.1.2.2 for closed cross-section members. Hand solutions are well established for doubly-

Formatted: text3a-title, Indent: Left: 0"
Formatted: text3, Indent: Left: 0", First line: 0", Tab stops: Not at 0.5" + 3.07" + 5.88"
Formatted: Font: Book Antiqua, 11 pt, Italic, Not Superscript/ Subscript, Not Raised by / Lowered by
Formatted: Font: Book Antiqua, 11 pt, Italic, Not Superscript/ Subscript, Not Raised by / Lowered by
Formatted: Font: Book Antiqua, 11 pt, Not Superscript/ Subscript, Not Raised by / Lowered by
Formatted: Font: Book Antiqua, 11 pt, Italic, Not Superscript/ Subscript, Not Raised by / Lowered by
Formatted: Font: Book Antiqua, 11 pt, Italic, Not Superscript/ Subscript, Not Raised by / Lowered by

and singly-symmetric sections, but not so for point symmetric sections (zees). F_e of point-symmetric sections is taken as half of the value for doubly-symmetric sections. Rational numerical analysis may be desirable in cases where a close to exact solution is required.

Members with holes

The global (Euler) buckling load, P_{cre} for columns and M_{cre} for beams, decreases when holes are present (Sarawit, 2003; Moen and Schafer, 2009b). A "weighted average" approach employing the net-section and gross-section properties can be utilized to approximate P_{cre} (Moen and Schafer, 2009c). For weak-axis or strong-axis flexural buckling of a column with *n* arbitrarily spaced holes or net-section regions:

$$P_{cre} = \frac{\pi^2 EI_{avg}}{(KL)^2} \qquad \text{(C-1.1.2-15}\sout{10}\text{)}$$

where

KL = effective column length

I_{avg} = "weighted average" of moment of inertia

$$= \left[\frac{I_g L_g + I_{net} L_{net} + T(I_g - I_{net})}{L}\right] \qquad \text{(C-1.1.2-}\sout{11}\text{16)}$$

where

I_g = gross section moment of inertia

L_g = total segment length without holes

I_{net} = net section moment of inertia

L_{net} = total length of holes or net-section regions

L = total member length

$= L_g + L_{net}$

$$T = \frac{L}{2\pi}\sum_{j=1}^{n}\cos\left(\frac{2\pi c_j}{L}\right)\sin\left(\frac{\pi L_{h,j}}{L}\right) \qquad \text{(C-1.1.2-17}\sout{12}\text{)}$$

where

$L_{h,j}$ = length of hole or net-section region j

c_j = distance from top of column to hole centerline or net-section region, see Figure C-1.1.2-4

$$L_{net} = \sum_{j=1}^{n} L_{h,j} \qquad \text{(C-1.1.2-18}\sout{13}\text{)}$$

If the holes or net section regions are spaced symmetrically about the longitudinal midheight of the column, then T=0. For example, T=0 for a column with two holes located in a column at c_1=L/3 and c_2=2L/3.

Formatted: text3a-title

Formatted: text3, Indent: Left: 0", First line: 0", Line spacing: single, Tab stops: Not at 0.5" + 2" + 3.07" + 3.75" + 5.88"

Formatted: eq 3, Line spacing: single, Tab stops: Not at 0.31" + 0.5" + 3.07" + 3.75" + 6.5"

Field Code Changed

Formatted: eq 3 text, Line spacing: single, Tab stops: Not at 0.31" + 0.5" + 3.07" + 3.75" + 6.5"

Formatted: eq 3 text, Line spacing: single, Tab stops: Not at 0.31" + 0.5" + 3.07" + 3.75" + 6.5"

Field Code Changed

Formatted: Font: Book Antiqua, Not Superscript/ Subscript, Lowered by 2 pt

Formatted: Font: Book Antiqua, 11 pt, Not Superscript/ Subscript, Not Raised by / Lowered by , Not Highlight

Formatted: Font: Book Antiqua, Not Superscript/ Subscript, Lowered by 2 pt

Formatted: Font: Book Antiqua, Not Superscript/ Subscript, Lowered by 2 pt

Formatted ...

Formatted ...

Formatted ...

Formatted ...

Formatted ...

Formatted ...

Field Code Changed

Formatted ...

Formatted ...

Formatted ...

Formatted ...

Formatted ...

Formatted ...

Field Code Changed

Formatted ...

Formatted ...

Formatted ...

Formatted ...

Formatted ...

Formatted ...

Formatted ...

Formatted ...

Formatted ...

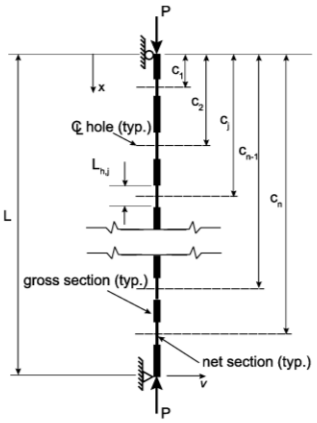

Figure C-1.1.2-4 A column with j = 1, 2 .. n holes or net section regions

The "weighted average" approach for flexural buckling can be extended to the general case of calculating P_{cre} for flexural, torsional and flexural-torsional buckling in columns as described in Moen and Schafer (2009c). For doubly- or singly-symmetric sections subjected to torsional or flexural-torsional buckling, the elastic flexural-torsional buckling load, P_{cre}, including the influence of holes, can be calculated with the following modifications to equations in Section C4.1.2:

$$P_{cre} = \frac{A_g}{2\beta}\left[(\sigma_{ex}+\sigma_t) - \sqrt{(\sigma_{ex}+\sigma_t)^2 - 4\beta\sigma_{ex}\sigma_t}\right] \qquad \text{(C-1.1.2-1914)}$$

where

$$\beta = 1 - \left(\frac{x_{o,avg}}{r_{o,avg}}\right)^2 \qquad \text{(C-1.1.2-2015)}$$

$$\sigma_{ex} = \frac{\pi^2 E I_{x,avg}}{A_g (K_x L_x)^2} \qquad \text{(C-1.1.2-2116)}$$

$$\sigma_t = \frac{1}{A_g r_{o,avg}^2}\left[GJ_{avg} + \frac{\pi^2 E C_{w,net}}{(K_t L_t)^2}\right] \qquad \text{(C-1.1.2-2217)}$$

The radius of gyration about the shear center is defined as $r_{o,avg}=(r_{x,avg}^2 + r_{y,avg}^2 + x_{o,avg}^2)^{0.5}$, where the "weighted average" x distance from the shear center to the centroid of the cross-section is $x_{o,avg}$

Formatted: Font: Book Antiqua, 12 pt, Not Superscript/ Subscript, Not Raised by / Lowered by

Formatted: Font: 11 pt, Not Superscript/ Subscript, Not Raised by / Lowered by

Formatted: Font: 11 pt, Not Superscript/ Subscript, Not Raised by / Lowered by

Formatted: Not Raised by / Lowered by

Formatted: eq 3, Indent: Left: 0", First line: 0", Line spacing: single, Tab stops: Not at 0.5" + 2" + 3.07" + 3.75" + 5.88"

Field Code Changed

Field Code Changed

Formatted: Not Superscript/ Subscript, Not Raised by / Lowered by

Formatted: Not Superscript/ Subscript, Not Raised by / Lowered by

Formatted: Font: Book Antiqua, 11 pt, Not Superscript/ Subscript, Not Raised by / Lowered by

Formatted: Tab stops: 0.75", Left

Formatted: Tab stops: 0.75", Left + 6.5", Right + Not at 5.88"

Field Code Changed

Field Code Changed

Formatted: Indent: Left: 0", First line: 0"

Formatted: Not Raised by / Lowered by

Formatted: Not Raised by / Lowered by

Formatted: Superscript, Not Raised by / Lowered by

Formatted: Not Raised by / Lowered by

Formatted: Superscript, Not Raised by / Lowered by

Formatted: Not Superscript/ Subscript, Not Raised by / Lowered by

Formatted: Not Raised by / Lowered by

Formatted: Superscript, Not Raised by / Lowered by

Formatted: Superscript, Not Raised by / Lowered by

Formatted: Not Raised by / Lowered by

$$x_{o,avg} = \frac{x_{o,g}L_g + x_{o,net}L_{net}}{L} \qquad \text{(C-1.1.2-1823)}$$

Note that the form of Eq. C-1.1.2-1823 is applicable to a column with holes spaced evenly about its midheight, and can be a viable approximation even when the holes are not evenly spaced.

The radii of gyration about the centroidal axes are $r_{x,avg} = (I_{x,avg} / A_{avg})^{0.5}$ and $r_{y,avg} = (I_{y,avg}/A_{avg})^{0.5}$, where $I_{x,avg}$, $I_{y,avg}$, and A_{avg} are calculated using the same form of Eq. C-1.1.2-2318. Note that the gross cross-sectional area, A_g, in Eqs. C-1.1.2-2114, C-1.1.2-2316, and C-1.1.2-2417 convert the uniform compressive stress at the ends of the column to a force and should not be confused with A_{avg}.

The St. Venant torsional constant, J_{avg}, including the influence of holes, can be calculated using the weighted average approach with the same form of Eq. C-1.1.2-2218. However, the warping torsion constant, C_w, does not follow the weighted average approximation, as the presence of holes prevents warping resistance from developing (Moen and Schafer 2009c). A viable approximation for warping stiffness at the net section is $C_{w,net}$. Note that all net section properties, e.g., $I_{x,net}$, $I_{y,net}$, A_{net}, $x_{o,net}$, $y_{o,net}$, J_{net}, and $C_{w,net}$, can be readily calculated with the built-in section property calculator in the freely available open source program CUFSM (Schafer and Ádány 2006) by setting the element thicknesses to zero at the hole(s), see Moen and Schafer (2010a).

The "weighted average" method is also applicable to cold-formed steel beams with holes. For example, an equivalent form of Eq. C3.1.2.1-14 can be written to calculate the critical elastic buckling moment of beams with singly- and doubly-symmetric cross-sections bending about the symmetry axis

$$M_{cre} = F_e S_f = C_b \frac{\pi}{K_y L_y}\sqrt{EI_{y,avg}\left(GJ_{avg} + EC_{w,net}\frac{\pi^2}{(K_t L_t)^2}\right)} \qquad \text{(C-1.1.2-2419)}$$

Note that holes are incorporated by replacing I_y and J with $I_{y,avg}$ and J_{avg} and by calculating $C_{w,net}$ assuming the cross-section thickness is zero at the hole(s).

Columns with perforation patterns

Perforation patterns in columns may be treated in the same manner as columns with larger, discrete holes with the following change:

$$\sigma_t = \frac{1}{A_g r_{o,avg}^2}\left[GJ_{avg} + \frac{\pi^2 EC_w}{(K_t L_t)^2}\right] \qquad \text{(C-1.1.2-25)}$$

The warping torsion constant C_w is equal to $C_{w,net}$ if n_t is equal to 1 and is equal to $C_{w,avg}$ for all other cases. The use of the weighted average warping torsion constant stems from a perforation pattern's ability to develop warping shear stresses in material located between perforations in pattern arrays. This behavior is observed in Smith and Moen (to appear).

1.1.3 Serviceability Determination

The provisions of this Appendix use a simplified approach to deflection calculations that assume the moment of inertia of the section for deflection calculations is linearly proportional to the strength of the section, determined at the allowable stress of interest. This approximation avoids lengthy effective section calculations for deflection determination.

Formatted: Tab stops: 6.5", Right + Not at 5.88"
Field Code Changed
Formatted: Indent: First line: 0"
Formatted: Not Raised by / Lowered by
Formatted: Not Raised by / Lowered by
Formatted: Not Raised by / Lowered by
Formatted: Superscript, Not Raised by / Lowered by
Formatted: Not Raised by / Lowered by
Formatted: Not Raised by / Lowered by
Formatted: Not Raised by / Lowered by
Formatted: Superscript, Not Raised by / Lowered by
Formatted: Not Raised by / Lowered by
Formatted: Not Raised by / Lowered by
Formatted: Not Raised by / Lowered by
Formatted: Not Raised by / Lowered by
Formatted: Not Raised by / Lowered by
Formatted: Not Raised by / Lowered by
Formatted: Not Raised by / Lowered by
Formatted: Not Raised by / Lowered by
Formatted: Not Raised by / Lowered by
Formatted: Not Raised by / Lowered by
Formatted: Not Raised by / Lowered by
Formatted: Not Raised by / Lowered by
Formatted: Not Raised by / Lowered by
Formatted: Not Raised by / Lowered by
Formatted: Tab stops: 6.5", Right + Not at 5.88"
Field Code Changed
Formatted ...
Formatted: Not Raised by / Lowered by
Formatted: Not Raised by / Lowered by
Formatted: Not Raised by / Lowered by
Formatted: Not Raised by / Lowered by
Formatted: Indent: Hanging: 0.4"
Formatted ...
Formatted ...
Field Code Changed
Formatted ...
Formatted: Font: Book Antiqua, 11 pt
Formatted: Centered

1.2 MEMBERS

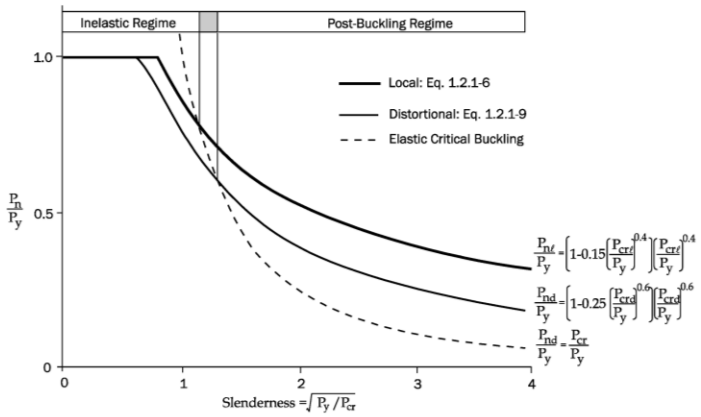

Figure C-1.2.1-1 Local and Distortional Direct Strength Curves for a Braced Column (Pne = Py)

1.2.1 Column Design

Commentary Section C4 provides a complete discussion on the behavior of cold-formed steel columns as it relates to the main *Specification*. This commentary addresses the specific issues raised by the use of the Direct Strength Method of Appendix 1 for the design of cold-formed steel columns. The thin-walled nature of cold-formed columns complicates behavior and design. Elastic buckling analysis reveals at least three buckling modes: local, distortional, and Euler (flexural, torsional, or flexural-torsional) that must be considered in design. Therefore, in addition to usual considerations for steel columns: material non-linearity (e.g., yielding), imperfections, and residual stresses, the individual role and potential for interaction of buckling modes must also be considered. The Direct Strength Method of this Appendix emerged through the combination of more refined methods for local and distortional buckling prediction, improved understanding of the post-buckling strength and imperfection sensitivity in distortional failures, and the relatively large amount of available experimental data.

Fully effective or compact columns are generally well predicted by conventional column curves (AISC, 2001; Galambos, 1998, etc.). Therefore, the long column strength, P_{ne}, follows the same practice as the main *Specification* and uses the AISC (2001) curves for strength prediction. The main *Specification* provides the long column strength in terms of a stress, F_n (Equations C4.1-2 and C4.1-3). In the Direct Strength Method this is converted from a stress to a strength by multiplying the gross area, A_g, resulting in the formulas for P_{ne} given in Appendix 1.

In the main *Specification*, column strength is calculated by multiplying the nominal column

buckling stress, F_n, by the effective area, A_e, calculated at F_n. This accounts for local buckling reductions in the actual column strength (i.e., local-global interaction). In the Direct Strength Method, this calculation is broken into two parts: the long column strength without any reduction for local buckling (P_{ne}) and the long column strength considering local-global interaction ($P_{n\ell}$).

The strength curves for local and distortional buckling of a fully braced column are presented in Figure C-1.2.1-1. The curves are presented as a function of slenderness, which in this case refers to slenderness in the local or distortional mode, as opposed to traditional long column slenderness. Inelastic and post-buckling regimes are observed for both local and distortional buckling modes. The magnitude of the post-buckling reserve for the distortional buckling mode is less than the local buckling mode, as may be observed by the location of the strength curves in relation to the critical elastic buckling curve.

The development and calibration of the Direct Strength provisions for columns are reported in Schafer (2000, 2002). The reliability of the column provisions was determined using the test data of Appendix Section 1.1.1.1 and the provisions of Chapter F of the main *Specification*. Based on a target reliability, β, of 2.5, a resistance factor, ϕ, of 0.84 was calculated for all the investigated columns. Based on this information the safety and resistance factors of Appendix Section 1.2.1 were determined for the pre-qualified members. For the United States and Mexico $\phi = 0.85$ was selected; while for Canada $\phi = 0.80$ since a slightly higher reliability, β, of 3.0 is employed. The safety factor, Ω, was back calculated from ϕ at an assumed dead to live load ratio of 1 to 5. Since the range of pre-qualified members is relatively large, extensions of the Direct Strength Method to geometries outside the pre-qualified set is allowed. Given the uncertain nature of this extension, increased safety factors and reduced resistance factors are applied in that case, per the rational analysis provisions of Section A1.2(b) of the main *Specification*.

The provisions of Appendix 1, applied to the columns of Section 1.1.1.1, are summarized in Figure C-1.2.1-2 below. The controlling strength is either by Appendix 1 Section 1.2.1.2, which considers local buckling interaction with long column buckling, or by Section 1.2.1.3, which considers the distortional mode alone. The controlling strength (minimum predicted of the two modes) is highlighted for the examined members by the choice of marker. Overall performance of the method can be judged by examination of Figure C-1.2.1-2. Scatter exists throughout the data set, but the trends in strength are clearly shown, and further, the scatter (variance) is similar to that of the main *Specification*.

The extension of the DSM approach to columns with holes utilizes the elastic buckling properties of a cold-formed steel column ($P_{cr\ell}$, P_{crd}, and P_{cre}) including the influence of holes to predict ultimate strength. In most cases, holes decrease $P_{cr\ell}$, P_{crd}, and P_{cre}, which increases a column's cross-section and global slenderness and lowers predicted strength. Simplified methods for predicting $P_{cr\ell}$, P_{crd}, and P_{cre} including holes are presented in Section 1.1.2. Alternatively, full finite element elastic eigen-buckling analysis can be performed.

The DSM strength prediction expressions have been modified to limit the maximum strength of a column with holes to the capacity of the net cross section, P_{ynet} (Moen and Schafer, 2011). A transition from P_{ynet}, through the inelastic regime, to the elastic buckling portion of the distortional buckling strength curve has also been included in the design provisions. The transition slope is dictated by the ratio of the net section capacity to gross section capacity, P_{ynet}/P_y, which was derived based on observed trends in column simulations to collapse reported in Moen and Schafer (2009b).

The development and calibration of the Direct Strength provisions for columns with holes was performed with experimental and simulation databases as reported in Moen and Schafer

Formatted: text1

Formatted: Font: Book Antiqua, 11 pt, Not Superscript/ Subscript, Not Raised by / Lowered by , Not Highlight

Formatted: text1, Indent: Left: 0"

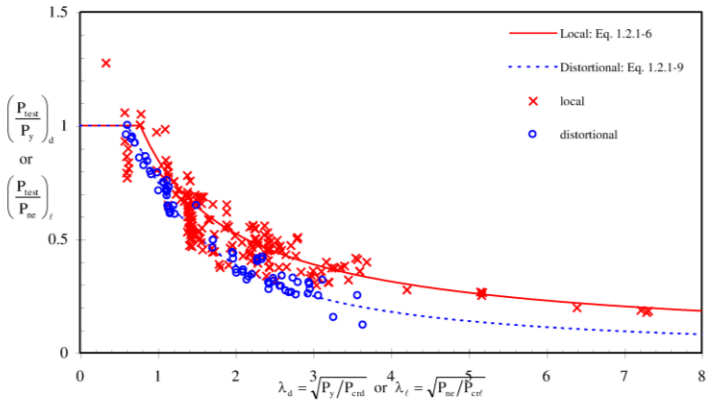

Figure C-1.2.1-2 Direct Strength Method for Concentrically Loaded Pin-Ended Columns

(2009b) and summarized in Moen and Schafer (2011). Note that both databases contained only lipped Cee cross-sections with discrete web holes because this is what was available in the research literature at the time. The philosophy of employing elastic buckling parameters ($P_{cr\ell}$, P_{crd}, P_{cre}) to predict the ultimate strength of cold-formed steel columns with holes was thoroughly validated in Moen and Schafer (2009b), and until more experiments are conducted, it is reasonable to assume that this philosophy holds true for other cross-section shapes.

Resistance factors were calculated by limit state with Chapter F of the main *Specification*. Based on a target reliability, β, of 2.5, the resistance factor, ϕ, was calculated as 0.94 (experiments) and 0.89 (simulations) for columns predicted to fail from local-global buckling interaction. For columns predicted to experience a distortional buckling failure mode, ϕ was calculated as 0.96 (experiments) and 0.91 (simulations).

Formatted: Normal

1.2.1.1 Flexural, Torsional, or Flexural-Torsional Buckling

As discussed in detail above, the strength expressions for long wavelength buckling of columns follow directly from Section C4 of the main *Specification*. These provisions are

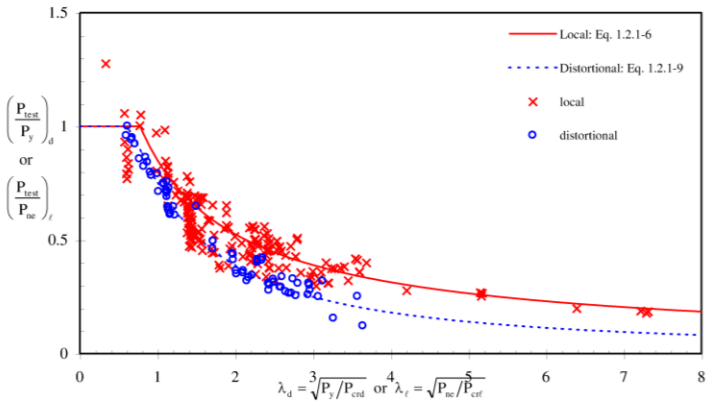

Figure C-1.2.1-2 Direct Strength Method for Concentrically Loaded Pin-Ended Columns

identical to those used for compact section hot-rolled columns in the AISC Specification (2001) and are fully discussed in the *Commentary* to Section C4. The axial elastic strength, P_{ne}, calculated in this section represents the upper bound capacity for a given column. Actual column strength is determined by considering reductions that may occur due to local buckling, and performing a separate check on the distortional mode. See Section 1.1.2 for information on rational analysis methods for calculation of P_{cre} considering columns with or without hole(s).

1.2.1.2 Local Buckling

The expression selected for local buckling of columns is shown in Figure C-1.2.1-1 and Figure C-1.2.1-2 and is discussed in Section 1.2.1. The potential for local-global interaction is presumed, thus the column strength in local buckling is limited to a maximum of the long column strength, P_{ne}. See Section 1.1.2 for information on rational analysis methods for calculation of $P_{cr\ell}$. For columns with holes, $P_{n\ell}$ is limited to P_{ynet} to reflect yielding and collapse of the net section when both local and global column slenderness are low.

1.2.1.3 Distortional Buckling

The expression selected for distortional buckling of columns is shown in Figure C-1.2.1-1 and Figure C-1.2.1-2 and is discussed in Section 1.2.1. Based on experimental test data and on the success of the Australian/New Zealand code (see Hancock et al., 2001 for discussion and Hancock et al. 1994 for further details) the distortional buckling strength is limited to P_y instead of P_{ne}. This presumes that distortional buckling failures are independent of long-column behavior, i.e., little if any distortional-global interaction exists. See Section 1.1.2 for information on rational analysis methods for calculation of P_{crd}.

Figure C-1.2.1-3 compares the distortional buckling strength prediction curve for a column without holes to the prediction curve for the same column with holes, where P_{ynet} =0.80 P_y. For the column with holes, P_{nd} is limited to a maximum strength of P_{ynet}. As distortional-slenderness increases, the prediction transitions from P_{ynet} to the same strength curve used for columns without holes. The transition is implemented to reflect the change in failure mode as slenderness increases, from yielding at the net section to elastic distortional buckling along the column.

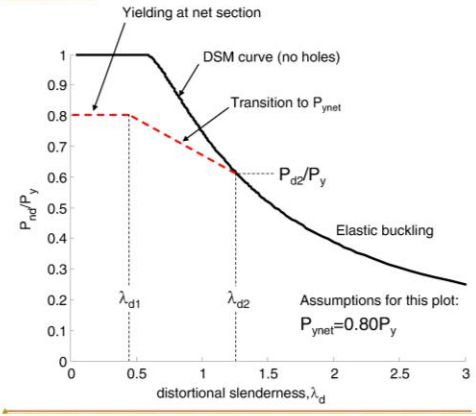

Figure C-1.2.1-3 DSM Distortional Buckling Strength Curve for a Column with Holes

Formatted: Font: Book Antiqua, 11 pt, Strikethrough, Not Superscript/ Subscript, Not Raised by / Lowered by

Formatted: Font: Book Antiqua, 11 pt, Not Superscript/ Subscript, Not Raised by / Lowered by

1.2.2 Beam Design

Commentary Section C3 provides a complete discussion on the behavior of cold-formed steel beams as it relates to the main *Specification*. This commentary addresses the specific issues raised by the use of the Direct Strength Method of Appendix 1 for the design of cold-formed steel beams.

The thin-walled nature of cold-formed beams complicates behavior and design. Elastic buckling analysis reveals at least three buckling modes: local, distortional, and lateral-torsional buckling (for members in strong-axis bending) that must be considered in design. The Direct Strength Method of this Appendix emerged through the combination of more refined methods for local and distortional buckling prediction, improved understanding of the post-buckling strength and imperfection sensitivity in distortional failures, and the relatively large amount of available experimental data.

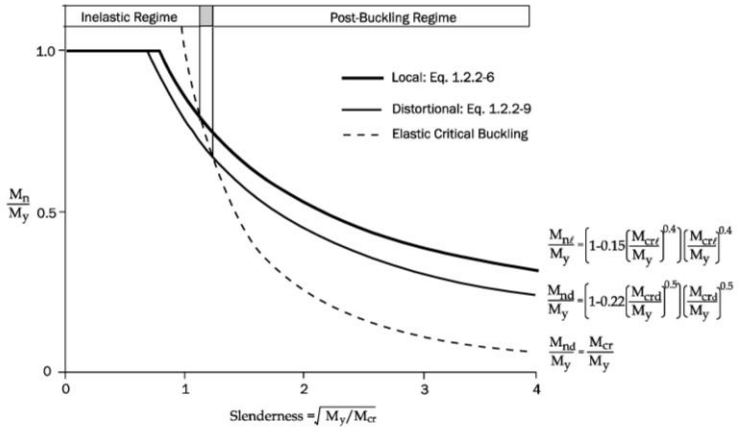

Figure C-1.2.2-1 Local and Distortional Direct Strength Curves for a Braced Beam (Mne = My)

The lateral-torsional buckling strength, M_{ne}, follows the same practice as the main *Specification*. The main *Specification* provides the lateral-torsional buckling strength in terms of a stress, F_c (Equations C3.1.2.1-2, -3, -4 and -5). In the Direct Strength Method, this is converted from a stress to a moment by multiplying by the gross section modulus, S_f, resulting in the formulas for M_{ne} given in Appendix 1.

In the main *Specification*, for beams that are not fully braced and locally unstable, beam strength is calculated by multiplying the predicted stress for failure in lateral-buckling, F_c, by the effective section modulus, S_c, determined at stress F_c. This accounts for local buckling reductions in the lateral-torsional buckling strength (i.e., local-global interaction). In the Direct Strength Method, this calculation is broken into two parts: the lateral-torsional buckling strength without any reduction for local buckling (M_{ne}) and the strength considering local-

global interaction ($M_{n\ell}$).

The strength curves for local and distortional buckling of a fully braced beam are presented in Figure C-1.2.2-1 and compared to the critical elastic buckling curve. While the strength in both the local and distortional modes exhibit both an inelastic regime and a post-buckling regime, the post-buckling reserve for the local mode is predicted to be greater than that of the distortional mode.

The reliability of the beam provisions was determined using the test data of Section 1.1.1.2 and the provisions of Chapter F of the main *Specification*. Based on a target reliability, β, of 2.5, a resistance factor, ϕ, of 0.90 was calculated for all the investigated beams. Based on this information the safety and resistance factors of Appendix Section 1.2.2 were determined for the pre-qualified members. For the United States and Mexico $\phi = 0.90$; while for Canada $\phi = 0.85$ because Canada employs a slightly higher reliability, β, of 3.0. The safety factor, Ω, is back calculated from ϕ at an assumed dead to live load ratio of 1 to 5. Since the range of pre-qualified members is relatively large, extensions of the Direct Strength Method to geometries outside the pre-qualified set is allowed. However, given the uncertain nature of this extension, increased safety factors and reduced resistance factors are applied in that case, per the rational analysis provisions of Section A1.2(b) of the main *Specification*.

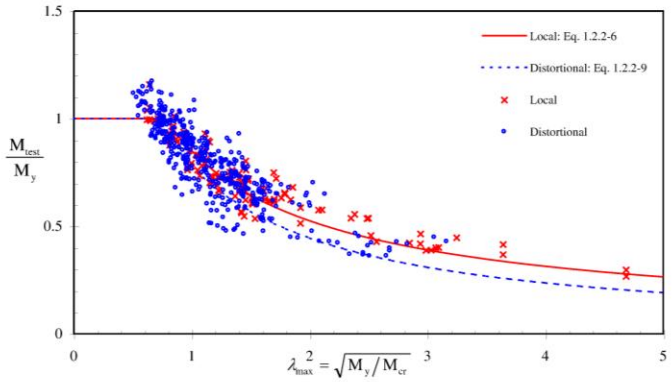

Figure C-1.2.2-2 Direct Strength Method for laterally braced beams

The provisions of Appendix 1, applied to the beams of Section 1.1.1.2, are summarized in Figure C-1.2.2-2. The controlling strength is determined either by Section 1.2.2.2, which considers local buckling interaction with lateral-torsional buckling, or by Section 1.2.2.3, which considers the distortional mode alone. The controlling strength (minimum predicted of the two modes) is highlighted for the examined members by the choice of marker. Overall performance of the method can be judged by examination of Figure C-1.2.2-2. The scatter shown in the data is similar to that of the main *Specification*.

1.2.2.1 Lateral-Torsional Buckling

As discussed in detail above, the strength expressions for lateral-torsional buckling of beams follow directly from Section C3 of the main *Specification* and are fully discussed in Section C3 of the *Commentary*. The lateral-torsional buckling strength, M_{ne}, calculated in this section represents the upperbound capacity for a given beam. Actual beam strength is determined by considering reductions that may occur due to local buckling and performing a separate check on the distortional mode. See Section 1.1.2 for information on rational analysis methods for calculation of M_{cre}.

1.2.2.2 Local Buckling

The expression selected for local buckling of beams is shown in Figures C-1.2.2-1 and C-1.2.2-2 and is discussed in Section 1.2.2. The use of the Direct Strength Method for local buckling and the development of the empirical strength expression is given in Schafer and Peköz (1998). The potential for local-global interaction is presumed; thus, the beam strength in local buckling is limited to a maximum of the lateral-torsional buckling strength, M_{ne}. For fully braced beams, the maximum M_{ne} value is the yield moment, M_y. See Section 1.1.2 for information on rational analysis methods for calculation of $M_{cr\ell}$.

1.2.2.3 Distortional Buckling

The expression selected for distortional buckling of beams is shown in Figures C-1.2.2-1 and C-1.2.2-2 and is discussed in Section 1.2.2. Based on experimental test data and on the success of the Australian/New Zealand code (see Hancock, 2001 for discussion) the distortional buckling strength is limited to M_y instead of M_{ne}. This presumes that distortional buckling failures are independent of lateral-torsional buckling behavior, i.e., little if any distortional-global interaction exists. See Section 1.1.2 for information on rational analysis methods for calculation of M_{crd}.

APPENDIX 1 REFERENCES

Acharya, V.V. and R.M. Schuster (1998), "Bending Tests of Hat Section with Multiple Longitudinal Stiffeners," *Proceedings of the Fourteenth International Specialty Conference on Cold-Formed Steel Structures*, University of Missouri-Rolla, Rolla, MO, October, 1998.

American Institute of Steel Construction (2001), *Manual of Steel Construction: Load and Resistance Factor Design*, 3rd Edition, American Institute of Steel Construction, Chicago, IL.

American Iron and Steel Institute (2002), *Cold-Formed Steel Design Manual*, American Iron and Steel Institute, Washington, DC.

Bambach, M.R., J.T. Merrick and G.J. Hancock (1998), "Distortional Buckling Formulae for Thin Walled Channel and Z-Sections with Return Lips," *Proceedings of the 14th International Specialty Conference on Cold-Formed Steel Structures*, University of Missouri-Rolla, Rolla, MO, October 1998, 21-38.

Bernard, E.S. (1993), "Flexural Behavior of Cold-Formed Profiled Steel Decking," Ph.D. Thesis, University of Sydney, Australia.

Chajes, A. (1974). *Principles of Structural Stability*, Prentice Hall College Div, Englewood Cliffs, NJ.

Cheung, Y.K. and L.G. Tham (1998), *Finite Strip Method*, CRC Press, 1998.

Cohen, J. M. (1987), "Local Buckling Behavior of Plate Elements," Department of Structural Engineering Report, Cornell University, Ithaca, NY, 1987.

Cook, R.D., D.S. Malkus and M.E. Plesha (1989), *Concepts and Applications of Finite Element Analysis,* John Wiley & Sons, Third Edition.

Davies, J.M. and C. Jiang (1996), "Design of Thin-Walled Beams for Distortional Buckling," *Proceedings of the Thirteenth International Specialty Conference on Cold-Formed Steel Structures*, University of Missouri-Rolla, Rolla, MO, October 1996, 141-154.

Davies, J.M., C. Jiang and V. Ungureanu (1998), "Buckling Mode Interaction in Cold-Formed Steel Columns and Beams," *Proceedings of the Fourteenth International Specialty Conference on Cold-Formed Steel Structures*, University of Missouri-Rolla, Rolla, MO, October 1998, 53-68.

Davies, J.M., P. Leach, D. Heinz (1994), "Second-Order Generalised Beam Theory." *Journal of Constructional Steel Research*, Elsevier, 31 (2-3) 221-242.

Desmond, T.P. (1977), "The Behavior and Design of Thin-Walled Compression Elements with Longitudinal Stiffeners," Ph.D. Thesis, Cornell University, Ithaca, NY, 1777.

Ellifritt, D., B. Glover and J. Hren (1997), "Distortional Buckling of Channels and Zees Not Attached to Sheathing," Report for the American Iron and Steel Institute, Washington DC, 1997.

El-Sawy, K.M., and A. S. Nazmy (2001). "Effect of aspect ratio on the elastic buckling of uniaxially loaded plates with eccentric holes." *Thin-Walled Structures*, 39(12), 983-998.

Elzein, A. (1991), *Plate Stability by Boundary Element Method*, Springer-Verlag, NY, 1991.

Galambos, T.V. (1998), *Guide to Stability Design Criteria for Metal Structures,* John Wiley & Sons, the Fifth Edition.

Hancock, G.J. (1997), "Design for Distortional Buckling of Flexural Members," *Thin-Walled Structures*, 27(1), 3-12, Elsevier Science Ltd.

Hancock, G.J., Y.B. Kwon and E.S. Bernard (1994), "Strength Design Curves for Thin-Walled Sections Undergoing Distortional Buckling," *Journal of Constructional Steel Research*, Elsevier, 31(2-3), 169-186.

Hancock, G.J., T.M. Murray and D.S. Ellifritt (2001), *Cold-Formed Steel Structures to the AISI Specification,* Marcell-Dekker, New York, NY.

Hancock, G.J., C.A. Rogers and R.M. Schuster (1996) "Comparison of the Distortional Buckling Method for Flexural Members with Tests." *Proceedings of the Thirteenth International Specialty Conference on Cold-Formed Steel Structures*, University of Missouri-Rolla, Rolla, MO, October 1998, 125-140.

Harik, I.E., X. Liu and R. Ekambaram (1991), "Elastic Stability of Pates with Varying Rigidities," Computers and Structures, 38 (2) 161-168.

Höglund, T. (1980), "Design of Trapezoidal Sheeting Provided with Stiffeners in the Flanges and Webs," *Swedish Council for Building Research*, Stockholm, Sweden, D28:1980.

Kawai, T., and H. Ohtsubo (1968). "A Method of Solution for the Complicated Buckling Problems of Elastic Plates with Combined Use of Rayleigh-Ritz's Procedure in the Finite Element Method." *Proceedings of the Second Conference on Matrix Methods in Structural Mechanics*, AFFDL-TR-68-150, Wright-Patterson Air Force Base, Ohio, 967-994.

König, J. (1978), "Transversally Loaded Thin-Walled C-Shaped Panels With Intermediate Stiffeners," *Swedish Council for Building Research*, Stockholm, Sweden, D7:1978.

Kwon, Y.B. and G.J. Hancock (1992), "Strength Tests of Cold-Formed Channel Sections undergoing Local and Distortional Buckling," *Journal of Structural Engineering*, ASCE, Vol. 117, No. 2, 1786 – 1803.

Kumai, T. (1952). "Elastic stability of the square plate with a central circular hole under edge thrust." *Reports of Research Institute for Applied Mechanics*, I(2).

LaBoube, R.A. and W. W. Yu (1978), "Structural Behavior of Beam Webs Subjected to Bending Stress," *Civil Engineering Study Structural Series*, 78-1, Department of Civil Engineering, University of Missouri-Rolla, Rolla, MO.

Lau, S.C.W., and G.J Hancock (1987),. "Distortional Buckling Formulas for Channel Columns," *Journal of Structural Engineering*, ASCE, Vol. 113, No. 5, 1063 – 1078.

Loughlan, J. (1979), "Mode Interaction in Lipped Channel Columns under Concentric or Eccentric Loading," Ph.D. Thesis, University of Strathclyde, Glasgow.

Miller, T.H. and T. Peköz (1994), "Load-Eccentricity Effects on Cold-Formed Steel Lipped- Channel Columns," *Journal of Structural Engineering*, ASCE, Vol. 120, No. 3, 805-823.

Moen, C.–D., and B.–W. Schafer (2009a). "Elastic buckling of thin plates with holes in compression or bending." *Thin-Walled Structures*, 47(12), 1597-1607.

Moen, C.D., and B.–W. Schafer (2009b). *Direct Strength Design for Cold-Formed Steel Members with Holes, Final Report*, American Iron and Steel Institute, Washington, D.C.

Moen, C.-D., and B.-W. Schafer, (2009c). "Elastic buckling of cold-formed steel columns and beams with holes." *Engineering Structures*, 31(12), 2812-2824.

Moen, C.–D., and B.–W. Schafer (2010a). "Direct Strength Design of Cold-Formed Steel Columns with Holes." 2010 Annual Technical Session and Meeting, Structural Stability Research Council, Orlando, FL.

Moen, C.–D., and B.–W. Schafer (2010b). "Extending Direct Strength Design to Cold-Formed Steel Beams with Holes." Twentieth International Specialty Conference on Cold-Formed Steel Structures, St. Louis, MO.

Moen, C.–D., and B.–W. Schafer (2011). "Direct Strength Method for Design of Cold-Formed Steel Columns with Holes." *ASCE Journal of Structural Engineering*, 137(5), 559-570.

Moreyra, M.E. (1993), "The Behavior of Cold-Formed Lipped Channels under Bending," M.S. Thesis, Cornell University, Ithaca, NY.

Mulligan, G.P. (1983), "The Influence of Local Buckling on the Structural Behavior of Singly-Symmetric Cold-Formed Steel Columns," Ph.D. Thesis, Cornell University, Ithaca, NY.

Papazian, R.P., R.M. Schuster and M. Sommerstein (1994), "Multiple Stiffened Deck Profiles," *Proceedings of the Twelfth International Specialty Conference on Cold-Formed Steel Structures*, University of Missouri-Rolla, Rolla, MO, October, 1994, 217-228.

Formatted: ref

Formatted: ref

Formatted: ref

Formatted: Font: (Default) Book Antiqua, 11 pt, Italic, Not Superscript/ Subscript, Not Raised by / Lowered by

Formatted: Font: (Default) Book Antiqua, 11 pt, Not Superscript/ Subscript, Not Raised by / Lowered by

Formatted: ref, Indent: Left: 0", First line: 0"

Formatted: Font: (Default) Book Antiqua, 11 pt, Not Superscript/ Subscript, Not Raised by / Lowered by

Formatted: Font: (Default) Book Antiqua, 11 pt, Not Superscript/ Subscript, Not Raised by / Lowered by

Formatted: Font: (Default) Book Antiqua, 11 pt, Not Superscript/ Subscript, Not Raised by / Lowered by

Formatted: ref

Formatted: Font: (Default) Book Antiqua, 11 pt, Italic, Not Superscript/ Subscript, Not Raised by / Lowered by

Formatted: Font: Book Antiqua, 11 pt, Italic, Not Superscript/ Subscript, Not Raised by / Lowered by

Formatted: Font: Book Antiqua, 11 pt, Not Italic, Not Superscript/ Subscript, Not Raised by / Lowered by

Formatted: Font: Book Antiqua, 11 pt, Not Superscript/ Subscript, Not Raised by / Lowered by

Phung, N., and W.W. Yu (1978), "Structural Behavior of Longitudinally Reinforced Beam Webs," *Civil Engineering Study Structural Series*, Department of Civil Engineering, 78-6, University of Missouri-Rolla, MO.

Polyzois, D., and P. Charnvarnichborikarn (1993), "Web-Flange Interaction in Cold-Formed Steel Z-Section Columns," *Journal of Structural Engineering*, ASCE, Vol. 119, No. 9, 2607-2628.

Pu, Y., M.H.R. Godley, R.G. Beale, H.H. Lau (1999), "Prediction of Ultimate Capacity of Perforated Lipped Channels," *Journal of Structural Engineering*, ASCE, Vol. 125, No. 5, 510-514.

Quispe, L., G.J. Hancock (2002), "Direct Strength Method for the Design of Purlins," *Proceedings of the 16th International Specialty Conference on Cold-Formed Steel Structures*, University of Missouri-Rolla, Rolla, MO, October 2002, 561-572.

Rhodes, J., and M. Macdonald (1996), "The Effects of Perforation Length on the Behaviour of Perforated Elements in Compression," *Proceedings of the 13th Internation Specialty Conference on Cold-Formed Steel Structures*, St. Louis, MO.

Rogers, C.A. (1995), "Interaction Buckling of Flange, Edge Stiffener and Web of C-Sections in Bending," M.S. Thesis, University of Waterloo, Ontario, Canada.

Sarawit, A. (2003). "Cold-Formed Steel Frame and Beam-Column Design," Ph.D. Thesis, Cornell University, Ithaca.

Schafer, B.W. (1997), "Cold-Formed Steel Behavior and Design: Analytical and Numerical Modeling of Elements and Members with Longitudinal Stiffeners," Ph.D. Thesis, Cornell University, Ithaca, NY.

Schafer, B.W. (2000), "Distortional Buckling of Cold-Formed Steel Columns: Final Report," Sponsored by the American Iron and Steel Institute, Washington, DC.

Schafer, B.W. (2001), "Progress Report 2: Test Verification of the Effect of Stress Gradient on Webs of Cee and Zee Sections," submitted to the AISI and MBMA, July 2001.

Schafer, B.W. (2002), "Local, Distortional, and Euler Buckling in Thin-walled Columns," *Journal of Structural Engineering*, ASCE, Vol. 128, No. 3, 289-299.

Schafer, B.W. (2002b), "Progress on the Direct Strength Method," *Proceedings of the 16th International Specialty Conference on Cold-Formed Steel Structures*, Orlando, FL. 647-662.

Schafer, B.W., and Ádány, S. (2006). "Buckling analysis of cold-formed steel members using CUFSM: conventional and constrained finite strip methods." *Proceeding of Eighteenth International Specialty Conference on Cold-Formed Steel Structures*, Orlando, FL.

Schafer, B.W., Sarawit, A., Peköz, T. (2006). "Complex edge stiffeners for thin-walled members." *Journal of Structural Engineering, ASCE*, Vol. 132, No. 2, 212-226.

Schafer, B.W., T. Peköz, (1998), "Direct Strength Prediction of Cold-Formed Steel Members using Numerical Elastic Buckling Solutions," *Proceedings of the Fourteenth International Specialty Conference on Cold-Formed Steel Structures,* University of Missouri-Rolla, Rolla, MO, October 1998.

Schafer, B.W. and T. Peköz, (1999), "Laterally Braced Cold-Formed Steel Flexural Members with Edge Stiffened Flanges." *Journal of Structural Engineering,* ASCE, Vol. 125, No. 2.

Schardt, R. (1989), *Verallgemeinerte Technische Biegetheorie [Generalized Beam Theory]*, Springer-Verlag, Berlin.

Formatted: Font: Book Antiqua, 11 pt, Superscript, Not Raised by / Lowered by

Formatted: ref

Formatted: Font: Book Antiqua, 11 pt, Italic, Not Superscript/ Subscript, Not Raised by / Lowered by

Schardt, R. and W. Schrade (1982), "Kaltprofil-Pfetten," Institut Für Statik, Technische Hochschule Darmstadt, Bericht Nr. 1, Darmstadt.

Schlack Jr., A.L. (1964). "Elastic stability of pierced square plates." *Experimental Mechanics*, 4(6), 167-172.

Schuster, R.M. (1992), "Testing of Perforated C-Stud Sections in Bending," Report for the Canadian Sheet Steel Building Institute, University of Waterloo, Waterloo Ontario, Canada.

Shan, M., R.A. LaBoube and W. W. Yu (1994), "Behavior of Web Elements with Openings Subjected to Bending, Shear and the Combination of Bending and Shear," *Civil Engineering Study Structural Series*, 94-2, Department of Civil Engineering, University of Missouri-Rolla, Rolla, MO.

Silvestre, N. and D. Camotim (2002a), "First-Order Generalised Beam Theory for Arbitrary Orthotropic Materials," *Thin-Walled Structures*, Elsevier. Vol. 40, 755-789.

Silvestre, N. and D. Camotim (2002b), "Second-Order Generalised Beam Theory for Arbitrary Orthotropic Materials," *Thin-Walled Structures*, Elsevier. Vol. 40, 791-820.

Smith, F.H. and C.D. Moen (to appear), "Elastic buckling solutions for thin-walled metal columns with perforation patterns," *Thin-Walled Structures*.

Thomasson, P. (1978), "Thin-walled C-shaped Panels in Axial Compression," *Swedish Council for Building Research*, D1:1978, Stockholm, Sweden.

Timoshenko, S.P., Gere, James M. (1961). *Theory of Elastic Stability*, McGraw-Hill, New York.

Willis, C.T. and B. Wallace (1990), "Behavior of Cold-Formed Steel Purlins under Gravity Loading," *Journal of Structural Engineering*, ASCE. Vol. 116, No. 8.

Yu, W.W. (2000), *Cold-Formed Steel Design*, John Wiley & Sons, Inc.

Zienkiewicz, O.C. and R.L. Taylor (1989), *The Finite Element Method: Volume 1 Basic Formulations and Linear Problems*, McGraw Hill, the Fourth Edition.

Zienkiewicz, O.C. and R.L. Taylor (1991), *The Finite Element Method: Volume 2 Solid and Fluid Mechanics Dynamics and Non-linearity*, McGraw Hill, the Fourth Edition.

Formatted: Font: Book Antiqua, 11 pt, Italic, Not Superscript/ Subscript, Not Raised by / Lowered by

Formatted: ref

Formatted: Font: Italic

Formatted: ref

Formatted: Font: Book Antiqua, 11 pt, Italic, Not Superscript/ Subscript, Not Raised by / Lowered by

APPENDIX C. PERFORATION PATTERN DESIGN EXAMPLE

DSM Design Example: Rack column with perforation pattern

This example problem investigates how strength of a perforated rack column may be determined using the Direct Strength Method (DSM). The section investigated is taken from research by Damien Koen at the University of Sydney. His thesis on capacity of pallet rack columns can be found at the following website:

http://prijipati.library.usyd.edu.au/handle/2123/3880

Problem statement

Using the Direct Strength Method, determine the compressive strength, P_n, of the 2550mm long 9024 cross-section experimentally tested by Koen (2008).

Background

Cross-sectional geometry - 9024 section (Figure A1, Koen, 2008)

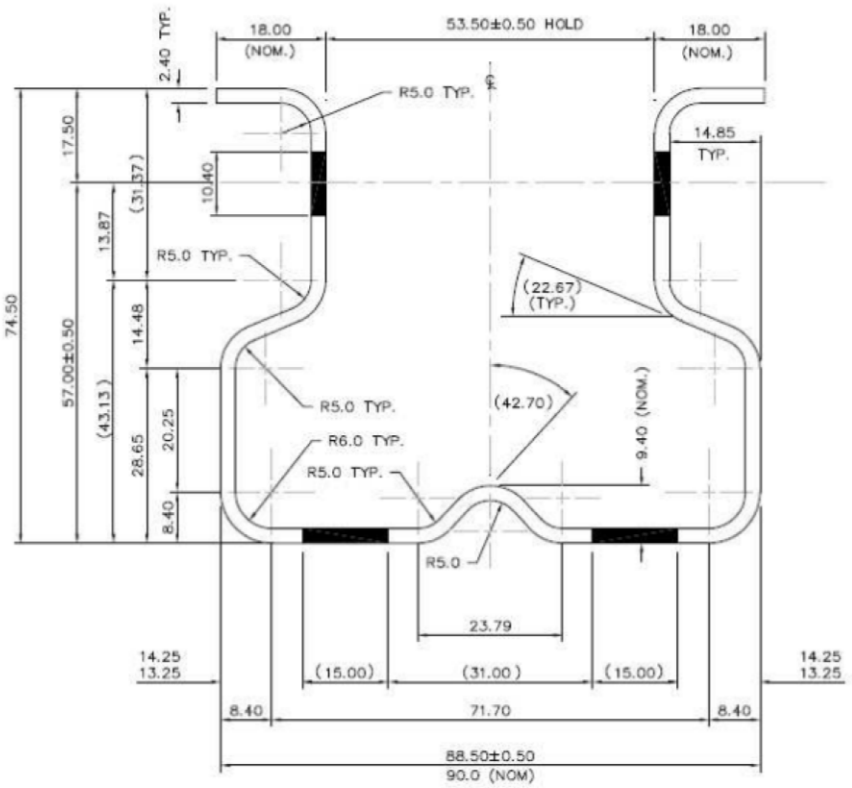

2.4mm UPRIGHT PROFILE EXTENDED REAR FLANGE SECTION DIMENSIONS

( ) = REFERENCE DIMENSION

Perforation geometry - 9024 section (Figure A2, Koen, 2008)

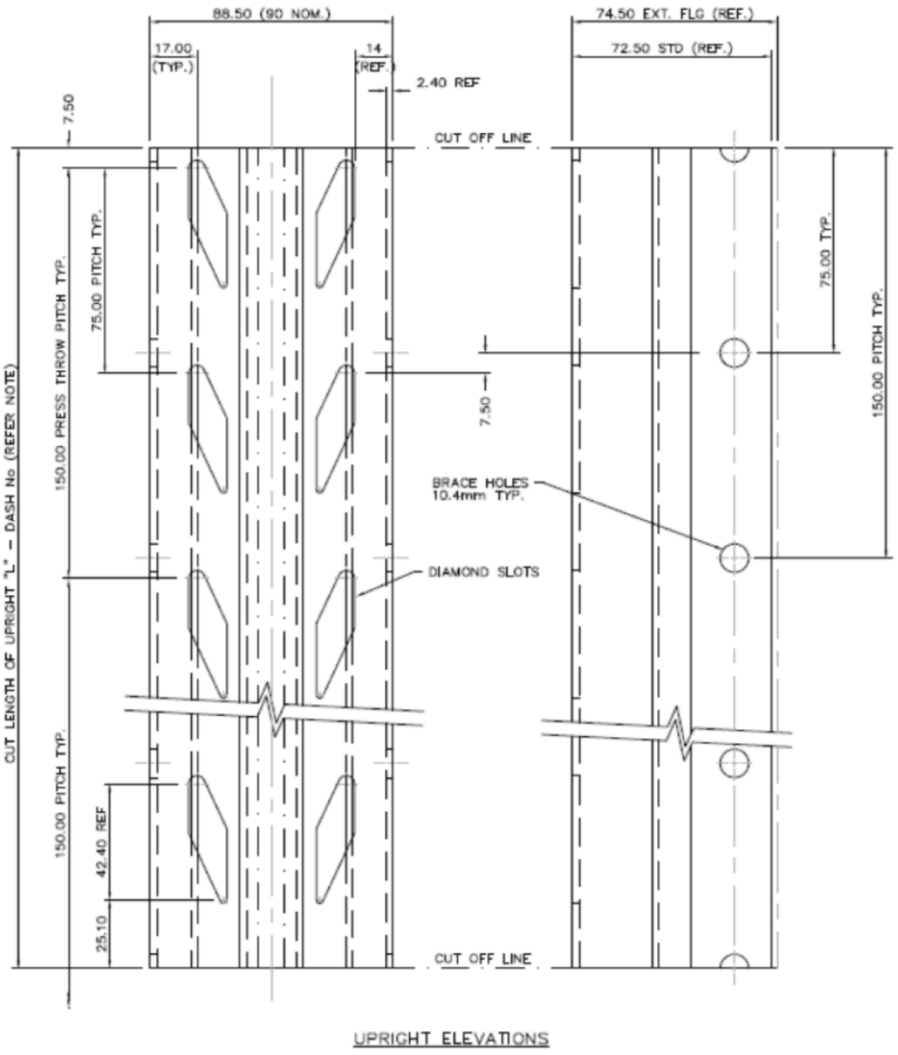

Model properties

Tensile coupon elastic modulus	$E := 225GPa$	(Table 4, Koen, 2008)
Tensile coupon yield stress	$F_y := 550MPa$	(Table 4, Koen, 2008)
Poisson's ratio	$\mu := 0.3$	(Appendix C4, Koen, 2008)
Measured member length	$L := 2547mm$	(Table 3, Koen, 2008)
Measured member thickness	$t := 2.39mm$	(pp 22, Koen, 2008)
Shear modulus	$G := \frac{E}{2 \cdot (1 + \mu)} = 86.5 \cdot GPa$	

Bracing and boundary conditions

"The support conditions at the top and bottom of the loaded upright were such that the upright could freely rotate at each end about the section's x-axis (see Figure A4 for axis system) only and was fixed against rotations about the y-axis and z-axis. The translational restraints allowed the upright to move in the vertical z-direction at the top where the load was applied, however all other translations were fixed." (pp 25, Koen, 2008)

"The rotational restraints at the ends of the uprights were positioned at the pivot point locations in the experimental tests. This was at a distance to the top and bottom ends of the uprights equal to 50mm and 60mm respectively." (pp 39, Koen, 2008)

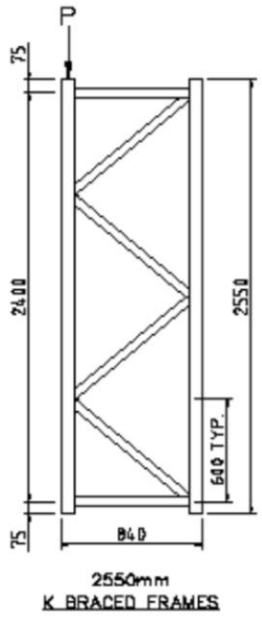

(Figure 1, Koen, 2008)

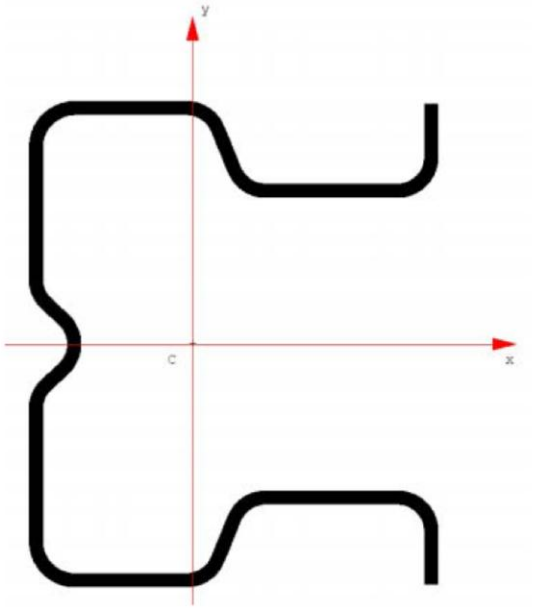

(Figure A4, Koen, 2008)

Because of CUFSM's naming convention, we will use the z-axis to represent Koen's y-axis, and the torsional axis, or t-axis, to represent Koen's z-axis.

Effective x-axis length $KL_x := L + 50mm + 60mm = 2657 \cdot mm$

Effective z-axis length $KL_z := \min(0.5L, 2 \cdot 600mm) = 1200 \cdot mm$

Effective t-axis length $KL_t := 0.5 \cdot L = 1273.5 \cdot mm$

Note that the effective z-axis length does not consider the bracing layout's contribution and is thus overly conservative. Koen has back calculated an effective length for this axis using the Euler buckling equation and a two dimensional buckling analysis. We will modify our effective z-axis length based on his findings (pp 66, Koen, 2008).

Modified effective z-axis length $KL_z := 896mm \cdot \frac{L}{2550mm} = 894.9 \cdot mm$

Gross and net section properties

The section properties presented are found using the cross-sectional property calculator within CUFSM.

Assumptions

Holes are treated using approximate rectangular perforations that bound the true diamond and circular perforation shapes. It is assumed that circular perforation shapes are located along the length of the cross-section such that they are alligned with the diamond shaped perforations. To treat the cross-section, the gross section and two separate cross-sections - one with both the diamond and circular perforations, another with just the diamond perforations - must be considered. Assumed perforation dimensions are as follows:

Diamond perforation length	$L_{h\_dmd} := 42.4mm$
Diamond perforation width	$d_{h\_dmd} := 15mm$
Diamond perforation longitudinal spacing	$s_{l\_dmd} := 75mm$
Circular perforation length	$L_{h\_crc} := 10.4mm$
Cicular perforation width	$d_{h\_crc} := 10.4mm$
Circular perforation longitudinal spacing	$s_{l\_crc} := 75mm$

Nodal coordinates

Nodal coordinates used to calculate gross cross-sectional properties are taken from information in Figure A1 and Figure A32 (Koen, 2008). These coordinates are modified to include perforations for net section calculations. A summary of the inputs used in CUFSM may be found in the supplementary Excel workbook.

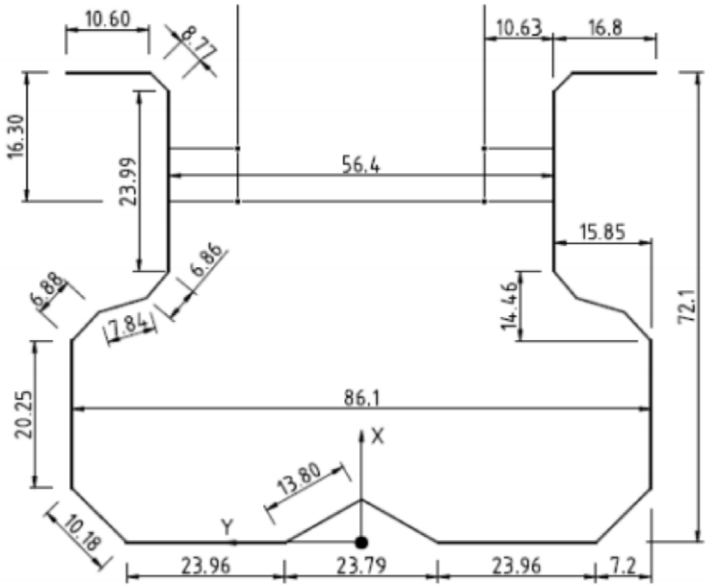

(Figure A32, Koen, 2008)

Gross section properties - 2.39mm thickness

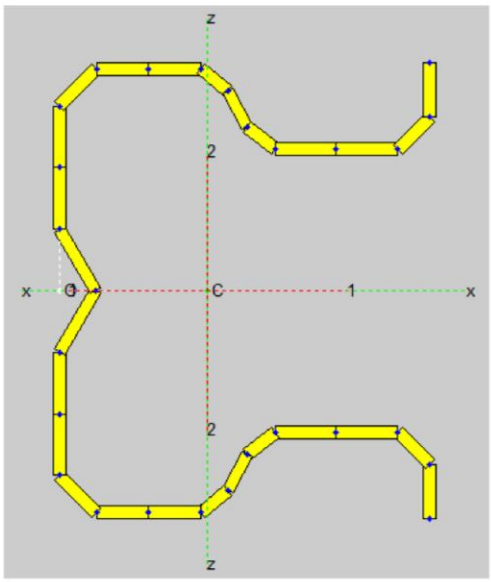

Area $A_g := 636.8\text{mm}^2$

Moment of inertia, x-axis $I_{xg} := 663300\text{mm}^4$

Moment of inertia, z-axis $I_{zg} := 430400\text{mm}^4$

Radius of gyration, x-axis $r_{xg} := \left(\frac{I_{xg}}{A_g}\right)^{0.5} = 32.27\cdot\text{mm}$

Radius of gyration, z-axis $r_{zg} := \left(\frac{I_{zg}}{A_g}\right)^{0.5} = 26.00\cdot\text{mm}$

St. Venant torsion constant $J_g := 1213\text{mm}^4$

Warping torsion constant $C_{wg} := 704500000\text{mm}^6$

Dist, centroid to shear center, x-axis $x_{og} := -63.88\text{mm}$

Radius of gyration, shear center $r_{og} := \left(r_{xg}^2 + r_{zg}^2 + x_{og}^2\right)^{0.5} = 76.15\cdot\text{mm}$

Net section A properties - 2.39mm thickness

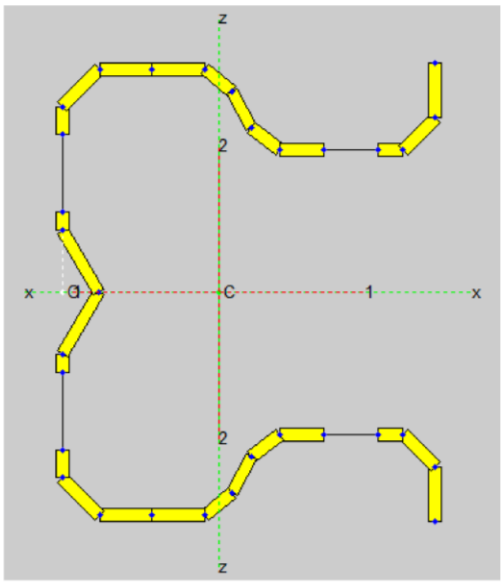

Area	$A_{nA} := 515.4\text{mm}^2$
Moment of inertia, x-axis	$I_{xnA} := 586600\text{mm}^4$
Moment of inertia, z-axis	$I_{znA} := 333100\text{mm}^4$
Radius of gyration, x-axis	$r_{xnA} := \left(\frac{I_{xnA}}{A_{nA}}\right)^{0.5} = 33.74\cdot\text{mm}$
Radius of gyration, z-axis	$r_{znA} := \left(\frac{I_{znA}}{A_{nA}}\right)^{0.5} = 25.42\cdot\text{mm}$
St. Venant torsion constant	$J_{nA} := 981.3\text{mm}^4$
Warping torsion constant	$C_{wnA} := 530800000\text{mm}^6$
Dist, centroid to shear center, x-axis	$x_{onA} := -64.35\text{mm}$
Radius of gyration, shear center	$r_{onA} := \left(r_{xnA}^2 + r_{znA}^2 + x_{onA}^2\right)^{0.5} = 76.98\cdot\text{mm}$

Net section B properties - 2.39mm thickness

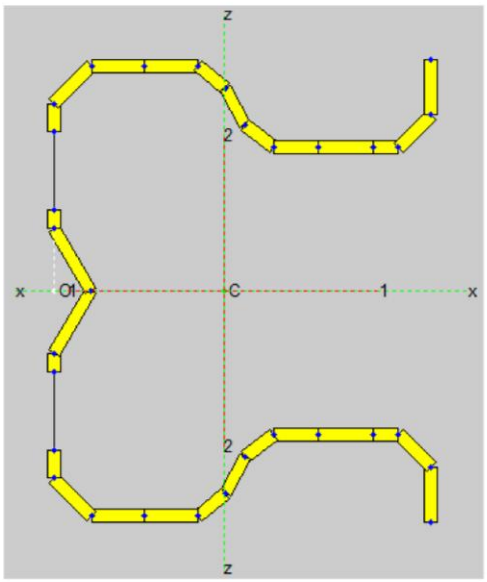

Area	$A_{nB} := 565.1\,mm^2$
Moment of inertia, x-axis	$I_{xnB} := 624100mm^4$
Moment of inertia, z-axis	$I_{znB} := 362900mm^4$
Radius of gyration, x-axis	$r_{xnB} := \left(\frac{I_{xnB}}{A_{nB}}\right)^{0.5} = 33.23 \cdot mm$
Radius of gyration, z-axis	$r_{znB} := \left(\frac{I_{znB}}{A_{nB}}\right)^{0.5} = 25.34 \cdot mm$
St. Venant torsion constant	$J_{nB} := 1076.mm^4$
Warping torsion constant	$C_{wnB} := 642700000mm^6$
Dist, centroid to shear center, x-axis	$x_{onB} := -69.97mm$
Radius of gyration, shear center	$r_{onB} := \left(r_{xnB}^2 + r_{znB}^2 + x_{onB}^2\right)^{0.5} = 81.50 \cdot mm$

Gross and net section squash loads - 2.39mm thickness

Gross section squash load	$P_y := A_g \cdot F_y = 350.2 \cdot kN$
Net section squash load	$P_{ynet} := \min\left(A_{nA}, A_{nB}\right) \cdot F_y = 283.5 \cdot kN$

Elastic buckling analysis

An elastic buckling analysis is the first step in determining the column capacity using the DSM. Simplified methods presented by Smith and Moen (to appear) will be used in calculating the critical elastic buckling loads - P_{crl}, P_{crd}, and P_{cre}.

Finite strip modeling assumptions

The 9024 cross-section leaves decisions to be made by the designer when modeling the shape for finite strip analyses:

1. Treatment of radiused corners - This will be done by using the gross-section model (see *Gross section properties*) with appropriate reduced thicknesses for the determination of the critical buckling loads. If an indistinct buckling mode arises, buckled half-wavelengths will be determined by the confined finite strip method using a simplified cross-section without corner radii as shown below:

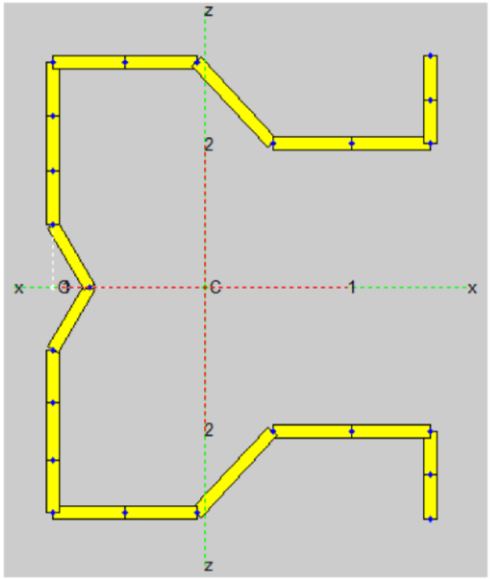

Reduced thicknesses should be used when finding half-wavelengths as perforations are known to affect this property (Smith and Moen, to appear). Half-wavelengths found using the sharp-corners model will be used to determine the critical buckling loads using results from the model with radii.

2. Treatment of boundary conditions - The effective lengths previously mentioned will be used to determine critical buckling loads. Half-wavelengths to be considered are taken from Appendix C2 (Koen, 2008).

Local buckling

Elemental Buckling

The model presented by Smith and Moen (to appear) to treat local buckling of cross-sections with perforation patterns determines a reduced thickness for elements within the cross-section that feature perforation patterns. The reduced thickness equation derived is applicable only to patterns that are centered within the element. While perforations located within the flange and web elements are not centered, we will assume the reduced thickness equations to remain applicable.

It should be noted that since a stiffener breaks the web into two different sections, the reduced web thickness will be found using the flat elements to either side of the stiffener.

Reduced flange element thickness

Number of longitudinal perforations $n_l := \text{ceil}\left(\frac{L}{s_{l\_crc}}\right) = 34$

Number of transverse perforations $n_t := 1$

Width of perforated flange element $b_f := 23.97\text{mm}$

Longitudinal perforation shape factor $\alpha := \frac{b_f}{\pi}\cdot\sin\left(\frac{\pi\cdot L_{h\_crc}}{b_f}\right) = 7.466\cdot\text{mm}$

Transverse perforation shape factor $\beta := \frac{b_f}{\pi}\cdot\sin\left(\frac{\pi\cdot d_{h\_crc}}{b_f}\right) = 7.466\cdot\text{mm}$

Longitudinal perforation pattern factor $X' := -1$

Transverse perforation pattern factor $Y' := \begin{cases} 0 & \text{if } n_t = 1 \\ -1 & \text{otherwise} \end{cases} = 0$

$$t_{rl\_fl} := t\cdot\left[1 - \frac{n_l\cdot n_t\cdot\left(L_{h\_crc}\cdot d_{h\_crc} - \mu\cdot d_{h\_crc}\cdot\alpha\cdot X' - \mu\cdot L_{h\_crc}\cdot\beta\cdot Y' + \alpha\cdot X'\cdot\beta\cdot Y'\right)}{L\cdot b_f}\right]^{\frac{1}{2}}$$

Reduced flange element thickness $t_{rl\_fl} = 2.301\cdot\text{mm}$

Reduced web element thickness

Number of longitudinal perforations $n_l := \text{ceil}\left(\frac{L}{s_{l\_dmd}}\right) = 34$

Number of transverse perforations $n_t := 1$

Width of perforated web element $b_w := 23.96\text{mm}$

Longitudinal perforation shape factor $\alpha := \frac{b_w}{\pi}\cdot\sin\left(\frac{\pi\cdot L_{h\_dmd}}{b_w}\right) = -5.051\cdot mm$

Transverse perforation shape factor $\beta := \frac{b_w}{\pi}\cdot\sin\left(\frac{\pi\cdot d_{h\_dmd}}{b_w}\right) = 7.037\cdot mm$

Longitudinal perforation pattern factor $X' := -1$

Transverse perforation pattern factor $Y' := \begin{cases} 0 & \text{if } n_t = 1 \\ -1 & \text{otherwise} \end{cases} = 0$

$$t_{rl\_w} := t\cdot\left[1 - \frac{n_l\cdot n_t\cdot\left(L_{h\_dmd}\cdot d_{h\_dmd} - \mu\cdot d_{h\_dmd}\cdot\alpha\cdot X' - \mu\cdot L_{h\_dmd}\cdot\beta\cdot Y' + \alpha\cdot X'\cdot\beta\cdot Y'\right)}{L\cdot b_w}\right]^{\frac{1}{2}}$$

Reduced web element thickness $t_{rl\_w} = 1.939\cdot mm$

Confined finite strip method local buckling half-wavelength using sharp-cornered, reduced thickness model

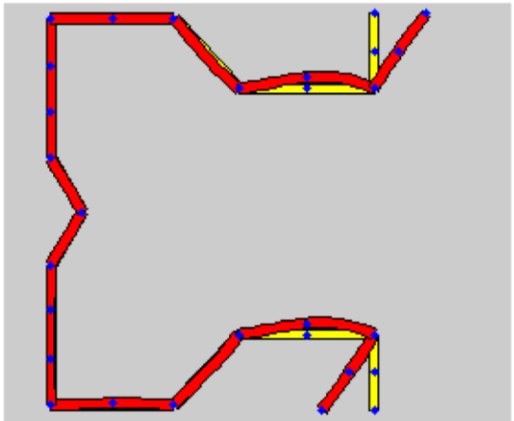

No distinct local buckling mode is present in the signature curve, thus the confined finite strip method is used to determine the local buckling half-wavelength. The local buckling half-wavelength to be used with the signature curve is $L_{cr\ell,h}$=40mm.

Note: reduced thicknesses from the rounded model are used for simplicity.

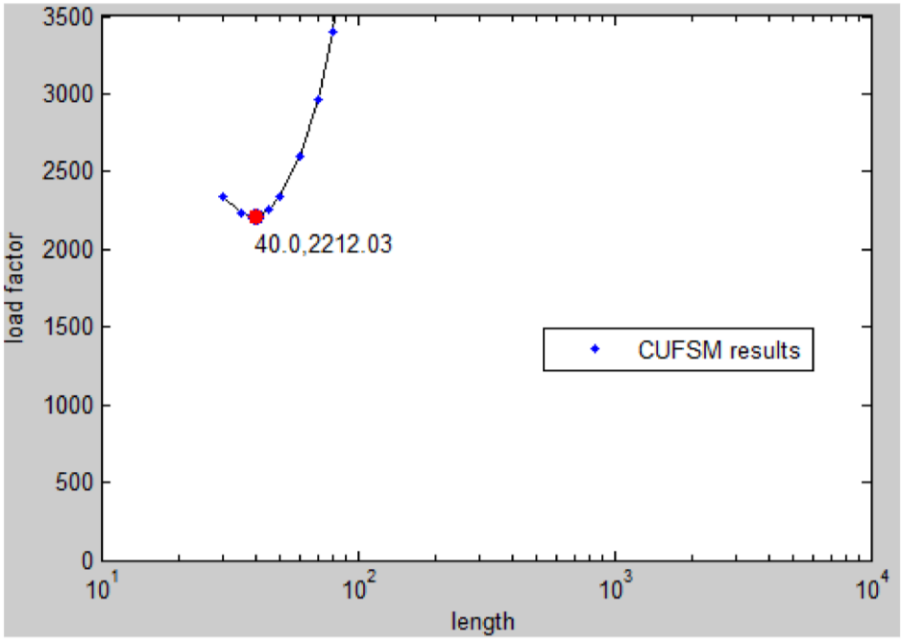

Elastic local buckling load using the rounded corner, reduced thickness model - plate failure mode

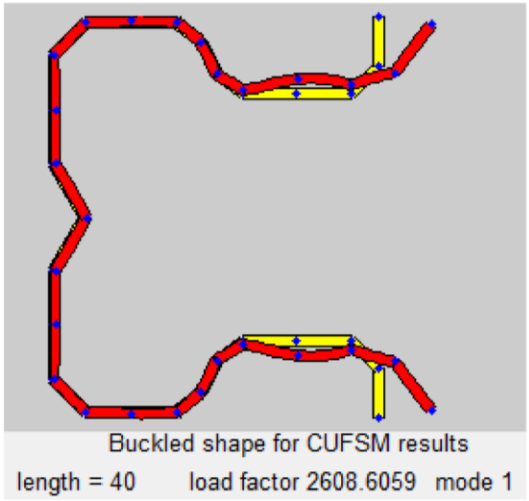

Plotted is the signature curve and buckled shape for local buckling at $L_{cr\ell,h}$=40mm. We can now say that the critical elastic buckling load including perforations for the plate failure mode is:

$$P_{crL\_plate} := 2609kN$$

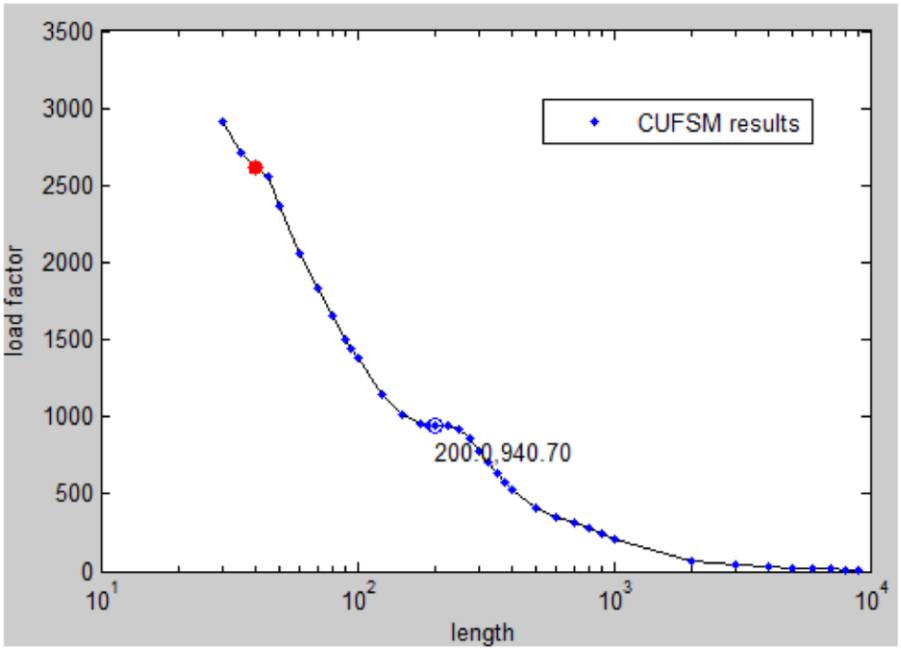

Sub-elemental Buckling

To address a potential failure mode of the section at the location of the hole, an approach similar to the one outlined by Moen and Schafer (2009) will be taken, as recommended by Smith and Moen (to appear). Of particular interest are "column strips" - material at the location of holes with two sides free to deform. Past research by Rhodes and Macdonald (1996) and Pu, et. al. (1999) have specified an effective length of the column strips to be near or equal to the length of perforations. For local buckling occuring in the column strip or unstiffened strip modes, the local buckling half-wavelength must satisfy $L_{cr} \leq L_h$.

Possible failures at perforation locations includ unstiffened or column strip buckling at web perforations, unstiffened or column strip buckling at flange holes, or column strip buckling between web and flange holes. Net section A will be used in the calculation of these failure modes. This may be overly conservative as the lengths of the flange and web holes are not equal.

Elastic local buckling load using the rounded corner, net section model - localized perforation failure mode

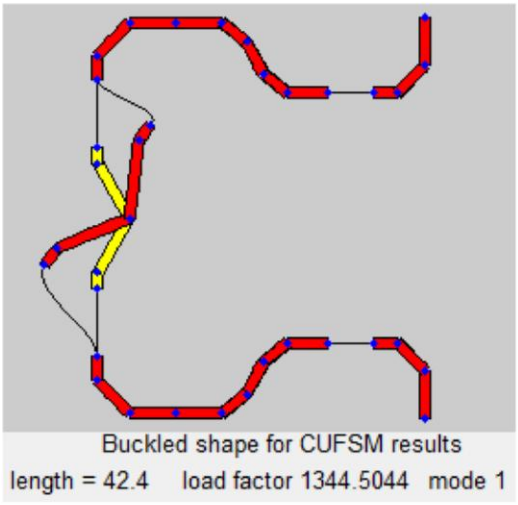

The worst case perforation localized buckling when considering effective lengths as previously discussed is the column strip local buckling between web perforations.

$$P_{crL\_perf} := 1345kN$$

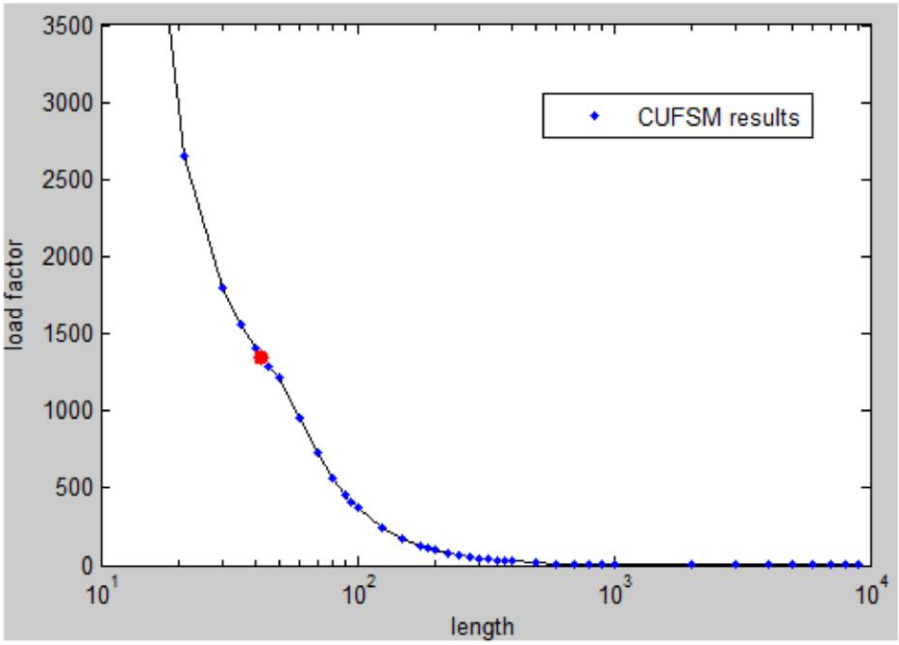

Worst case local buckling

Local buckling now becomes the minimum of these different failure modes.

$$P_{crL} := \min\left(P_{crL\_plate}, P_{crL\_perf}\right) = 1345 \cdot kN$$

Distortional buckling

Smith and Moen's method for distortional buckling was determined using a single flat web element (2013). The presence of the stiffener in the web of the 9024 shape may cause the section to be more prone to asymmetric distortional buckling or flexural-symmetric-distortional interaction.

Because the presence of a web stiffener has not been addressed by research, the application of the reduced thickness leaves the user with design choices. Because the method considers the full width of the web when calculating and applying the reduced thickness, this will be done. For this calculation, the width of the web will not consider the additional material due to the height of the stiffener as ignoring this material is more conservative.

Reduced full web thickness

Number of longitudinal perforations $n_l = 34$

Number of transverse perforations $n_t := 2$

Full web width $h_o := 71.70mm$

$$t_{rd\_w} := t \cdot \left(1 - \frac{n_l \cdot n_t \cdot L_{h\_dmd} \cdot d_{h\_dmd}}{L \cdot h_o} \right)^{\frac{1}{3}}$$

Reduced full element thickness $t_{rd\_w} = 2.184 \cdot mm$

Investigation of finite strip results

While there is a distinct distortional buckling mode in the signature curve, when examining distortional buckling in more detail it is apparent that this load is not the minimum for distortional buckling. To determine the half-wavelength, the confined finite strip method is used, again applying the reduced thickness to simulate the effects of perforations.

Confined finite strip method distortional buckling half-wavelength using sharp-cornered, reduced thickness model

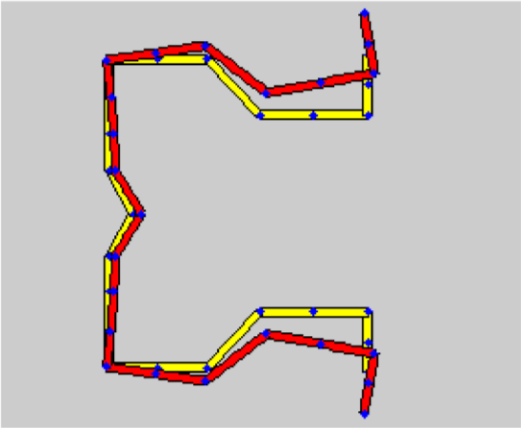

Buckled shape for CUFSM results
length = 700 load factor 438.4195 mode 1

The local buckling half-wavelength to be used with the signature curve is $L_{crd,h}$=700mm. This buckling shape may be located in a higher mode than the mode 1 that is plotted on the signature curve. If a more obvious minima is found in another mode near 700mm, it will be used instead as the sharp corners of this model may affect half-wavelength. Effective member lengths are greater than 700mm so their influence on distortional buckling is not necessary to consider.

Note: reduced thicknesses from the rounded model are used for simplicity.

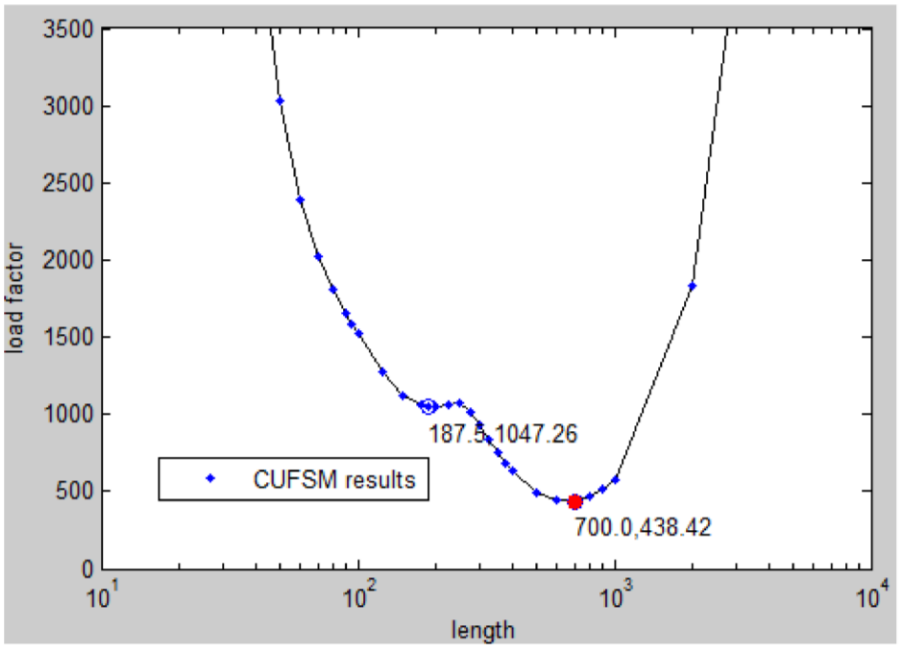

Elastic distortional buckling load using the rounded corner, reduced thickness model

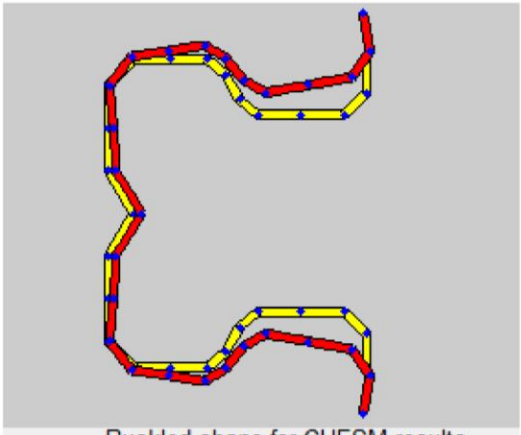

Buckled shape for CUFSM results

length = 600 load factor 437.857 mode 2

Modes 1 and 2 are plotted on the signature curve. A more obvious minima was found for distortional buckling was found (600mm) in mode 2 for distortional buckling near the one suggesand by the confined finite strip analysis. Buckled shapes for modes 1 and 2 are plotted. Mode 1 shows flexural-torsional buckling and asymmetric distortional buckling mixing. Since this mode shape was not shown by the confined finite strip results, it is not used. Instead, because mode 2 shows a buckled shape consistent with the one from the confined finite strip analysis, it is used.

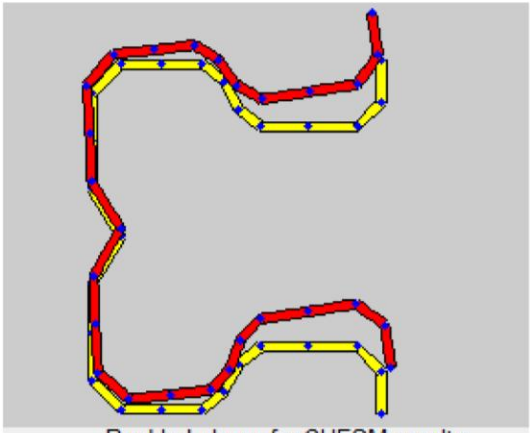

Buckled shape for CUFSM results

length = 600 load factor 375.7608 mode 1

We can now say that:

$$P_{crd} := 437.9kN$$

Note that this elastic buckling load is 45 percent of the distinct one located on the signature curve. Also note that the distinct mode is at a half-wavelength that is less than 3 times the greatest outside dimension of 90mm (200mm < 270mm), but is significantly greater than the outside dimension. These limits for discerning local and distortional buckling are mentioned in the Direct Strength Design Guide (AISI, 2006).

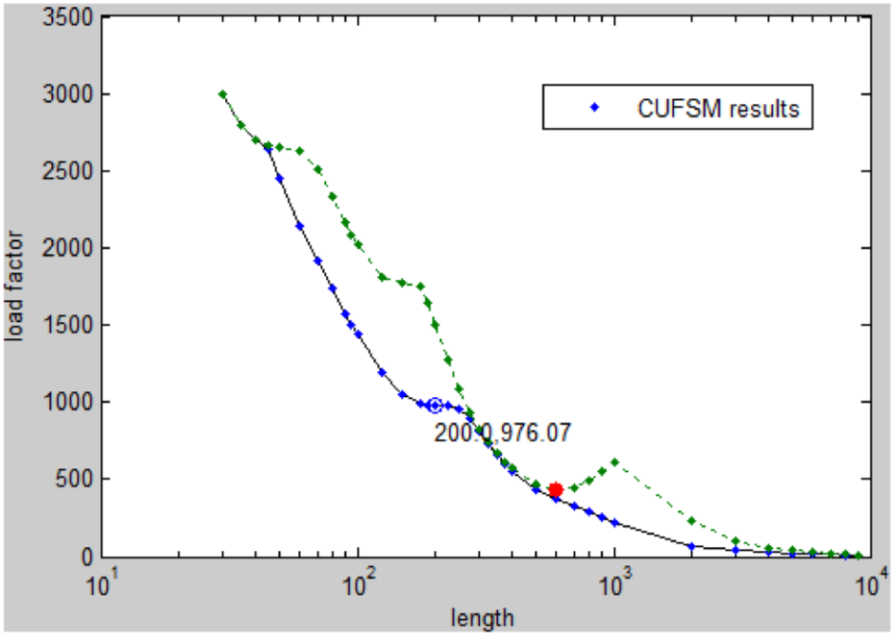

Global buckling

Two different methods to treat global buckling are presented by Smith and Moen (2013) and both will be examined: the modified classic cubic buckling equations and the weighted properties method. While stiffeners were not present in shapes of their research, it is assumed the methods to be general enough to account for their presence.

Bracing conditions must be considered when evaluating elastic global buckling loads. These conditions are described by the effective column lengths:

Effective x-axis length	$KL_x = 2657 \cdot mm$
Effective z-axis length	$KL_z = 894.9 \cdot mm$
Effective torsional-axis length	$KL_t = 1273.5 \cdot mm$

Flexural buckling will occur in the x-axis direction. This corresponds to bracing in the perpendicular axis and thus it must be evaluated at a half-wavelength of 894.9mm. Flexural-torsional buckling occurs in the z and torsional axes. Treatment of this will be done in one of three ways:

1. Using correct KL values in the modified classic cubic buckling equation to to determine $P_{cr,ft,h}$.

2. Using correct KL values in the unmodified classic cubic buckling equation to find $P_{cr,ft,nh}$ and modifying it using the weighted properties method to find $P_{cr,ft,h}$.

3. Using the worst case effective length to find to $P_{cr,ft,nh}$ because CUFSM does not allow for different half-wavelengths to be considered for different axes, and modifying it using the weighted properties method to find $P_{cr,ft,h}$.

Flexural buckling

Weighted Properties

The first step to calculating flexural buckling is the determination of the weak axis wieghted average moment of inertia. Though the perforation patterns may not lie completely symmetric along the length of the member, or, also for our case with smaller circular perforation alligned symmetrically with the larger diamond perforation, because the patterns are continuous along the member and at frequent spacing, we will assume pattern symmetry to simplify calculations (if perforations are not symmetric, a procedure described by Moen and Schafer (2009) should be used). These calculations are greatly simplified by the fact that spacing of the flange and web holes is the same (s_{l_dmd} and s_{l_crc}=75mm).

Length of net section A $L_{nA} := n_l \cdot L_{h\_crc} = 353.6 \cdot mm$

Length of net section B $L_{nB} := n_l \cdot \left(L_{h\_dmd} - L_{h\_crc}\right) = 1088 \cdot mm$

Length of gross section $L_g := L - L_{nA} - L_{nB} = 1105.4 \cdot mm$

Weighted moment of inertia about the z-axis

$$I_{zavg} := \frac{I_{zg} \cdot L_g + I_{znA} \cdot L_{nA} + I_{znB} \cdot L_{nB}}{L} = 388058 \cdot mm^4$$

Modified classic cubic buckling equation

$$P_{cre\_f\_h\_1} := \frac{\pi^2 \cdot E \cdot I_{zavg}}{\left(KL_z\right)^2} = 1076 \cdot kN$$

Unperforated finite strip model using weighted properties method

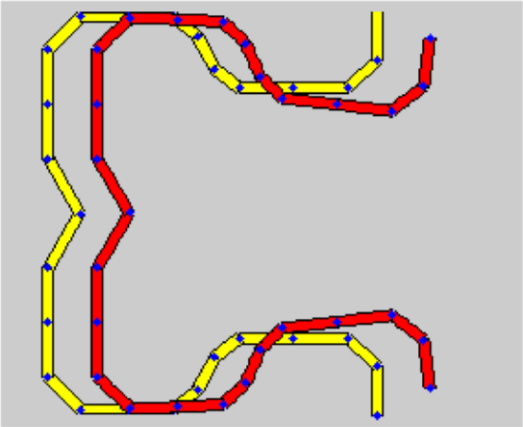

Flexural buckling at L_{cre}=894.9mm was present in mode 3. Calculating $P_{cre,f,nh}$ including the presence of holes:

$$P_{cre\_f\_nh\_2} := 1110.kN$$

$$P_{cre\_f\_h\_2} := P_{cre\_f\_nh\_2} \cdot \frac{I_{zavg}}{I_{zg}}$$

$$P_{cre\_f\_h\_2} = 1001 \cdot kN$$

This elastic buckling mode is more conservative and accurate as it eliminates error from the rigid body assumption and includes modal interaction.

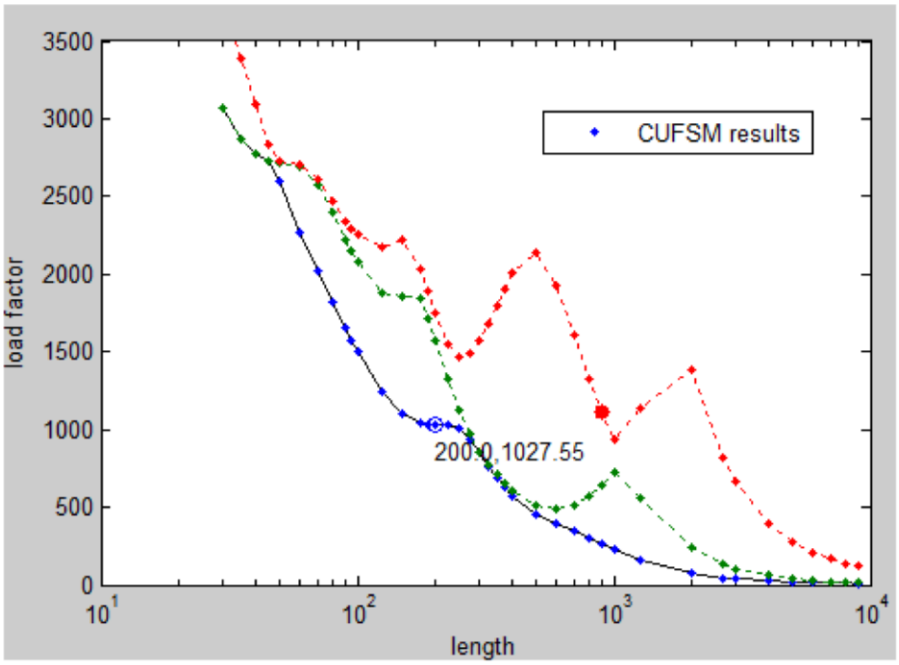

Flexural-torsional buckling

Weighted Properties

The first step to calculating flexural-torsional buckling is the determination of the wieghted average properties that will be used in the approximate methods. As mentioned previously, it will be assumed that holes are symmetric within patterns and patterns are symmetric within the member length.

Length of net section A $L_{nA} = 353.6 \cdot mm$

Length of net section B $L_{nB} = 1088 \cdot mm$

Length of gross section $L_g = 1105.4 \cdot mm$

Weighted x distance from centroid to shear center

$$x_{oavg} := \frac{x_{og} \cdot L_g + x_{onA} \cdot L_{nA} + x_{onB} \cdot L_{nB}}{L} = -66.55 \cdot mm$$

Weighted radius of gyration about the shear center

$$r_{oavg} := \frac{r_{og} \cdot L_g + r_{onA} \cdot L_{nA} + r_{onB} \cdot L_{nB}}{L} = 78.55 \cdot mm$$

Weighted St. Venant torsional constant

$$J_{avg} := \frac{J_g \cdot L_g + J_{nA} \cdot L_{nA} + J_{nB} \cdot L_{nB}}{L} = 1122 \cdot mm^4$$

Weighted warping torsional constant

$$C_{wavg} := \frac{C_{wg} \cdot L_g + C_{wnA} \cdot L_{nA} + C_{wnB} \cdot L_{nB}}{L} = 6.540 \times 10^8 \cdot mm^6$$

Weighted moment of inertia about the x-axis

$$I_{xavg} := \frac{I_{xg} \cdot L_g + I_{xnA} \cdot L_{nA} + I_{xnB} \cdot L_{nB}}{L} = 635907 \cdot mm^4$$

Modified classic cubic buckling equation

$$\beta_h := 1 - \left(\frac{x_{oavg}}{r_{oavg}} \right)^2 = 0.282$$

$$\sigma_{exh} := \frac{\pi^2 \cdot E \cdot I_{xavg}}{A_g \cdot (KL_x)^2} = 314.1 \cdot MPa$$

$$\sigma_{th} := \frac{1}{A_g \cdot r_{oavg}^2} \cdot \left[G \cdot J_{avg} + \frac{\pi^2 \cdot E \cdot C_{wavg}}{(KL_t)^2} \right] = 252.6 \cdot MPa$$

$$P_{cre\_ft\_h\_1} := \frac{A_g}{2\beta_h} \cdot \left[(\sigma_{exh} + \sigma_{th}) - \sqrt{(\sigma_{exh} + \sigma_{th})^2 - 4\beta_h \cdot \sigma_{exh} \cdot \sigma_{th}} \right] = 96.44 \cdot kN$$

Weighted average method using classic cubic buckling equation

$$\beta := 1 - \left(\frac{x_{og}}{r_{og}}\right)^2 = 0.296$$

$$\sigma_{ex} := \frac{\pi^2 \cdot E \cdot I_{xg}}{A_g \cdot (KL_x)^2} = 327.6 \cdot MPa$$

$$\sigma_t := \frac{1}{A_g \cdot r_{og}^2} \cdot \left[G \cdot J_g + \frac{\pi^2 \cdot E \cdot C_{wg}}{(KL_t)^2} \right] = 289.7 \cdot MPa$$

$$P_{cre\_ft\_nh\_2} := \frac{A_g}{2\beta} \cdot \left[(\sigma_{ex} + \sigma_t) - \sqrt{(\sigma_{ex} + \sigma_t)^2 - 4\beta \cdot \sigma_{ex} \cdot \sigma_t} \right] = 106.45 \cdot kN$$

$$P_{cre\_ft\_h\_2} := P_{cre\_ft\_nh\_2} \cdot \frac{C_{wavg}}{C_{wg}} \cdot \frac{J_{avg}}{J_g} = 91.43 \cdot kN$$

Unperforated finite strip model using weighted properties method

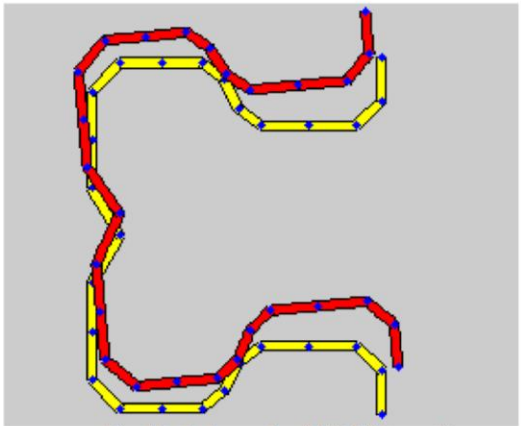

Since CUFSM does not allow separate braced lengths to be considered, we will use $L_{cre}=KL_x$=2657mm in calculating $P_{cre,ft,h}$.

$$P_{cre\_ft\_nh\_3} := 46.80kN$$

$$P_{cre\_ft\_h\_3} := P_{cre\_ft\_nh\_3} \cdot \frac{C_{wavg}}{C_{wg}} \cdot \frac{J_{avg}}{J_g}$$

$$P_{cre\_ft\_h\_3} = 40.20 \cdot kN$$

This elastic buckling mode is overly conservative. It is recommended to use one of the previous methods when effective lengths are not equal.

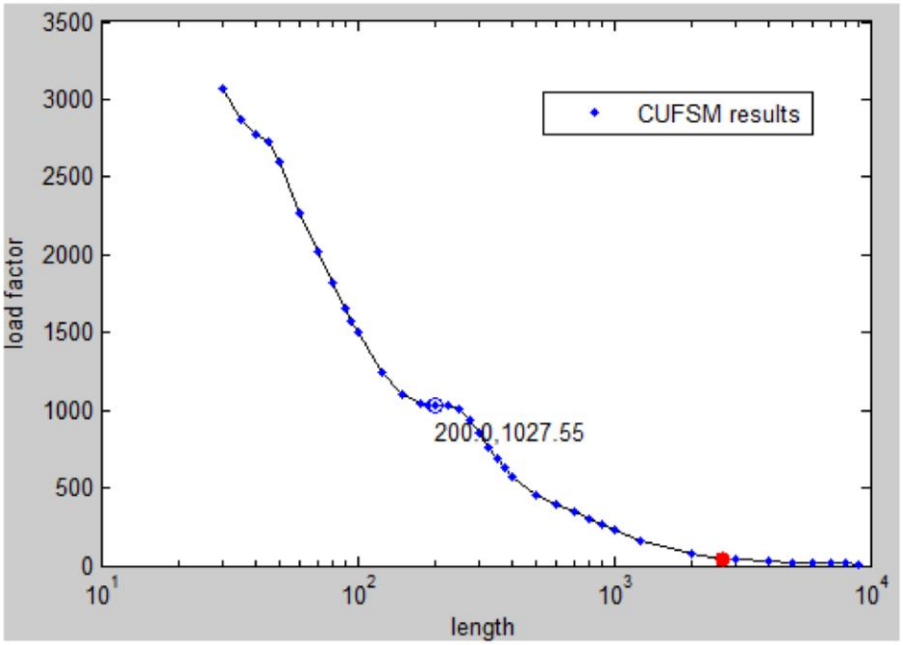

Global buckling load for use with the DSM

The worst case of flexural and torsional-flexural buckling will control elastic global buckling. However, when comparing the approximate buckling loads found for either mode, addition consideration must be given.

For flexural buckling, there is only one effective length to be considered so both the finite strip method approximation and the classic cubic buckling equation can be directly compared. The rigid body assumption of the classic cubic buckling equation introduces error into the elastic buckling load and ignores any modal interaction. Because of this, the lesser of the two loads will be used for flexural buckling.

$$P_{cre\_f\_h} := \min\left(P_{cre\_f\_h\_1}, P_{cre\_f\_h\_2}\right) = 1001 \cdot kN$$

For flexural-torsional buckling, there are two different effective lengths to be considered and only the classic cubic buckling equation can consider both at once. Because of this, the assumption made for the finite strip approach to use the greatest effective length is overly conservative and thus one of the classic cubic buckling equations should be used. There are pros and cons to both of the classic cubic buckling equation methods for flexural torsional buckling and Smith and Moen (2013) do not reccommend one method over another. The weighted properties approach requires less calculations as $x_{o,avg}$, $r_{o,avg}$, and $I_{x,avg}$ are not required, however, their inclusion into the modified classic cubic buckling equation provides it with a greater background in behavior. Because of the latter point, the modified classic cubic buckling equation will be used for flexural-torsional buckling.

$$P_{cre\_ft\_h} := P_{cre\_ft\_h\_1} = 96.44 \cdot kN$$

The critical elastic global buckling load can now be found:

$$P_{cre} := \min\left(P_{cre\_ft\_h}, P_{cre\_f\_h}\right) = 96.44 \cdot kN$$

A summary of the inputs from the elastic buckling analysis:

$P_y = 350.2 \cdot kN$

$P_{ynet} = 283.5 \cdot kN$

$P_{crL} = 1345 \cdot kN$

$P_{crd} = 437.9 \cdot kN$

$P_{cre} = 96.44 \cdot kN$

Global buckling strength per DSM 1.2.1.1

$$\lambda_c := \sqrt{\frac{P_y}{P_{cre}}} \qquad \lambda_c = 1.906$$

global slenderness (including influence of holes) (Eq. 1.2.1-3)

$$P_{ne} := \begin{cases} \left(0.658^{\lambda_c^2}\right) \cdot P_y & \text{if } \lambda_c \le 1.5 \\ \left(\frac{0.877}{\lambda_c^2}\right) \cdot P_y & \text{if } \lambda_c > 1.5 \end{cases}$$

(Eq. 1.2.1-1) (Eq. 1.2.1-2)

$P_{ne} = 84.6 \cdot kN$ column capacity, global buckling limit state (including the influence of holes)

Local buckling check per DSM 1.2.1.2

$$\lambda_L := \sqrt{\frac{P_{ne}}{P_{crL}}} \qquad \lambda_L = 0.251$$

(subscript "L" = "ℓ")

local slenderness (including influence of holes) (Eq. 1.2.1-7)

$$P_{nL} := \min\left[P_{ynet}, \left[\left[1 - 0.15 \cdot \left(\frac{P_{crL}}{P_{ne}}\right)^{0.4}\right]\left(\frac{P_{crL}}{P_{ne}}\right)^{0.4} \cdot P_{ne}\right]\right]$$

(Eq. 1.2.1-6) (Eq. 1.2.1-8)

$P_{nL} = 139.747 \cdot kN$ column capacity, local-global buckling interaction limit state (including the influence of holes)

Distortional buckling check per DSM 1.2.1.3

$$\lambda_d := \sqrt{\frac{P_y}{P_{crd}}} \qquad \lambda_d = 0.894$$

distortional slenderness (including influence of holes) (Eq. 1.2.1-12)

$$\lambda_{d1} := 0.561 \cdot \left(\frac{P_{ynet}}{P_y} \right) \qquad \lambda_{d1} = 0.454 \qquad \text{(Eq. 1.2.1-16)}$$

$$\lambda_{d2} := 0.561 \cdot \left[14 \left(\frac{P_y}{P_{ynet}} \right)^{0.4} - 13 \right] \qquad \lambda_{d2} = 1.254 \qquad \text{(Eq. 1.2.1-17)}$$

$$P_{d2} := \left[1 - 0.25 \cdot \left(\frac{1}{\lambda_{d2}} \right)^{1.2} \right] \cdot \left(\frac{1}{\lambda_{d2}} \right)^{1.2} \cdot P_y \qquad P_{d2} = 216 \cdot kN \qquad \text{(Eq. 1.2.1-18)}$$

$$P_{nd} := \begin{cases} P_{ynet} & \text{if } \lambda_d \le \lambda_{d1} \qquad \text{(Eq. 1.2.1-13)} \\ \left[P_{ynet} - \left(\frac{P_{ynet} - P_{d2}}{\lambda_{d2} - \lambda_{d1}} \right) \cdot \left(\lambda_d - \lambda_{d1} \right) \right] & \text{if } \lambda_{d1} < \lambda_d \le \lambda_{d2} \qquad \text{(Eq. 1.2.1-14)} \\ \left[\left[1 - 0.25 \cdot \left(\frac{P_{crd}}{P_y} \right)^{0.6} \right] \left(\frac{P_{crd}}{P_y} \right)^{0.6} \cdot P_y \right] & \text{if } \lambda_d > \lambda_{d2} \qquad \text{(Eq. 1.2.1-11)} \end{cases}$$

$P_{nd} = 246.4 \cdot kN$ column capacity, distortional buckling limit state (including the influence of holes)

Predicted compressive capacity per DSM 1.2

$P_n := \min\left(\left(P_{ne} \;\; P_{nL} \;\; P_{nd} \right) \right) \qquad P_n = 84.576 \cdot kN$

This load is conservative when compared to the average ultimate static load determined experimentally by Koen.

$P_{2550\_u\_s} := 103.0kN$ (Table 8, Koen, 2008)

It is believed that this conservatism arises from the assumption that bracing does not reduce the effective lengths in the x and torsional axes.

Design compressive capacity per DSM

The geometry of this section does not fall within the "pre-qualified" columns of DSM Section 1.1.1.1 as lipped c-sections with web stiffeners do not include the complex lips of rack uprights. Thus the lower ϕ and higher Ω of DSM Section 1.2.1 must be used for determining design strength.

LRFD: $\phi_c := 0.80 \qquad \phi_c \cdot P_n = 67.7 \cdot kN$

ASD: $\Omega_c := 2.00 \qquad \frac{P_n}{\Omega_c} = 42.3 \cdot kN$

Discussion of influence of the perforation pattern

Looking at the bigger picture, we can examine the reduction in strength that the perforation pattern causes. For the 9024 section, flexural torsional buckling controls and sees no interaction with local buckling. Using this knowledge, we can calculate P_n excluding holes:

$$\lambda_c := \sqrt{\frac{P_y}{P_{cre\_ft\_nh\_2}}} \qquad \lambda_c = 1.814$$ global slenderness (including influence of holes) (Eq. 1.2.1-3)

$$P_{ne} := \begin{cases} \left(0.658^{\lambda_c^2}\right) \cdot P_y & \text{if } \lambda_c \le 1.5 \\ \left(\frac{0.877}{\lambda_c^2}\right) \cdot P_y & \text{if } \lambda_c > 1.5 \end{cases}$$ (Eq. 1.2.1-1) (Eq. 1.2.1-2)

$P_{ne} = 93.4 \cdot kN$ column capacity, global buckling limit state (excluding the influence of holes)

We already know that P_{ne} will govern strength for the unperforated section. This leads us to the comparison in strength of the section with and without perforations.

$$\frac{P_n}{P_{ne}} = 0.906$$

By ignoring perforations in the 2550mm length column, we could potentially over predict capacity by 10 percent.

The influence of holes is likely more pronounced for shorter column lengths. We will examine this influence by using Smith and Moen's (2013) prediction methods to determine stub column strength.

Problem statement

Using the Direct Strength Method, determine the compressive strength, P_n, of the 373.5mm long 9024 cross-section experimentally tested by Koen (2008).

Background

Cross-sectional geometry - 9024 section

See previous

Perforation geometry - 9024 section

See previous

Model properties

Measured member length $L := 373.5mm$ (Table 5, Koen, 2008)

For other properties, see previous

Bracing and boundary conditions

"The base and cap plates were fixed for all translations and rotations other than vertical displacement at the top." (pp 32, Koen, 2008)

Effective x-axis length	$KL_x := 0.5 \cdot L = 186.8 \cdot mm$
Effective z-axis length	$KL_z := 0.5 \cdot L = 186.8 \cdot mm$
Effective t-axis length	$KL_t := 0.5 \cdot L = 186.8 \cdot mm$

Gross and net section properties

See previous

Elastic buckling analysis

The purpose of a stub column test is to eliminate the influence of global buckling modes. To simplify our analysis, we will assume $P_{ne}=P_y$ (the same as saying P_{cre} is extremely large). We can use information from the previous elastic buckling calculations on local buckling, as $L_{cr}<KL$. We must now examine distortional buckling at a half-wavelength equal to KL. It was previously mentioned that the Direct Strength Design Guide (AISI, 2006) reccommends using three times the greatest outside dimension to discern distortional buckling; however, this leaves buckled half-wavelengths between one and three times the greatest outside dimension unnaccounted for by local or distortional buckling. This is a problem as a mode within these lengths is less than that of local buckling. Because it makes no sense to treat a buckled shape with half-wavelengths greater than the greatest outside dimension as local buckling, we will treat this mode as distortional for use with the DSM equations. Note that the reduced thickness model for distortional buckling was used in this analysis.

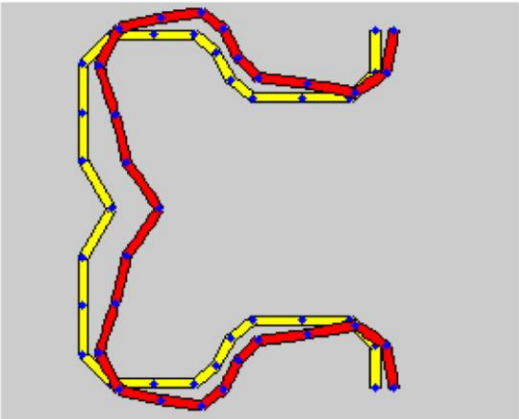

Buckled shape for CUFSM results

length = 186.8 load factor 978.4703 mode 1

$P_{crd} := 978.5kN$

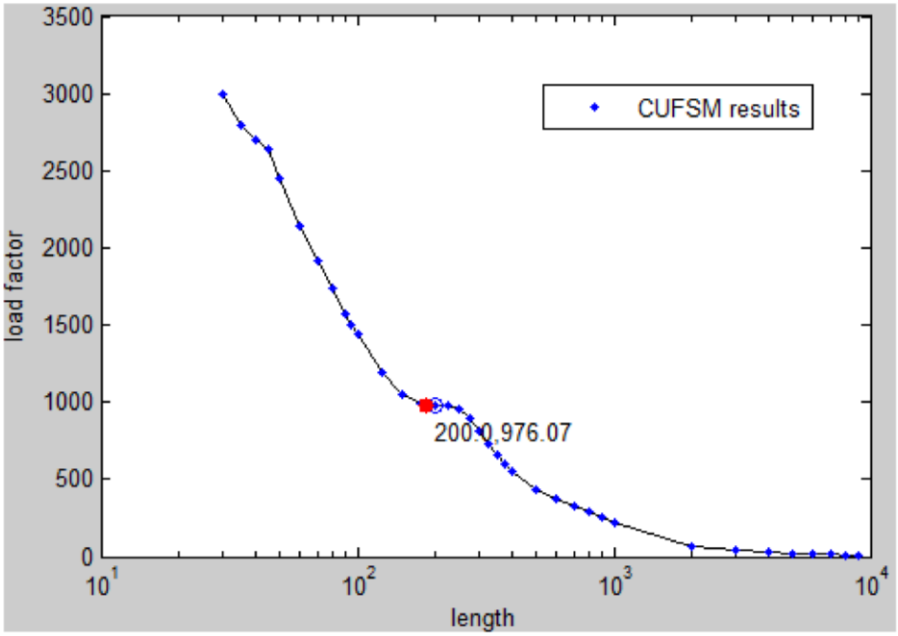

A summary of the inputs from the elastic buckling analysis:

$P_y = 350.2 \cdot kN$

$P_{ynet} = 283.5 \cdot kN$

$P_{crL} = 1345 \cdot kN$

$P_{crd} = 978.5 \cdot kN$

$P_{cre} := 1000000kN$ (Assumed to be extremely large)

Global buckling strength per DSM 1.2.1.1

$\lambda_c := \sqrt{\frac{P_y}{P_{cre}}}$ $\lambda_c = 0.019$ global slenderness (including influence of holes) (Eq. 1.2.1-3)

$$P_{ne} := \begin{cases} \left(0.658^{\lambda_c^2}\right) \cdot P_y & \text{if } \lambda_c \le 1.5 \\ \left(\frac{0.877}{\lambda_c^2}\right) \cdot P_y & \text{if } \lambda_c > 1.5 \end{cases}$$

(Eq. 1.2.1-1)

(Eq. 1.2.1-2)

$P_{ne} = 350.2 \cdot kN$ column capacity, global buckling limit state (including the influence of holes)

Local buckling check per DSM 1.2.1.2

$$\lambda_L := \sqrt{\frac{P_{ne}}{P_{crL}}} \qquad \lambda_L = 0.51 \qquad \text{local slenderness (including influence of holes)} \qquad \text{(Eq. 1.2.1-7)}$$

(subscript "L" = "ℓ")

$$P_{nL} := \min\left[P_{ynet}, \left[\left[1 - 0.15\cdot\left(\frac{P_{crL}}{P_{ne}}\right)^{0.4}\right]\left(\frac{P_{crL}}{P_{ne}}\right)^{0.4}\cdot P_{ne}\right]\right] \qquad \text{(Eq. 1.2.1-6)} \quad \text{(Eq. 1.2.1-8)}$$

$P_{nL} = 283.47\cdot kN$ column capacity, local-global buckling interaction limit state (including the influence of holes)

Distortional buckling check per DSM 1.2.1.3

$$\lambda_d := \sqrt{\frac{P_y}{P_{crd}}} \qquad \lambda_d = 0.598 \qquad \text{distortional slenderness (including influence of holes)} \qquad \text{(Eq. 1.2.1-12)}$$

$$\lambda_{d1} := 0.561\cdot\left(\frac{P_{ynet}}{P_y}\right) \qquad \lambda_{d1} = 0.454 \qquad \text{(Eq. 1.2.1-16)}$$

$$\lambda_{d2} := 0.561\cdot\left[14\left(\frac{P_y}{P_{ynet}}\right)^{0.4} - 13\right] \qquad \lambda_{d2} = 1.254 \qquad \text{(Eq. 1.2.1-17)}$$

$$P_{d2} := \left[1 - 0.25\cdot\left(\frac{1}{\lambda_{d2}}\right)^{1.2}\right]\cdot\left(\frac{1}{\lambda_{d2}}\right)^{1.2}\cdot P_y \qquad P_{d2} = 216\cdot kN \qquad \text{(Eq. 1.2.1-18)}$$

$$P_{nd} := \begin{cases} P_{ynet} & \text{if } \lambda_d \le \lambda_{d1} \qquad \text{(Eq. 1.2.1-13)} \\ \left[P_{ynet} - \left(\frac{P_{ynet} - P_{d2}}{\lambda_{d2} - \lambda_{d1}}\right)\cdot\left(\lambda_d - \lambda_{d1}\right)\right] & \text{if } \lambda_{d1} < \lambda_d \le \lambda_{d2} \qquad \text{(Eq. 1.2.1-14)} \\ \left[\left[1 - 0.25\cdot\left(\frac{P_{crd}}{P_y}\right)^{0.6}\right]\left(\frac{P_{crd}}{P_y}\right)^{0.6}\cdot P_y\right] & \text{if } \lambda_d > \lambda_{d2} \qquad \text{(Eq. 1.2.1-11)} \end{cases}$$

$P_{nd} = 271.3\cdot kN$ column capacity, distortional buckling limit state (including the influence of holes)

Predicted compressive capacity per DSM 1.2

$$P_n := \min\left(\left(P_{ne}\ \ P_{nL}\ \ P_{nd}\right)\right) \qquad P_n = 271.314\cdot kN$$

This load is nearly the same as the one determined by Koen.

$P_{3735\_u\_s} := 270kN$ (Table 5, Koen, 2008)

Assuming that local buckling will not govern for the unperforated shape, we can determine the ultimate strength of the unperforated shape by examining distortional buckling at the same half-wavelength using the unreduced section.

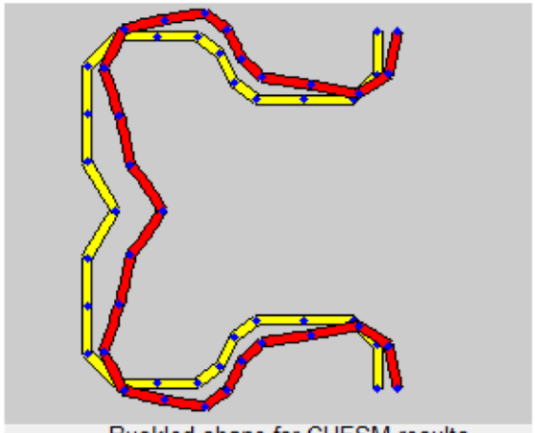

$P_{crd} := 1028.kN$

$P_{ynet} := P_y$ (Unperforated)

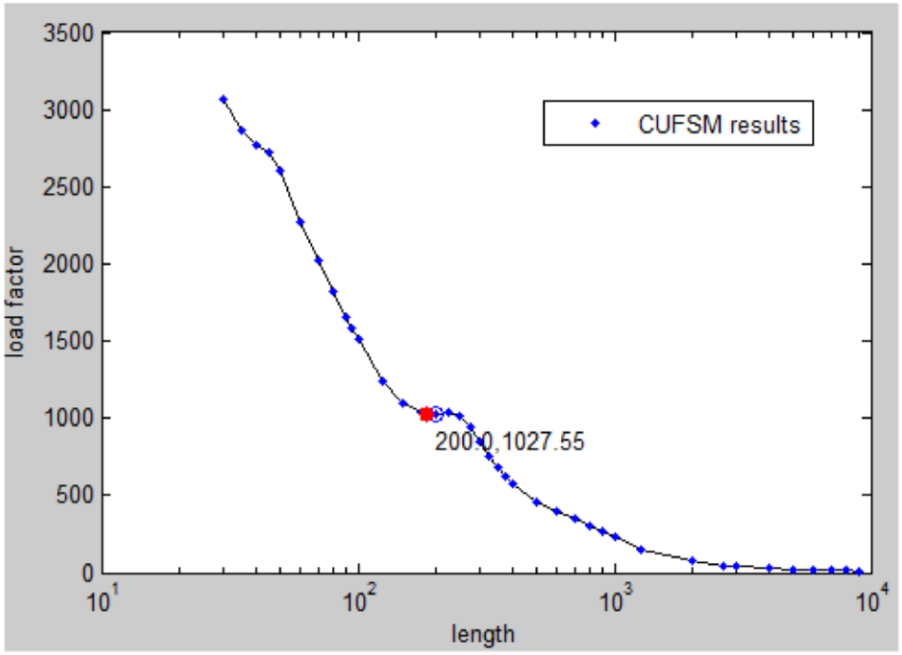

Distortional buckling check per DSM 1.2.1.3

$\lambda_d := \sqrt{\frac{P_y}{P_{crd}}}$ $\lambda_d = 0.584$ distortional slenderness (including influence of holes) (Eq. 1.2.1-12)

$$\lambda_{d1} := 0.561 \cdot \left(\frac{P_{ynet}}{P_y} \right) \qquad \lambda_{d1} = 0.561 \qquad \text{(Eq. 1.2.1-16)}$$

$$\lambda_{d2} := 0.561 \cdot \left[14 \left(\frac{P_y}{P_{ynet}} \right)^{0.4} - 13 \right] \qquad \lambda_{d2} = 0.561 \qquad \text{(Eq. 1.2.1-17)}$$

$$P_{d2} := \left[1 - 0.25 \cdot \left(\frac{1}{\lambda_{d2}} \right)^{1.2} \right] \cdot \left(\frac{1}{\lambda_{d2}} \right)^{1.2} \cdot P_y \qquad P_{d2} = 350.2 \cdot kN \qquad \text{(Eq. 1.2.1-18)}$$

$$P_{nd} := \begin{cases} P_{ynet} \text{ if } \lambda_d \le \lambda_{d1} & \text{(Eq. 1.2.1-13)} \\ \left[P_{ynet} - \left(\frac{P_{ynet} - P_{d2}}{\lambda_{d2} - \lambda_{d1}} \right) \cdot \left(\lambda_d - \lambda_{d1} \right) \right] \text{ if } \lambda_{d1} < \lambda_d \le \lambda_{d2} & \text{(Eq. 1.2.1-14)} \\ \left[\left[1 - 0.25 \cdot \left(\frac{P_{crd}}{P_y} \right)^{0.6} \right] \left(\frac{P_{crd}}{P_y} \right)^{0.6} \cdot P_y \right] \text{ if } \lambda_d > \lambda_{d2} & \text{(Eq. 1.2.1-11)} \end{cases}$$

$P_{nd} = 349.5 \cdot kN$ column capacity, distortional buckling limit state (excluding the influence of holes)

We have established that P_{nd} will govern strength for the unperforated stub column and thus we can compare the reduction in strength perforations cause.

$$\frac{P_n}{P_{nd}} = 0.776$$

By ignoring perforations in the 373.5mm length stub column, we over predict capacity by more than 20 percent.

Final thoughts

The examples presented highlight two things:

The first is that the Direct Strength Method in conjunction with elastic buckling prediction methods developed by Smith and Moen (2013) have the potential to accurately predict column strength for rack columns with perforation patterns.

The second is that boundary conditions, especially in longer columns, have a great effect on predicted strength. A conservative assumption may cause an engineer to significantly overdesign a section; an unconservative assumption may cause a member to be significantly underdesigned.

APPENDIX D. PERFORATION PATTERN FACTORS

Longitudinal and transverse perforation pattern factors, *X* and *Y*, account for the average effect of a perforation's location on local buckling due to the removal of material's effect on strain energy. The effect of varying these factors on the mean and coefficient of variation of ABAQUS to predicted results for local buckling was studied and results are shown in two dimensional contour plots in the following figure. While having a separate cases for *X* and *Y* for different perforation pattern parameters can improve coefficient of variation results and, in the case of the transverse perforation pattern factor, these different cases can be explained by the effect perforations have on the in-plane stress distribution (Pennington Vann 1971), it is both conservative and simpler to use $X=Y=-1$.

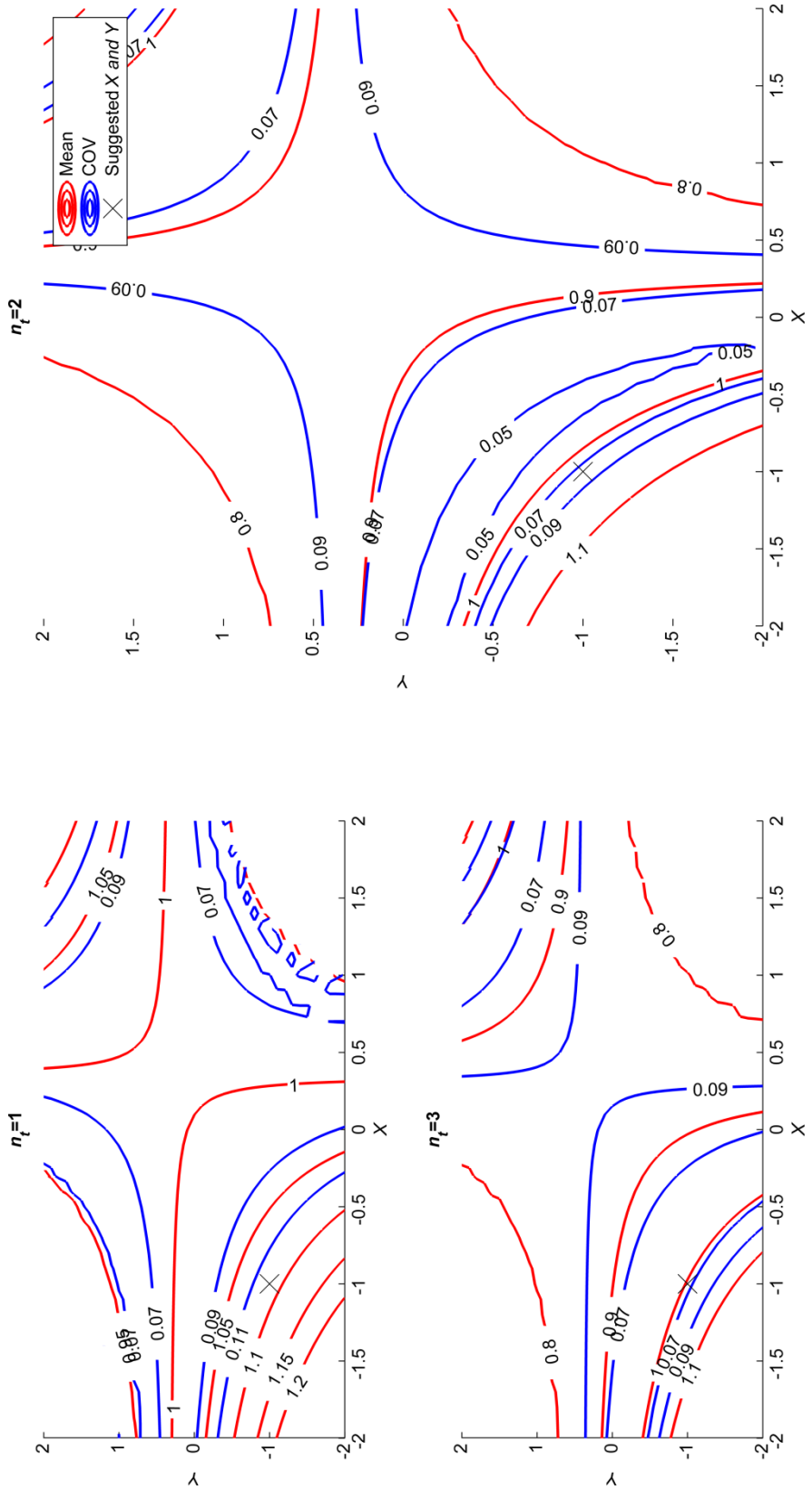

Fig. 21 Study of longitudinal and transverse perforation pattern factors effect on ABAQUS to predicted results for local buckling